6 *Dynamics of Air Pollutants over the Northeastern Iberian Peninsula by Using ECHAM5/MESSy and MM5-EMICAT2000-CMAQ Models*

6.1 Introduction

The complex topography of the northeastern Iberian Peninsula (NEIP) induces an extremely complicated structure of the flow because of the development of mesoscale phenomena that interact with synoptic flows. The characteristics of the breezes have important effects in the dispersion of pollutants emitted. In addition, the flow can be even more complex because of the non-homogeneity of the terrain, the land-use and the types of vegetation. In these situations, the structure of the flow is extremely complicated because of the superposition of circulations of different scale.

The objective of the present study is to search for the origin of the high levels of photochemical pollutants over the Western Mediterranean Basin (WMB), and specifically, over the northeastern Iberian Peninsula during summertime. The global circulation model ECHAM5, together with MESSy, provides a coupled chemistry-climate model, which was used to describe the patterns of pollutants over the WMB. In order to study the northeastern Iberian Peninsula with a higher resolution, the MM5-EMICAT2000-CMAQ model was implemented to reproduce the diurnal cycle of air pollutants and then to help understanding the relative importance of processes involved at a high space (1h) and temporal (2km) resolution. The episode of 13-16 August, 2000 (described previously in Section 2.1) was selected to perform simulations, since it is shown to be a recursive weather pattern over the Mediterranean area during summertime (Jorba *et al.*, 2004).

An evaluation of ECHAM5/MESSy and MM5-EMICAT2000-CMAQ is performed using data from air quality stations in the northeastern Iberian Peninsula belonging to the Environmental Department of Catalonia Government (Spain). Extensive ambient data are found for O_3, CO and NO_x in the area during the episode of 13-16 August, 2000; and therefore an assessment of the results of the first layer of the models respect to these pollutants is shown. The LIDAR vertical profiles by Pérez *et al.* (2004) allow us performing a vertical qualitative evaluation of the behavior of the model when describing the layering of pollutants that are observed with the LIDAR measurements over the northeastern Iberian Peninsula.

Results show the dynamics and the origin of tropospheric air pollutants for ozone and also for carbon monoxide, since O_3 presents a short lifetime during summer (in the order of hours or a few days), meanwhile CO may act as a tracer to describe the origin of polluted air masses, since its lifetime in the Western Mediterranean during summer is in the order of months.

The troposphere was divided in three different zones in order to facilitate the analysis and description of physic-chemical phenomena: low troposphere, middle troposphere and upper troposphere. In addition, a quantification of the tropospheric ozone and carbon monoxide in the northeastern Iberian Peninsula is performed according to the different phenomena taking part in the dynamics of the pollutants in the area of study: (1) emissions-photochemical cycle; (2) convective transport; (3) advective transport; (4) dry and wet deposition; and (5) stratosphere-troposphere exchange.

6.2 Methodology: Description of Models

Two different approaches were used in this work in order to describe the dynamics of photochemical pollutants. For the Western Mediterranean Basin, the general circulation model (GMC) used in this study is the European Centre Hamburg Model version 5 (ECHAM5) (Roeckner *et al.*, 2003) coupled with MECCA chemistry, in order to describe processes at a regional-global scale. When a more detailed description of dynamical processes is needed, the MM5-EMICAT2000-CMAQ model represents local-regional photochemistry. Further description of these ECHAM5/MESSy is presented below. The description of MM5-EMICAT2000-CMAQ can be found in Section 2.2.

6.2.1 European Center Hamburg Model version 5 (ECHAM5)

The ECHAM5 model used a horizontal resolution of about 1.8° x 1.8° and a time step of 900 s (T63). ECHAM5 global circulation model has been coupled to the Modular Earth Submodel System (MESSy), developed at Max Planck Institute for Chemistry (Mainz, Germany), that provides a generalized structure, which allows studying feedback mechanisms between various bio-geochemical processes, and extending ECHAM5 into a fully coupled chemistry-climate model. The model distinguishes 19 hybrid σ-p layers between the surface and the top level at 10 hPa. Tracer transport is calculated with a semi-Lagrangian advection scheme (Rasch and Williamson, 1990). Additional vertical transports are included through the parameterization of vertical diffusion and convection.

Because the model does not represent typical stratospheric chemistry, ozone in the stratosphere is parameterized with results from a 2D troposphere-stratosphere chemistry model (Brühl and Crutzen, 1988). Additionally, the model applies an ozone-potential vorticity (PV) correlation in the extra-tropical lower stratosphere to preserve longitudinal variability of ozone associated with the meandering and breaking of the jet streams (Roelofs and Lelieveld, 2000b). The parameterization is applied above the extra-tropical tropopause while transport and mixing in the tropopause region is simulated by the model.

The model considers a separate stratospheric ozone tracer, referred to as O_3s. The concentration of O_3s is equal to that of ozone in the grids where stratospheric ozone is prescribed (Roelofs and Lelieveld, 2000a). O_3s is transported from the stratosphere into the troposphere along with the calculated air motions (Kentarchos and Roelofs, 2003), where it is photochemically destroyed or removed by dry deposition. The difference between O_3 and O_3s is a measure of ozone that originates from photochemical production, mainly in the troposphere (O_3t).

The representation of emissions is an essential component of ECHAM5/MESSy chemistry-climate model. Emission inventories were derived from EDGAR 3.2 database, and are described in detail by van Aardenne *et al.* (2001). This inventory includes the emissions of CO_2, CO, CH4, NMVOCs, SO_2, NO_x, N_2O and NH_3. In EDGAR, emissions are calculated on the basis of information related to activity data, emission factors and other explanatory variables. The underlying information is organized by (sub)source category, by country or region, or as gridded maps, for a number of sources by season. Databases describe anthropogenic source categories such as fossil fuel production and combustion, industrial production, agricultural practices, waste handling, and land use-related activities.

MECCA (Module Efficiently Calculating the Chemistry of the Atmosphere) chemistry model, developed at Max Planck Institute for Chemistry (Mainz, Germany) was coupled to ECHAM5 global circulation model through MESSy interface. The current mechanism of MECCA consists of three contributions: (1) tropospheric chemistry adapted from von Kuhlmann *et al.* (2003); (2) the chemical mechanism for the stratosphere adapted from Steil *et al.* (1998); and (3) tropospheric halogen and sulfur chemistry by von Glasow *et al.* (2003). In addition to the gas-phase chemistry, the submodule MECCA-MBL provides the possibility of calculating chemical reactions in aerosols.

6.2.2 Backtrajectory Analysis

In order to have a detailed picture of the possible origin of air masses over the northeastern Iberian Peninsula, backtrajectory analysis by means of HYSPLIT trajectory model (Draxler *et al.*, 1998) was undergone for the episode here studied (13-16 August, 2000) using MM5 meteorological model outputs. Simulations were performed in four nested domains (Figure 6.1), which essentially covered Europe (Domain 1, D1), the Iberian Peninsula (Domain 2, D2), the northeastern Iberian Peninsula (Domain 3, D3) and the Catalonia area (Domain 4, D4). D1 is formed by 35 x 50 grid points in the horizontal with 72-km grid-point spacing; D2, 61 x 49 24-km cells; D3, 93 x 93 6-km cells; and D4, 151 x 151 2-km cells.

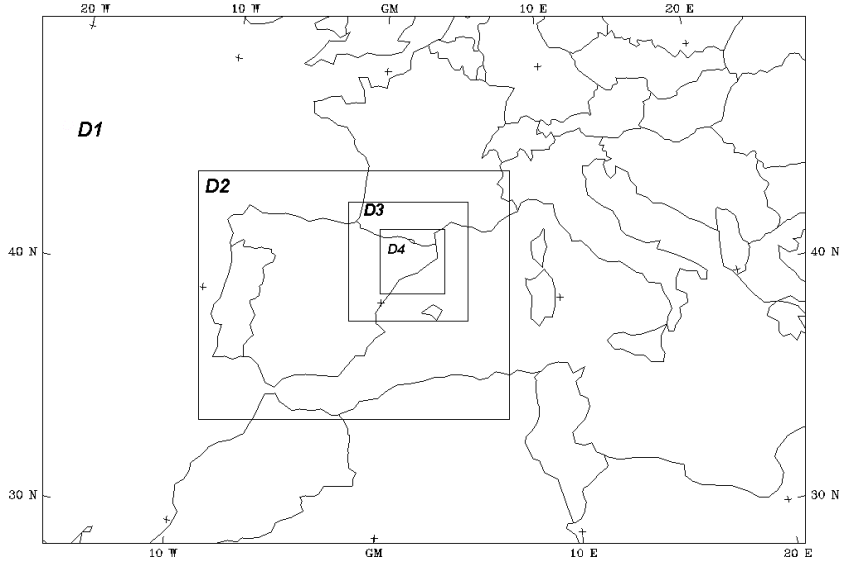

Figure 6.1. Four-nested domain configuration for backtrajectory analysis. D1: 35x50 72-km cells. D2: 61x49 24-km cells. D3: 93x93 6-km cells. D4: 151x151 2-km cells.

6.3 Evaluation of ECHAM5/MESSy and MM5-EMICAT2000-CMAQ

Air quality stations hourly data averaged over the domain of study were used in order to evaluate the performance of both ECHAM5/MESSy and MM5-EMICAT2000-CMAQ when forecasting ground-level O_3, CO and NO_x over the episode of 13-16 August, 2000. Hourly measures of ambient pollutants were provided by 48 air quality surface stations in northeastern Spain, which belong to the Environmental Department of the Catalonia Government (Spain).

Despite a surface measurement represents a value only at a given horizontal location and height, while the concentration predicted by the model represents a volume-averaged value, performance of the models for the different photochemical pollutants was statistically evaluated by comparing the first-layer simulations results and the values measured in the air quality stations of the domain under study. Statistic parameters are shown in Table 6.1.

The vertical evaluation of air quality models is not a straightforward task since of the non-availability of measurements. A possible approach is through the use of LIDAR techniques, which provide vertical values for the stratification of pollutants over a certain domain (Duclau *et al.*, 2002). For the episode selected (13-16 August, 2000), Pérez *et al.* (2004) performed measurements using an elastic-backscatter LIDAR on 14 August, 2000, over the city of Barcelona in order to analyze the vertical stratification of pollutants layers. In this section we compare the simulation results with the profiles generated by the LIDAR campaign.

6.3.1 Evaluation of ECHAM5/MESSy and MM5-EMICAT2000-CMAQ with Air Quality Stations Data from the Northeastern Iberian Peninsula

The European Directive 2002/3/EC relating to ozone in ambient air establishes an uncertainty of 50% as the quality objective for modeling assessment methods. This uncertainty is defined as the maximum error of the measured and calculated concentration levels.

Table 6.1. Statistical figures considered in the evaluation of ECHAM5/MESSy and MM5-EMICAT2000-CMAQ*.

Mean Bias (MB)	$\mathrm{MB} = \frac{1}{N}\sum_{1}^{N}(\mathrm{Model}-\mathrm{Obs})$
Mean Normalized Bias Error (MNBE)	$\mathrm{MNBE} = \frac{1}{N}\sum_{1}^{N}\left(\frac{(\mathrm{Model}-\mathrm{Obs})}{\mathrm{Obs}}\right)\cdot 100\%$
Mean Fractionalized Bias (MFB)	$\mathrm{MFB} = \frac{1}{N}\sum_{1}^{N}\left(\frac{(\mathrm{Model}-\mathrm{Obs})}{\left(\frac{\mathrm{Model}+\mathrm{Obs}}{2}\right)}\right)\cdot 100\%$
Mean Absolute Gross Error (MAGE)	$\mathrm{MAGE} = \frac{1}{N}\sum_{1}^{N}\lvert\mathrm{Model}-\mathrm{Obs}\rvert$
Mean Normalized Gross Error (MNGE)	$\mathrm{MNGE} = \frac{1}{N}\sum_{1}^{N}\left(\frac{\lvert\mathrm{Model}-\mathrm{Obs}\rvert}{\mathrm{Obs}}\right)\cdot 100\%$
Normalized Mean Error (NME)	$\mathrm{NME} = \frac{\sum_{1}^{N}\lvert\mathrm{Model}-\mathrm{Obs}\rvert}{\sum_{1}^{N}\mathrm{Obs}}\cdot 100\%$
Normalized Mean Bias (NMB)	$\mathrm{NMB} = \frac{\sum_{1}^{N}(\mathrm{Model}-\mathrm{Obs})}{\sum_{1}^{N}(\mathrm{Obs})}\cdot 100\%$
Root Mean Square Error (RMSE)	$\mathrm{RMSE} = \sqrt{\frac{1}{N}\sum_{1}^{N}(\mathrm{Model}-\mathrm{Obs})^2}$
Unpaired Peak Accuracy (UPA)	$\mathrm{UPA} = \frac{\mathrm{Model}_{max}-\mathrm{Obs}_{max}}{\mathrm{Obs}_{max}}\cdot 100\%$

*Model: modeled (data obtained from simulations)
Obs: observations (ambient data)
N: number of observations

In addition, the US Environmental Protection Agency has developed guidelines (US EPA, 1991) for a minimum set of statistical measures to be used for these evaluations where monitoring data are sufficiently dense, that are summarized in Chapter 5 of this Dissertation. Those statistical figures considered are the mean normalized bias error (MNBE); the mean normalized gross error for concentrations above a prescribed threshold (MNGE), and the unpaired peak prediction accuracy (UPA).

Table 6.2 collects the results of statistical analyses. Although there is no criterion set forth for a satisfactory model performance, US EPA (1991) suggested values of ±10–15% for MNBE, ±15–20% for the UPA and 30–35% for the MNGE to be met by modeling simulations of O_3 have been considered for regulatory applications. In addition, results for the evaluation of ECHAM5/MESSy and MM5-EMICAT2000-CMAQ in the location of several air quality stations is shown in Figure 6.2 for urban (Barcelona and Vic), industrial (Alcover and Mataró) and background (Agullana and Begur) environments.

Table 6.2. Standards to be met by photochemical models and the results obtained for ECHAM5/MESSy and MM5-EMICAT2000-CMAQ during the episode of 13-16 August, 2000.

		Ozone							
	EPA Goal	***13 August, 2000***		***14 August, 2000***		***15 August, 2000***		***16 August, 2000***	
Observed peak (μg m^{-3})		**157**		**177**		**189**		**171**	
		ECHAM5	**CMAQ**	**ECHAM5**	**CMAQ**	**ECHAM5**	**CMAQ**	**ECHAM5**	**CMAQ**
Modeled peak (μg m^{-3})		**137**	**189**	**151**	**170**	**159**	**167**	**163**	**180**
UPA (%)	<±20	-12.7	14.4	-14.7	-3.8	-15.9	-11.7	-4.7	5.2
MNBE (%)	<±15	12.4	-2.1	13.1	-11.0	14.3	-10.3	15.8	-5.6
MNGE (%)	<35	19.2	16.8	27.6	19.8	28.6	21.7	31.3	26.7

The objective set in the Directive 2002/3/EC (deviation of 50% for the 1-hr averages during daytime) is achieved for the whole period of study for both ECHAM5/MESSy and MM5-EMICAT2000-CMAQ. The modeled episode peak (189 μg m^{-3}) is well captured by both models (163 μg m^{-3} and 188 μg m^{-3} in the case of ECHAM5/MESSy and CMAQ, respectively). The unpaired peak accuracy is negative during the simulated episode when considering ECHAM5/MESSy outputs; this underprediction ranges from -16% to -5%. Peak accuracy is overestimated by CMAQ on the first and last day of simulations (14.4% and 5.2%, respectively) and underestimated on the central days of the episode (–3.8% and –11.7%). Both models, despite considering different approaches and resolutions, met the objective of ±20% set by US EPA for UPA; and hence, they are accurate tools in order to forecast the ozone peak levels.

The O_3 bias of ECHAM5/MESSy is positive on each day of the simulation, progressively increasing from 12.4% until 15.8% on the last day of the episode. This positive value may the due to an excessive accumulation of O_3 during this low-pressure gradient situation or an underestimation of the drainage flows over the region. On the contrary, MM5-EMICAT2000-CMAQ underpredicts average values, showing values of MNBE that are negative on each day, ranging from –2.1% on the first day of simulation until –11.0% on 14 August, 2000. This negative bias may suggest that the O_3-production chemistry may not be sufficiently reactive in CMAQ. US EPA goals of ±15% are both achieved by MM5-EMICAT2000-CMAQ and ECHAM5/MESSy; but the latter presents higher positive values of bias indicating a slight overestimation of mean values.

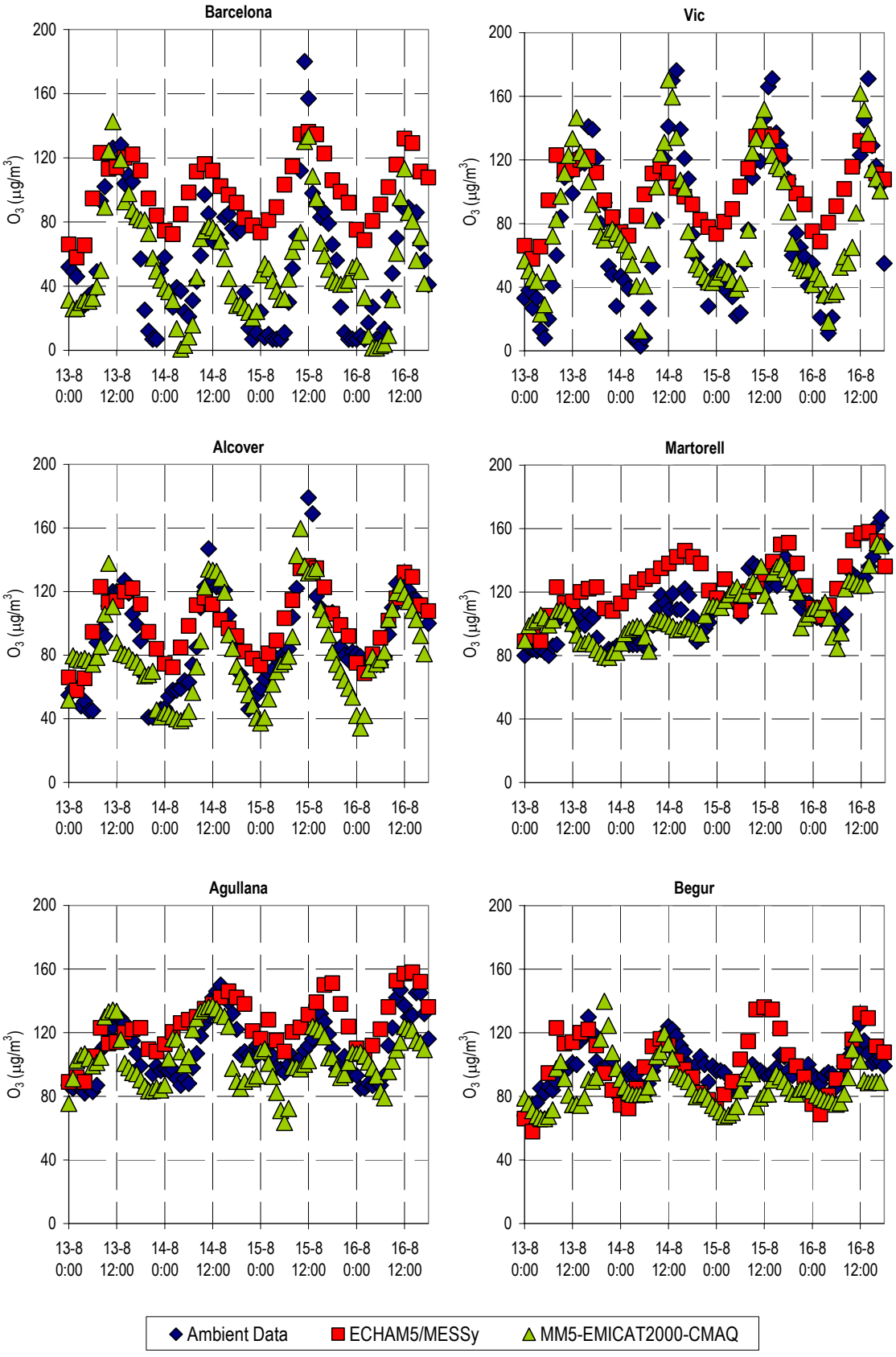

Figure 6.2. Ozone evaluation of ECHAM5/MESSy (red squares) and CMAQ (green triangles) with several air quality stations data (blue diamonds) in the domain of the northeastern Iberian Peninsula: urban (Barcelona and Vic), industrial (Alcover and Mataró) and background (Agullana and Begur).

The mean normalized gross error increases from 13 August until 16 August, 2000 in simulations with both models (19% to 31% for ECHAM5/MESSy and 17% to 27% for CMAQ). This increment may be due to deviations in meteorological predictions that enlarge with the time of simulation (Jiménez *et al.*, 2004). However, the MNGE derived from the results achieve the EPA goals for a discrete evaluation on all episode days for both models (<35%).

Table 6.3 indicates the results of the evaluation of ECHAM5/MESSy and MM5-EMICAT2000-CMAQ with different statistical parameters for ozone, carbon monoxide and nitrogen oxides against ambient data from 48 air quality stations located in the northeastern Iberian Peninsula. Evaluation against 1649 measurements is performed in the case of ozone. Results for O_3 show a correlation of 0.62 and 0.74 for ECHAM5/MESSy and MM5-EMICAT2000-CMAQ, correspondingly. The mean bias (20.0 $\mu g\ m^{-3}$ and 0.5 $\mu g\ m^{-3}$ for ECHAM5/MESSy and CMAQ) indicates a tendency to overprediction of values that is more stressed in the global circulation model. The root mean square error is also lower for the regional model CMAQ (12.7 $\mu g\ m^{-3}$) than in the case of the global circulation model (37.2 $\mu g\ m^{-3}$). Hence, coarser grid smoothens the concentration of ozone respect to finer grids, overestimating minimum values and underestimating maximum values (Jang *et al.*, 1995; Jiménez *et al.*, 2004), and this is clearly observed in the presented simulations.

Simulations for CO and NO_x tend to show much larger bias and error than the similar statistics of ozone for the same simulation. As noted by Russell and Dennis (2000), currently air quality models show a pervasive tendency towards underprediction of precursors. Despite there are no references in the goals to be achieved in the evaluation of O_3 precursors predicted by air quality models, results with bias between -20% and -50% are accepted (Russell and Dennis, 2000). In the case of CO, the correlation coefficient between the observed and predicted carbon monoxide concentrations for the 907 observation values during this episode is 0.34 for ECHAM5/MESSy and 0.57 for CMAQ, and hence correlating worse than ozone in the domain of study. The mean bias is -104.2 $\mu g\ m^{-3}$ and -102.3 $\mu g\ m^{-3}$, respectively, for ECHAM5/MESSy and CMAQ. The root mean square error is 285.8 $\mu g\ m^{-3}$ for ECHAM5/MESSy and 242.9 $\mu g\ m^{-3}$ for CMAQ. In the case of NO_x, Both ECHAM5/MESSy and CMAQ behave between these limits, with results of -20% and -9%, respectively, if the normalized bias is considered. A tendency towards the smoothening of NO_x values (underprediction of peak values; overprediction of minimum and average concentrations) is exhibited in ECHAM5/MESSy evaluation, and this is also observed in the coefficient of variation. Despite this differences, the performance of both models respect NO_x concentrations follows similar pattern for statistics shown in Table 6.3. The correlation coefficient between the observed and predicted nitrogen oxides concentrations at 48 stations is 0.56 for ECHAM5/MESSy and 0.75 for CMAQ, while the mean bias is -14.5 $\mu g\ m^{-3}$ and -5.5 $\mu g\ m^{-3}$, in that order. The root mean square error is 41.1 $\mu g\ m^{-3}$ and 35.4 $\mu g\ m^{-3}$ for the global and the regional model.

Summarizing, the simulation with the coarser grid (ECHAM5/MESSy) underestimates maximum ozone, carbon monoxide and nitrogen oxides levels with regards to the fine grid of MM5-EMICAT2000-CMAQ, since the grid resolution highly influences the formation and loss processes of pollutants, (especially photochemistry and vertical transport). Hence, the average volume defined by the model's horizontal grid spacing must be sufficiently small to allow the air quality to be reproduced accurately (Jiménez *et al.*, 2004).

Table 6.3. Results of the evaluation of O_3 and CO with ECHAM5/MESSy and MM5-EMICAT2000-CMAQ models against data from 48 air quality stations located in the northeastern Iberian Peninsula*.

Ozone (O_3)						
	Observations	***ECHAM5***	***CMAQ***		***ECHAM5***	***CMAQ***
Mean ($\mu g\ m^{-3}$)	**63.7**	**88.2**	**64.7**	*n*	**1649**	
SD ($\mu g\ m^{-3}$)	**37.4**	**16.7**	**31.5**	*R*	**0.62**	**0.74**
CV (%)	**58.7%**	**18.9%**	**48.6%**	*MB ($\mu g\ m^{-3}$)*	**20.0**	**0.5**
Max ($\mu g\ m^{-3}$)	**189.0**	**163.0**	**188.0**	*MNBE (%)*	**46.8%**	**37.9%**
95th ($\mu g\ m^{-3}$)	**123.0**	**157.0**	**113.9**	*MFB (%)*	**21.1%**	**5.6%**
75th ($\mu g\ m^{-3}$)	**92.0**	**118.3**	**83.5**	*MAGE ($\mu g\ m^{-3}$)*	**25.9**	**9.8**
50th ($\mu g\ m^{-3}$)	**61.0**	**86.7**	**66.9**	*MNGE (%)*	**70.9%**	**64.1%**
25th ($\mu g\ m^{-3}$)	**33.0**	**70.3**	**43.0**	*NME (%)*	**42.2%**	**30.8%**
5th ($\mu g\ m^{-3}$)	**9.2**	**52.6**	**10.0**	*NMB (%)*	**28.0%**	**1.7%**
Min ($\mu g\ m^{-3}$)	**1.0**	**49.4**	**0.1**	*RMSE ($\mu g\ m^{-3}$)*	**37.2**	**12.7**
Carbon Monoxide (CO)						
	Observations	***ECHAM5***	***CMAQ***		***ECHAM5***	***CMAQ***
Mean ($\mu g\ m^{-3}$)	**908.1**	**788.4**	**826.5**	*n*	**907**	
SD ($\mu g\ m^{-3}$)	**325.0**	**265.3**	**287.2**	*R*	**0.34**	**0.57**
CV (%)	**35.8%**	**31.6%**	**34.8%**	*MB ($\mu g\ m^{-3}$)*	**-104.2**	**-102.3**
Max ($\mu g\ m^{-3}$)	**2000.0**	**1610.0**	**1832.3**	*MNBE (%)*	**-3.1%**	**-8.0%**
95th ($\mu g\ m^{-3}$)	**1450.0**	**1275.0**	**1584.3**	*MFB (%)*	**-12.2%**	**-13.1%**
75th ($\mu g\ m^{-3}$)	**1100.0**	**1000.0**	**1010.1**	*MAGE ($\mu g\ m^{-3}$)*	**311.6**	**188.4**
50th ($\mu g\ m^{-3}$)	**900.0**	**850.0**	**797.1**	*MNGE (%)*	**35.1%**	**18.6%**
25th ($\mu g\ m^{-3}$)	**650.0**	**510.0**	**556.6**	*NME (%)*	**35.9%**	**35.1%**
5th ($\mu g\ m^{-3}$)	**450.0**	**480.0**	**379.3**	*NMB (%)*	**-13.2%**	**-22.8%**
Min ($\mu g\ m^{-3}$)	**300.0**	**475.0**	**271.0**	*RMSE ($\mu g\ m^{-3}$)*	**285.8**	**242.9**
Nitrogen Oxides (NO_x)						
	Observations	***ECHAM5***	***CMAQ***		***ECHAM5***	***CMAQ***
Mean ($\mu g\ m^{-3}$)	**59.5**	**66.6**	**54.0**	*n*	**907**	
SD ($\mu g\ m^{-3}$)	**45.5**	**43.9**	**51.7**	*R*	**0.56**	**0.75**
CV (%)	**76.4%**	**66.0%**	**95.6%**	*MB ($\mu g\ m^{-3}$)*	**-14.5**	**-5.5**
Max ($\mu g\ m^{-3}$)	**279.3**	**190.0**	**283.0**	*MNBE (%)*	**-10.5%**	**-6.1%**
95th ($\mu g\ m^{-3}$)	**149.0**	**123.0**	**164.7**	*MFB (%)*	**-26.3%**	**-23.8%**
75th ($\mu g\ m^{-3}$)	**79.5**	**90.0**	**73.3**	*MAGE ($\mu g\ m^{-3}$)*	**31.9**	**26.3**
50th ($\mu g\ m^{-3}$)	**47.6**	**72.0**	**37.5**	*MNGE (%)*	**43.0%**	**62.7%**
25th ($\mu g\ m^{-3}$)	**27.7**	**25.0**	**16.8**	*NME (%)*	**44.3%**	**44.4%**
5th ($\mu g\ m^{-3}$)	**9.8**	**16.0**	**3.7**	*NMB (%)*	**-20.2%**	**-9.2%**
Min ($\mu g\ m^{-3}$)	**2.8**	**15.0**	**1.2**	*RMSE ($\mu g\ m^{-3}$)*	**41.1**	**35.4**

* As a difference from US EPA statistics indicated in Table 6.2, no threshold has been applied.

The large averaging volumes used by regional models are feared to lead to unacceptable errors for many species that are formed via nonlinear chemical reactions (e.g. ozone and its precursors), particularly in areas with significant chemical gradients, such as cities (Russell and

Dennis, 2000). Meanwhile having a finer grid is important for addressing ozone processes in urban and industrial areas, rural areas allow larger grids to capture the nonlinearity of the ozone process. However, simulation of the Western Mediterranean Basin and the northeastern Iberian Peninsula combining ECHAM5/MESSy and MM5-EMICAT2000-CMAQ is a reliable methodology that provides the possibility of describing the dynamics and processes of pollutants on a regional and global scale, and this is the basis for the description of different scale circulations.

6.3.2 Vertical Evaluation of ECHAM5/MESSy and MM5-EMICAT2000-CMAQ Profiles

The vertical profiles obtained over the city of Barcelona (41.361N – 2.181E) with the global model ECHAM5/MESSy and the regional model MM5-EMICAT2000-CMAQ are shown in Figure 6.3. The first approaches to the results indicate that profiles are comparable; and both models simulate a realistic ozone gradient between the boundary layer and the free troposphere with differences between both models that focus principally in the definition of the planetary boundary layer.

The vertical resolution of CMAQ is finer in the lower troposphere and shows a more detailed layering of pollutants within the mixing layer. Hence, ECHAM5/MESSy provides values of concentrations between 500m and 1000m that are slightly higher than CMAQ model. A relatively coarse vertical resolution of the lower troposphere leads to artificial vertical exchange between the boundary layer and the free troposphere; this enhances NO_x venting from the planetary boundary layer (Wang *et al.*, 1998) so that free tropospheric O_3 formation may be overestimated in the models with coarse resolutions.

Considering the results of LIDAR profiles shown in Pérez *et al.* (2004), the low troposphere showed multiple layers above the mixing layer at 700-800m between 1400UTC and 1500UTC. Simulations with MM5-EMICAT2000-CMAQ capture this feature (both for O_3 and CO); this layer is due to re-circulations over coastal and pre-coastal mountain ranges. However, the coarser resolution of ECHAM5/MESSy (both vertically and horizontally) is not able to capture this feature of the flow (Figure 6.3). According to Roelofs *et al.* (2003), the horizontal and vertical resolutions included in ECHAM5/MESSy model may be too coarse to accurately represent some of the relevant boundary conditions in detail (e.g., height and stability of the land-sea breeze circulations).

Another layer was depicted with LIDAR measurements between 1600-2300m, and this is observable both with the regional and the global climate-chemistry model, especially in the case of photochemical O_3, with concentrations of 105 $\mu g\ m^{-3}$. This layer is formed by the return flow of the breeze and forcings caused by nearby coastal and pre-coastal mountain ranges. It is remarkable that this layer is also observed for CO simulations, depicting a layer with low concentrations of this pollutant (260 $\mu g\ m^{-3}$), but rich in ozone and aerosols. Last, a layer with a peninsular origin was observed upper 3500m with the LIDAR measurements. Simulations with

both models indicate a layer with a relatively high content of CO (over 300 μg m^{-3}) between 2600 and 4000 m. In the case of O_3, the vertical profile of this pollutant due to diffusion processes makes this layer difficult to distinguish from the layer below (1600-2300m) and other possible layers above.

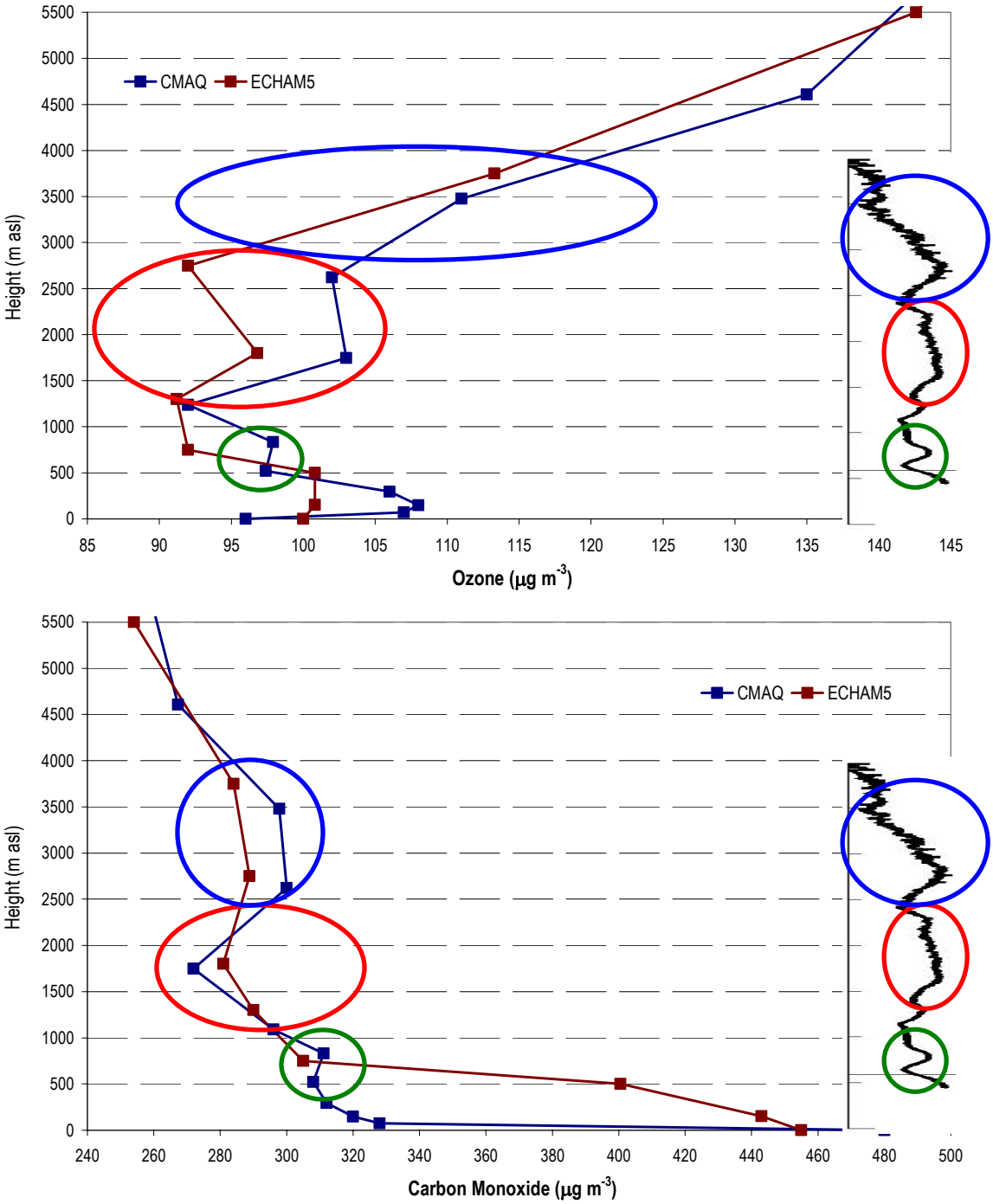

Figure 6.3. Layering of pollutants overt the city of Barcelona, for O_3 (up) and CO (down), on 14 August, 2000, at 1500UTC. Multiple layers appear at 700-800 m (green), 1600-2300m (red) and 2600-4000m (blue). Results from CMAQ (blue), ECHAM5/MESSy (red) and LIDAR profiles (black) by Pérez *et al.* (2004).

6.4 Processes Controlling Ozone Dynamics in the Western Mediterranean Basin and the Northeastern Iberian Peninsula

The episode considered in this work for the analysis of processes over the Western Mediterranean Basin corresponds to 13-16 August, 2000, which is a characteristic situation of photochemical pollution by ozone in during summertime in the WMB. According to Martín-Vide (1984), it can be classified as a low pressure gradient. The day was characterized by a weak synoptic forcing, so that mesoscale phenomena, induced by the particular geography of the region would be dominant. This situation is associated with weak winds in the lower troposphere and high maximum temperatures. A high sea level pressure and almost non-existent surface pressure gradients over the domain characterize this day, with slow northwesterlies aloft. Under this weak synoptic forcing, strong insolation promotes the development of prevailing mesoscale flows associated with the local orography (mountain and valley breezes), while the difference of temperature between the sea and the land enhances the development of sea-land breezes (Barros *et al.*, 2003).

6.4.1 Lower Troposphere: Regional Re-Circulations

In summer, a strong-west surface pressure difference (>20 hPa) is generated between the Azorean high and Asian monsoon low-pressure regimes (see Chapter 2, Figures 2.3 and 2.4). This quasi-permanent weather system causes northerly flows in the lower troposphere over the Mediterranean, feeding into the trade winds further south. The flow is strongest and most persistent in August (Lelieveld *et al.*, 2002). The Azorean anticyclone dominated the Iberian Peninsula during the episode of 13-16 August, 2000, with very low-pressure gradients. In the surface, the anticyclone dorsal of 1020 hPa has penetrated into the western Mediterranean littoral inducing a low-pressure gradient over the whole region. Because of the high-pressure areas over the Mediterranean, a generalized subsidence is observable, allowing the accumulation of pollutants in the area.

The backwards trajectories ending in the boundary layer and the lower troposphere (Figure 6.4) point to a local origin of air masses mainly due to re-circulation processes, which are common in the Western Mediterranean Basin during this kind of synoptic situation (Millán *et al.*, 1992; Millán *et al.*, 1997; Pérez *et al.*, 2004). The backtrajectories at ground level indicate a regional re-circulation over the Mediterranean Sea, meanwhile backtrajectories at 500m account for a coastal origin of air masses from Valencia-Castellón area, with a strong industrial influence. This pattern keeps constant until 2500m.

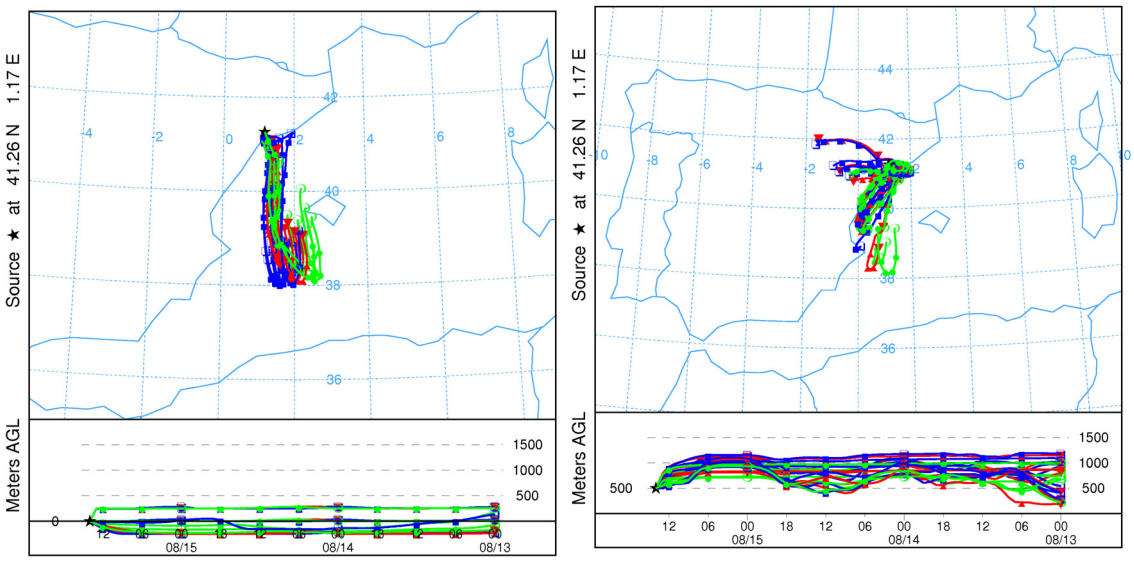

Figure 6.4. Ensemble backtrajectories arriving at ground level (left) and 500m (right) at the domain of the Iberian Peninsula on 15 August, 2000, at 1200UTC. Backtrajectories show a regional origin of air masses, both from the Mediterranean Sea (surface) or Valencia-Castellón coast (500m).

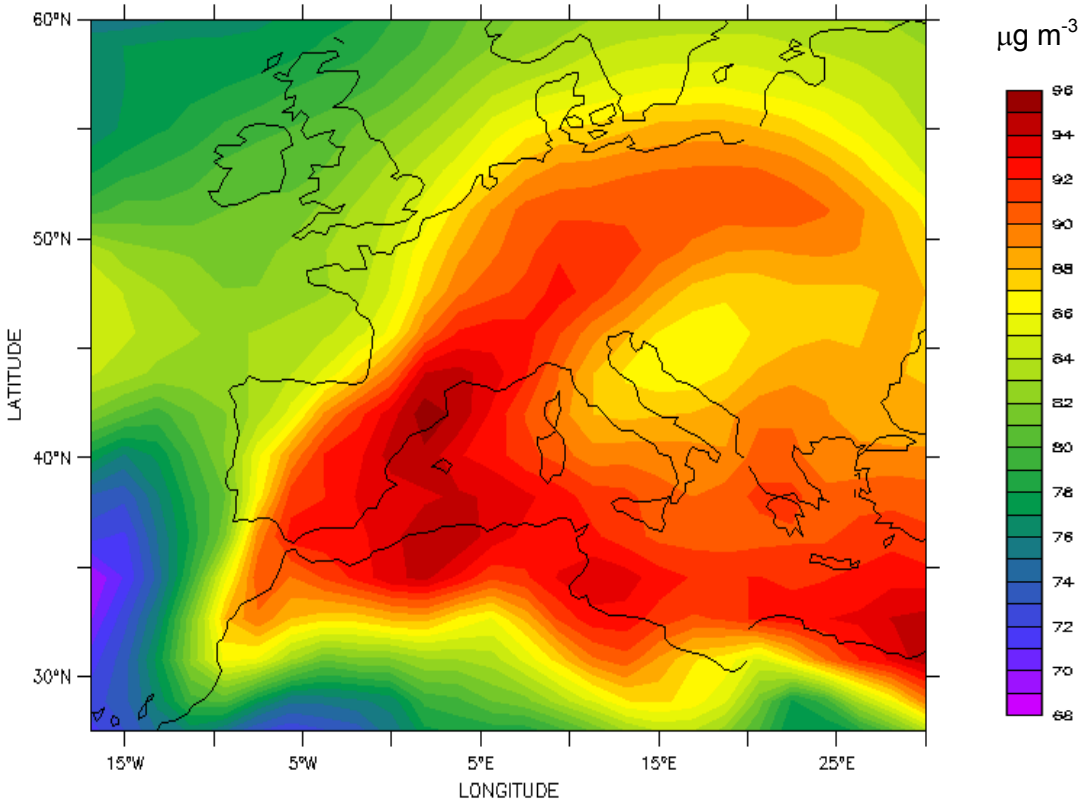

Figure 6.5. Average concentration of O_3 ($\mu g\ m^{-3}$) in the lower troposphere of the Western Mediterranean Basin during the episode of 13-16 August, 2000.

The occurrence of regional re-circulations at low levels represents 45% of the yearly flow transport patterns over the area of study (Jorba *et al.*, 2004) and these situations are associated with local-regional episodes of air pollution in the lower troposphere of the whole Western Mediterranean Basin, which result in high levels of O_3 (Figure 6.5) within the boundary layer (Toll and Baldasano, 2000; Barros *et al.*, 2003).

Therefore, during 13-16 August, 2000, the accumulation of photochemical pollutants is observed in the entire troposphere of the Western Mediterranean Basin under the planetary boundary layer, as indicated for total O_3 amounts in Figure 6.6. Levels of 189 $\mu g\ m^{-3}$ are simulated inland, in Vic (latitude 41.842 N and longitude 2.305 E), downwind the main important emitter area (Barcelona Geographical Area). Therefore, the European Information Threshold of 180 $\mu g\ m^{-3}$ established in Directive 2002/3/EC is exceeded in the area for the considered episode. Similar concentrations are also predicted in the industrial zone of Tarragona.

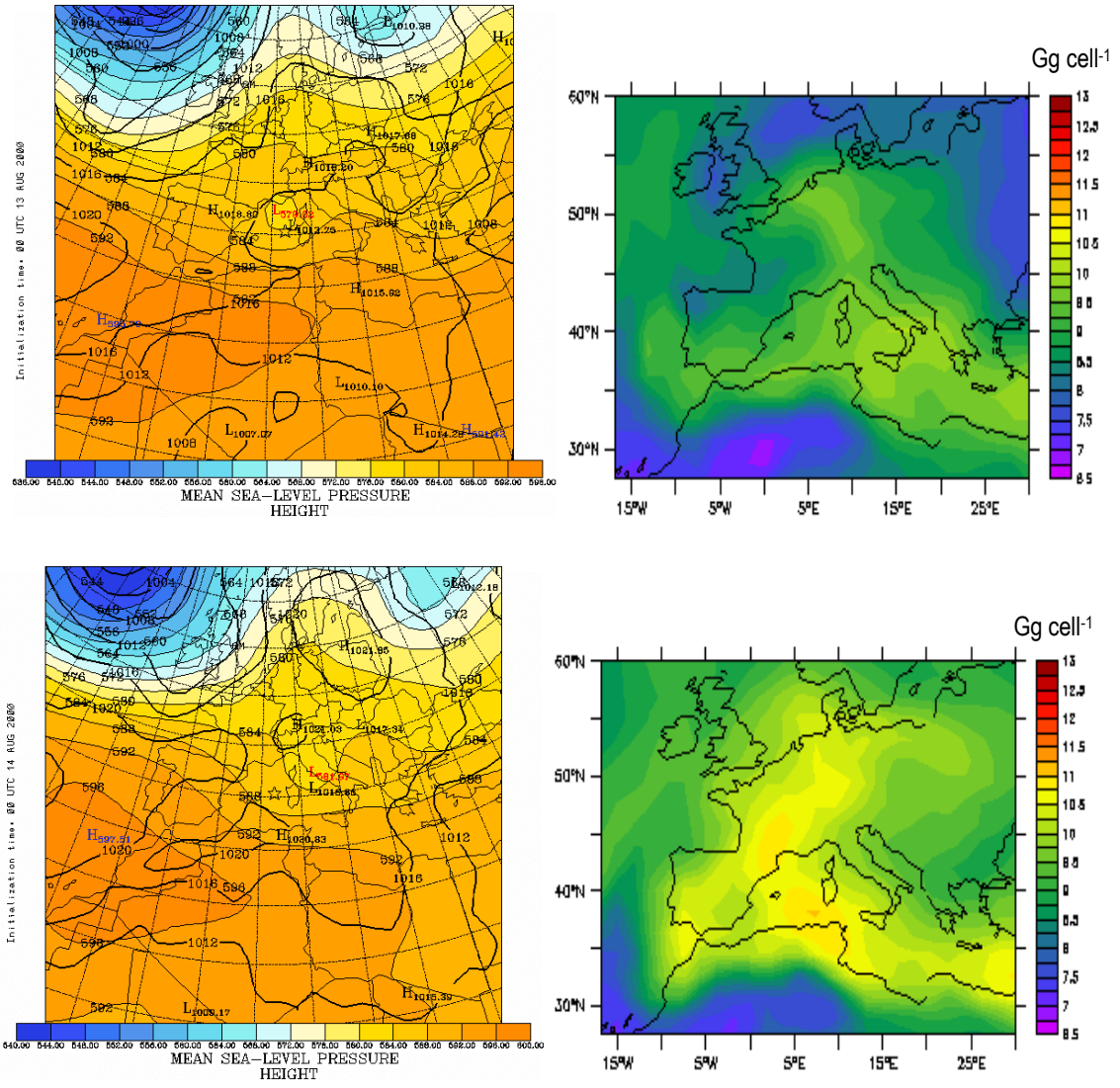

Figure 6.6. Meteorological analysis at surface and 500hPa (left) and accumulation of the tropospheric column of O_3 (Gg $cell^{-1}$) (right) in the Western Mediterranean Basin during the episode of 13 August, 2000 (up) to 16 August, 2000 (down).

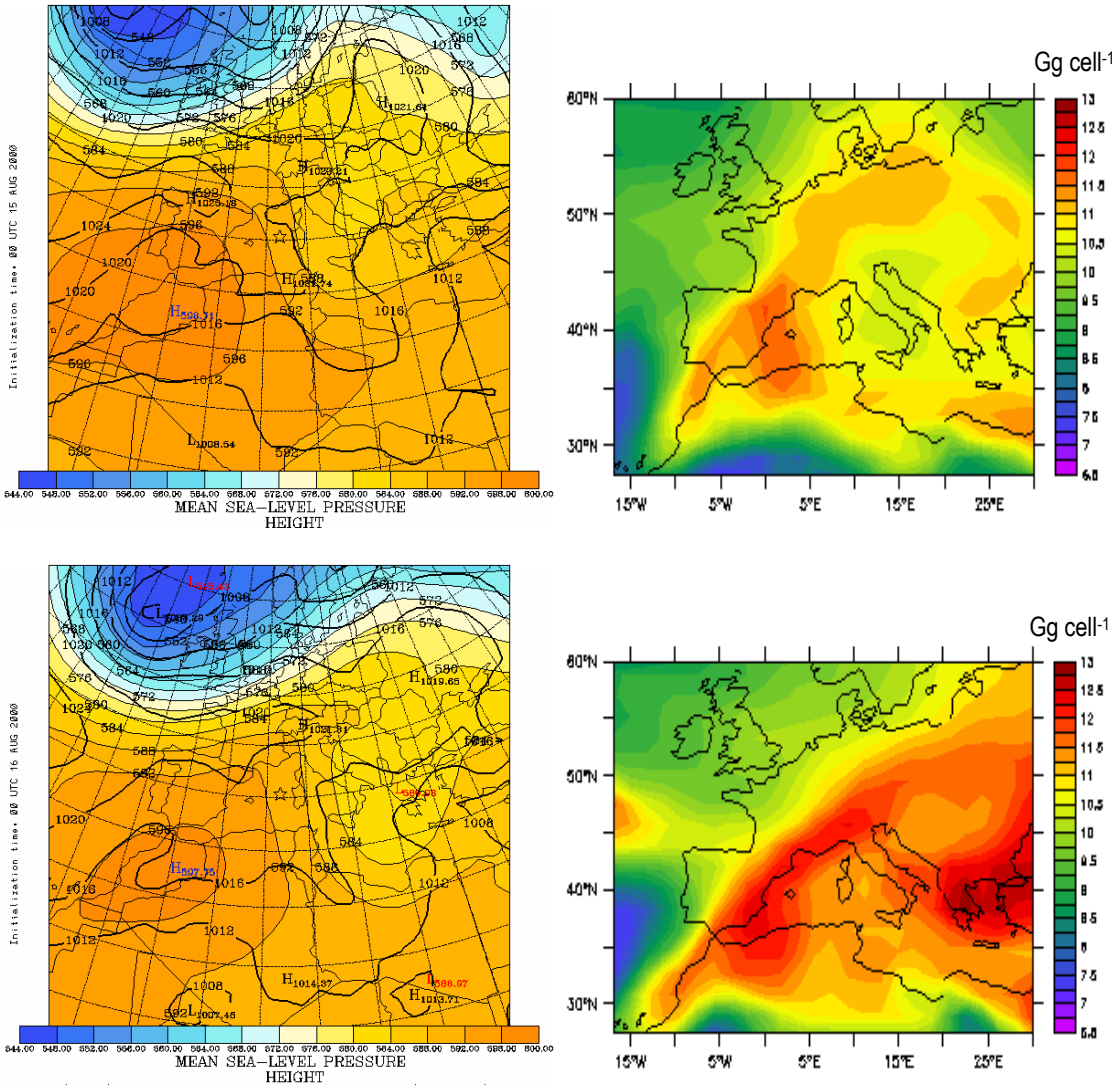

Figure 6.6 (continued). Meteorological analysis at surface and 500hPa (left) and accumulation of the tropospheric column of O_3 (Gg cell^{-1}) (right) in the Western Mediterranean Basin during the episode of 13 August, 2000 (up) to 16 August, 2000 (down).

Figure 6.7 shows the ozone patterns on 14 August, 2000, at 0600UTC. The maintenance of the anticyclonic circulation over the northeastern Iberian Peninsula at this time from the previous day is remarkable. At night, the whole eastern Iberian coast presented down-slope winds over the mountains and general offshore breeze flows. The canalization between the Pyrenees and the Central Massif introduced northwestern flows into the Mediterranean. The offshore flows produce drainage of pollutants towards the coast through the river valleys. As the day advanced, a well developed sea-breeze regime was established along the entire domain with breeze circulation cells up to 2000m height, over the mixing height achieving 800m (Sicard *et al.*, 2003). From 0800UTC, the onshore winds are well developed along the eastern coast, intensifying the anticyclonic circulation and deflecting to the east the flow between the Pyrenees and the Central Massif.

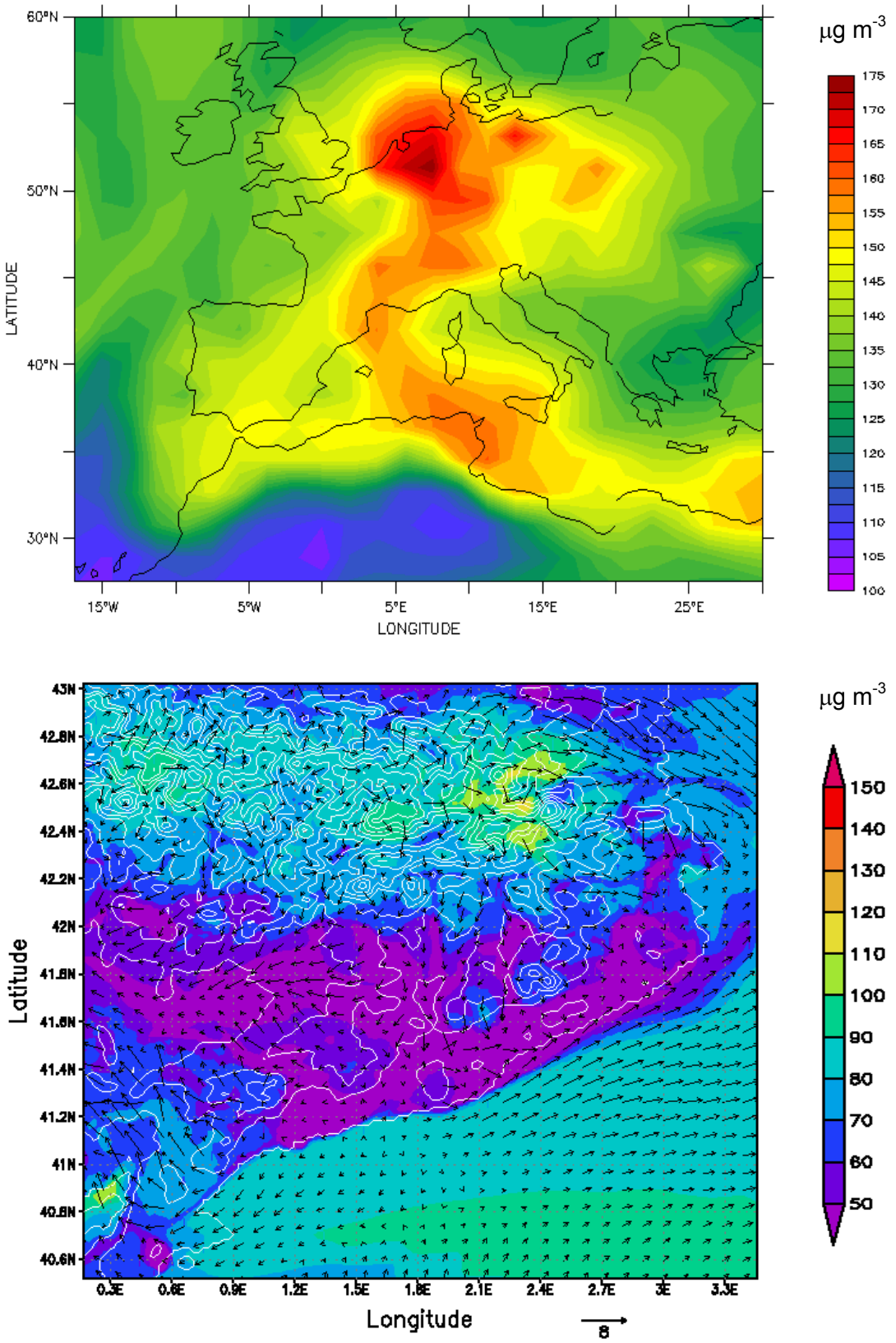

Figure 6.7. Ozone concentrations (μg m^{-3}) simulated with ECHAM5/MESSy model (up) and O_3 concentrations (μg m^{-3}) and wind field vectors at ground-level over the northeastern Iberian Peninsula with MM5-EMICAT2000-CMAQ (down) on 14 August, 2000, at 0600UTC.

At noon, pollutants departing from Barcelona area, as the main emitter zone, and the line coast are transported inland following the breeze front (Figure 6.8), since they arrive at Plana de Vic (70-km downwind Barcelona), where winds calm and allow ozone and its precursors to accumulate, meeting values over the European Information Threshold of 180 $\mu g\ m^{-3}$. At the same time, in the southern domain of the northeastern Iberian Peninsula (industrial area of Tarragona), during the morning, katabatic winds weaken and a clear breeze regime is observed, with the development of anabatic and valley winds. The high ozone concentrations achieved in the southern part of the domain are produced because the intensity of the breeze is not capable to overcome the littoral mountain range and therefore appearing a local maximum downwind the industrial area of Tarragona (Figure 6.9).

Inland the northeastern Iberian Peninsula, in the area of Plana de Vic, the flow is conditioned by the presence of the pre-Pyrenees and the northwesterly wind aloft, allowing the creation of re-circulations that provoke the accumulation of ozone in the area. This pattern keeps constant during the afternoon (Figure 6.10), but the breeze gains intensity and adds to the upslope winds transporting pollutants over the pre-littoral mountain ranges. Around 1900-2000UTC, the photochemical activity ceases, the see-breeze regime loses intensity and winds in the coast weaken (Figure 6.11). Inland, at the east part of the domain, strong south winds are observed, which translates into a transport of ozone that adds to the quenching procedure of photochemical ozone by its reaction with nitrogen monoxide. At night, inland winds calm with the development of a weak land-breeze, with drainages in the valleys and katabatic winds. The dynamics depicted above for photochemical pollutants (ozone, carbon monoxide, nitrogen oxides and volatile organic compounds) are shown for a daily cycle in Figures 6.12 to 6.23.

Another feature of the flows within the low troposphere is the canalization between the Pyrenees and the Central Massif, which introduces Atlantic air masses with a northwesterly origin into the northeastern Iberian Peninsula during the whole episode, as stated by Gangoiti *et al.* (2001). However, from simulations with ECHAM5/MESSy and MM5-EMICAT2000-CMAQ it may be observed that the concentration of photochemical pollutants in these air masses is low, since of its Atlantic origin.

An important characteristic of the entire domain is the presence of re-circulations due to the orographic forcing. The strength of the sea breeze and the complex orography of the eastern Iberian coast produce several vertical injections and layering of pollutants. As the sea breeze front advances inland reaching the mountain ranges, orographic injections occur at different altitudes, with a later return to the coast (Figure 6.24). Mechanical re-circulation of air pollutants occurs at Collserola Mountain (~500m). At noon, the breeze has reached the first mountainous chain, and here it is reinforced by anabatic winds producing upward motions up to 1500-2000m.

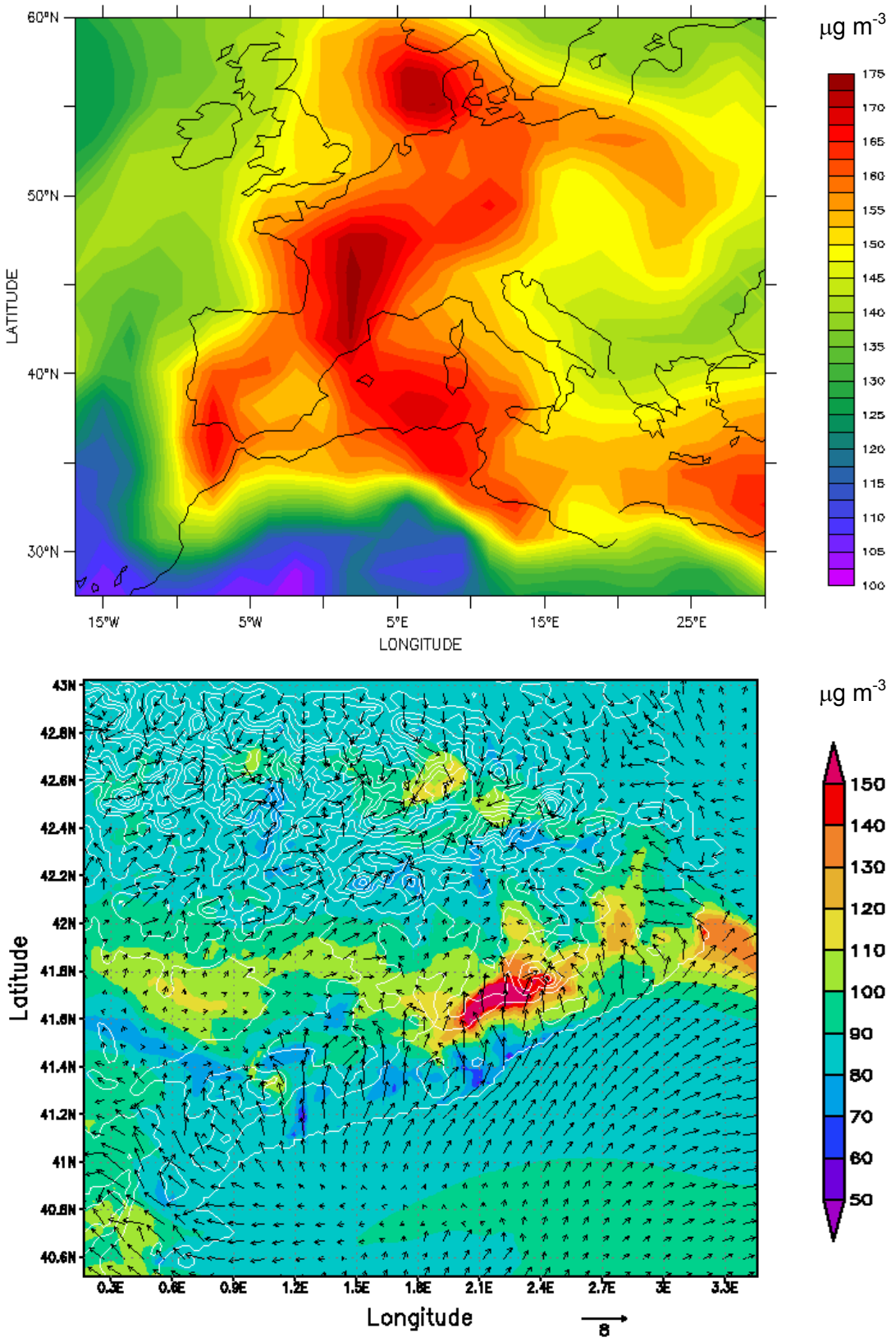

Figure 6.8. Ozone concentrations (µg m^{-3}) simulated with ECHAM5/MESSy model (up) and O_3 concentrations (µg m^{-3}) and wind field vectors at ground-level over the northeastern Iberian Peninsula with MM5-EMICAT2000-CMAQ (down) on 14 August, 2000, at 1200UTC.

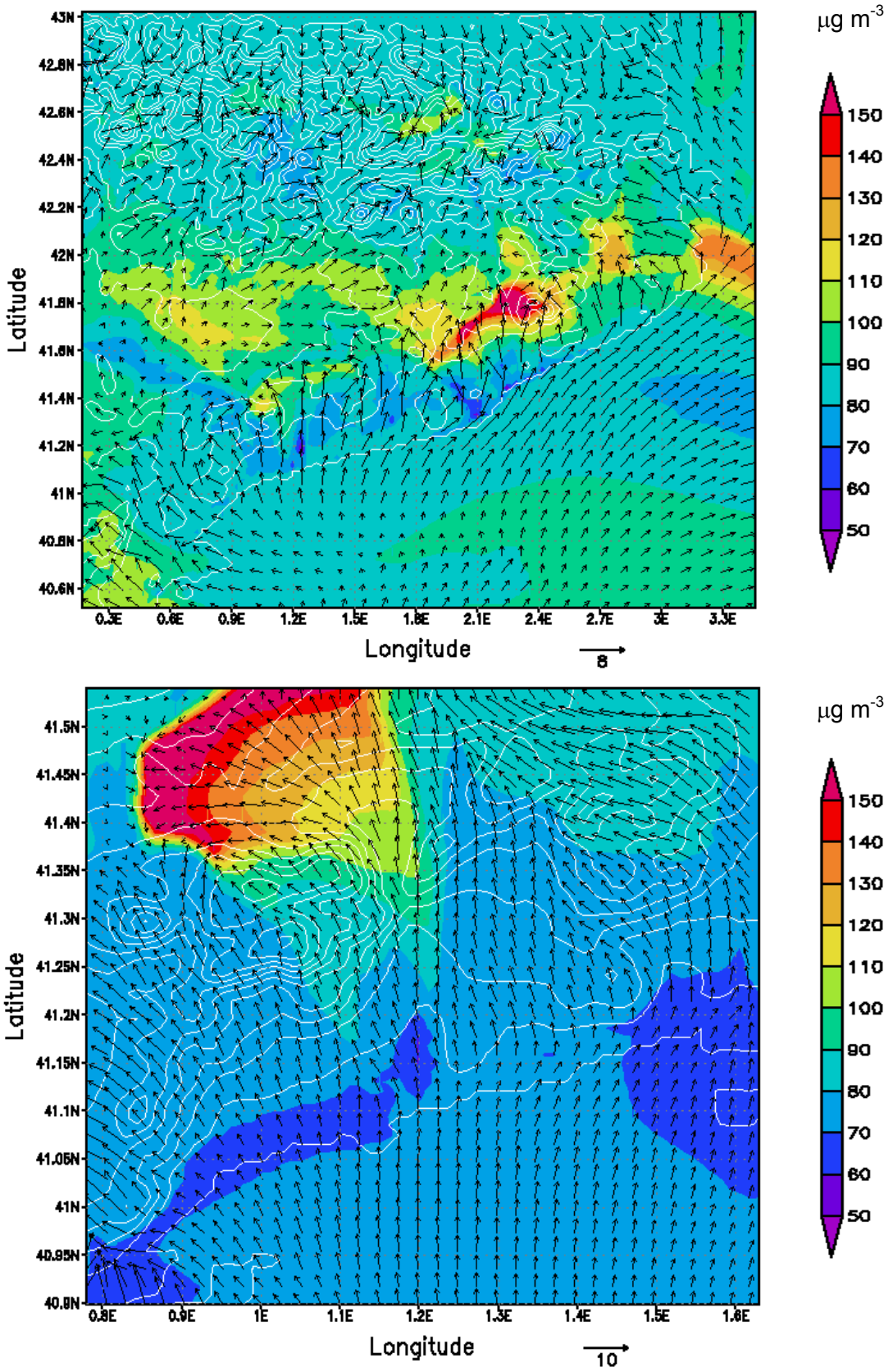

Figure 6.9. Wind field vectors and ozone concentrations (μg m^{-3}) over the northeastern Iberian Peninsula on 14 August, 2000, at 1100UTC, for the whole domain (up) and the industrial area of Tarragona (down).

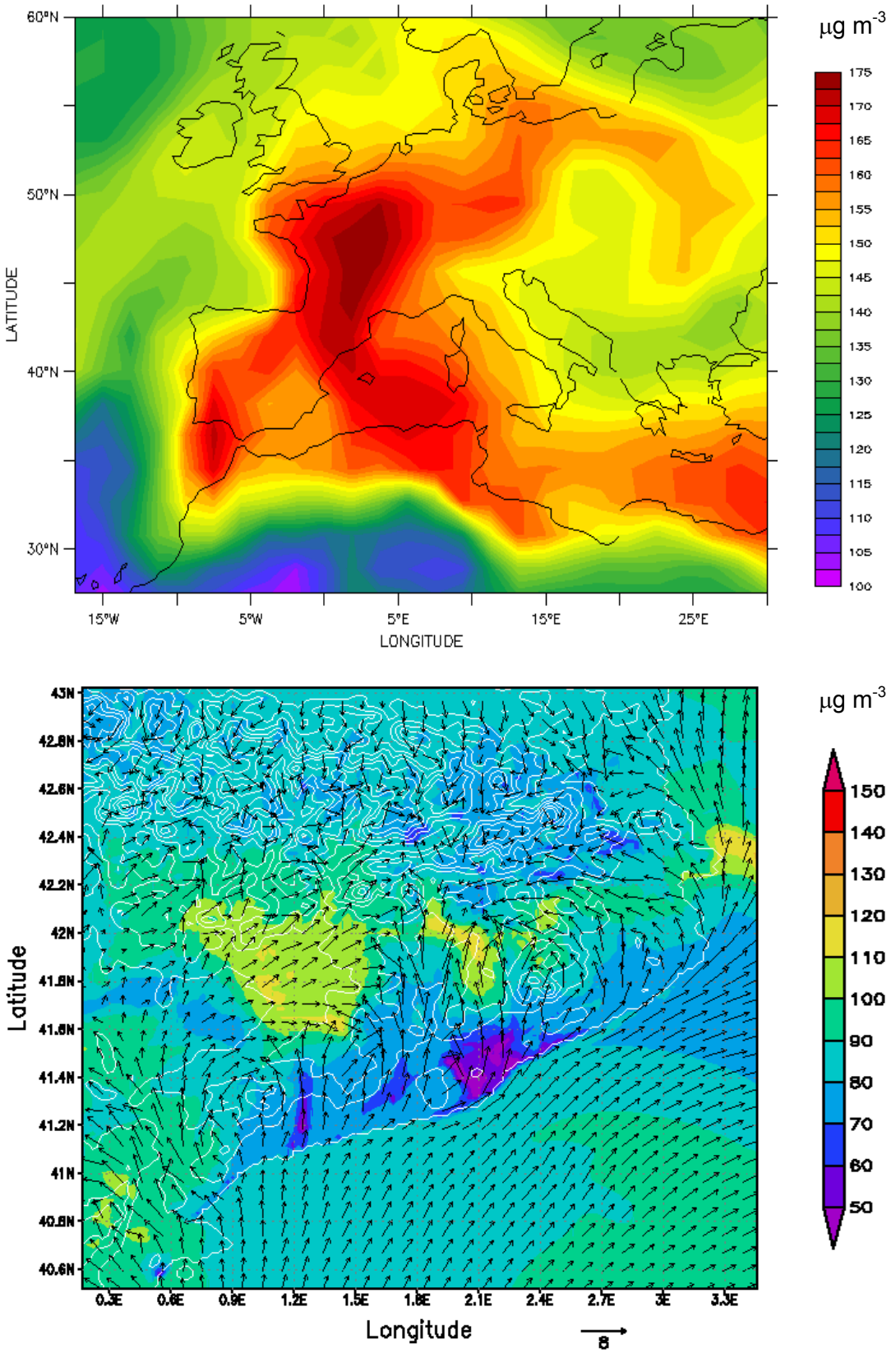

Figure 6.10. Ozone concentrations (μg m^{-3}) simulated with ECHAM5/MESSy model (up) and O_3 concentrations (μg m^{-3}) and wind field vectors at ground-level over the northeastern Iberian Peninsula with MM5-EMICAT2000-CMAQ (down) on 14 August, 2000, at 1600UTC.

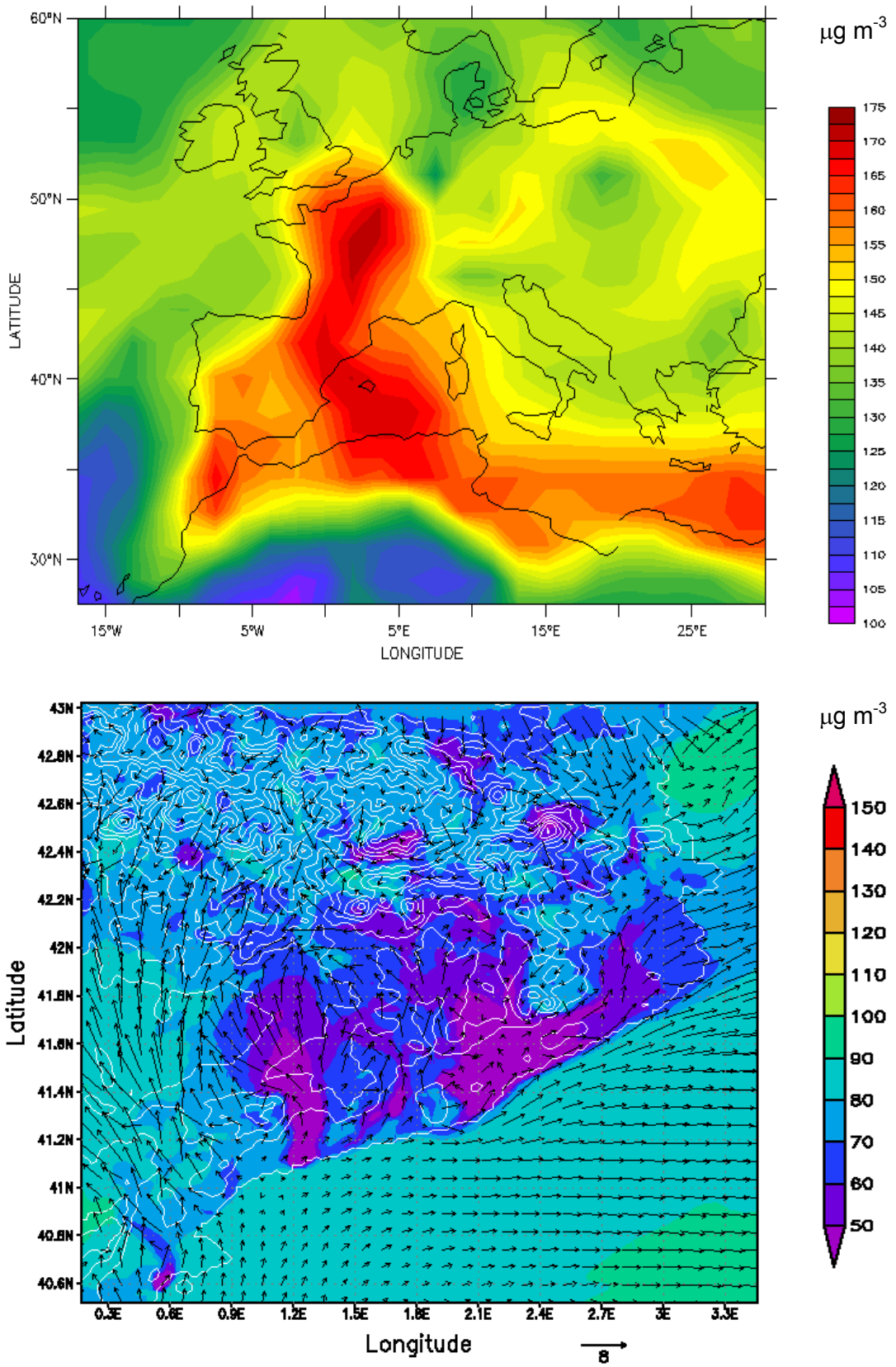

Figure 6.11. Ozone concentrations (μg m^{-3}) simulated with ECHAM5/MESSy model (up) and O_3 concentrations (μg m^{-3}) and wind field vectors at ground-level over the northeastern Iberian Peninsula with MM5-EMICAT2000-CMAQ (down) on 14 August, 2000, at 2000UTC.

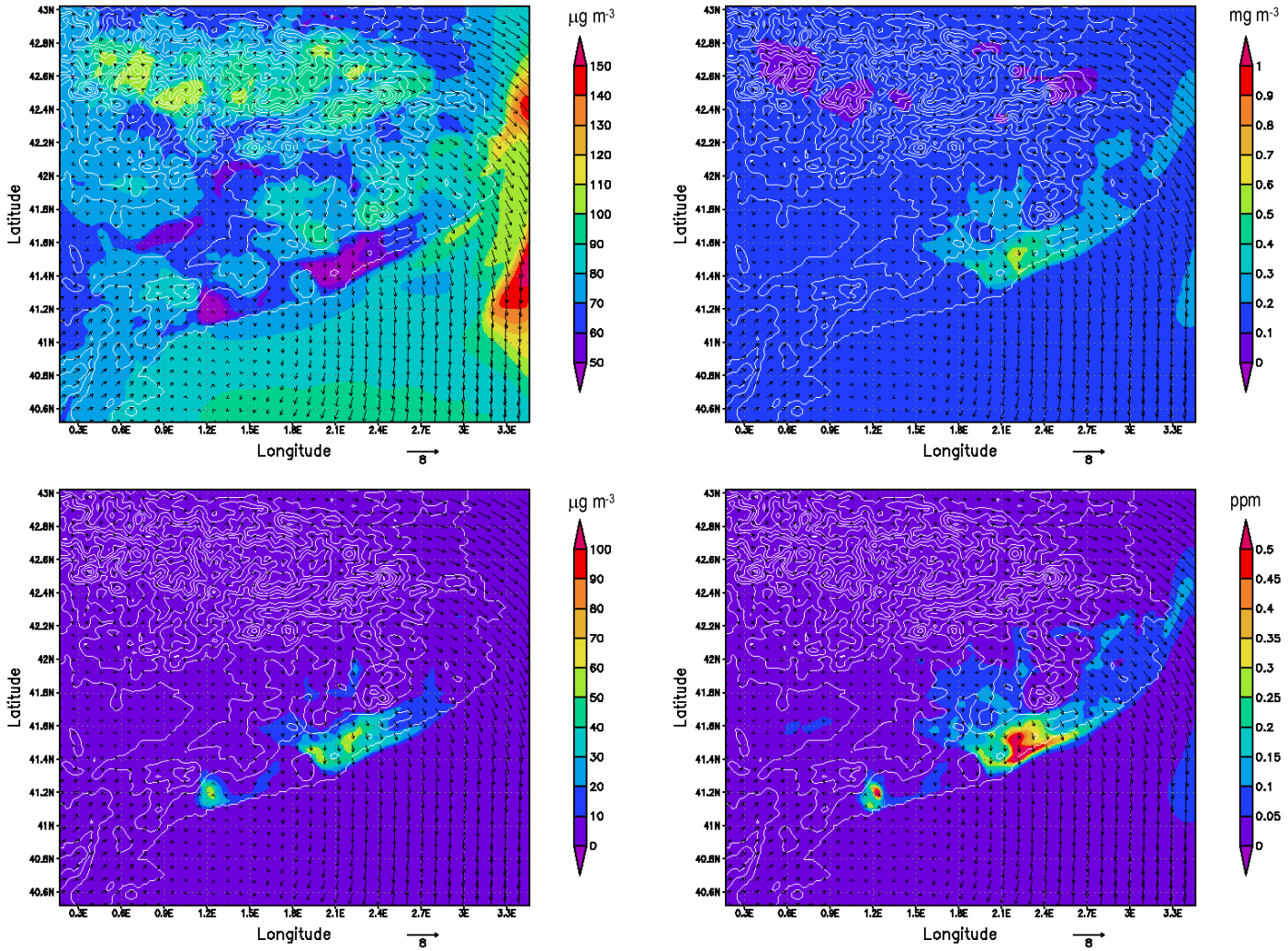

Figure 6.12. Surface concentration of O_3 (µg m^{-3}, up-left); CO (mg m^{-3}, up-right); NO_x (µg m^{-3}, down-left) and VOCs (ppm) at 0000UTC on 14 August, 2000.

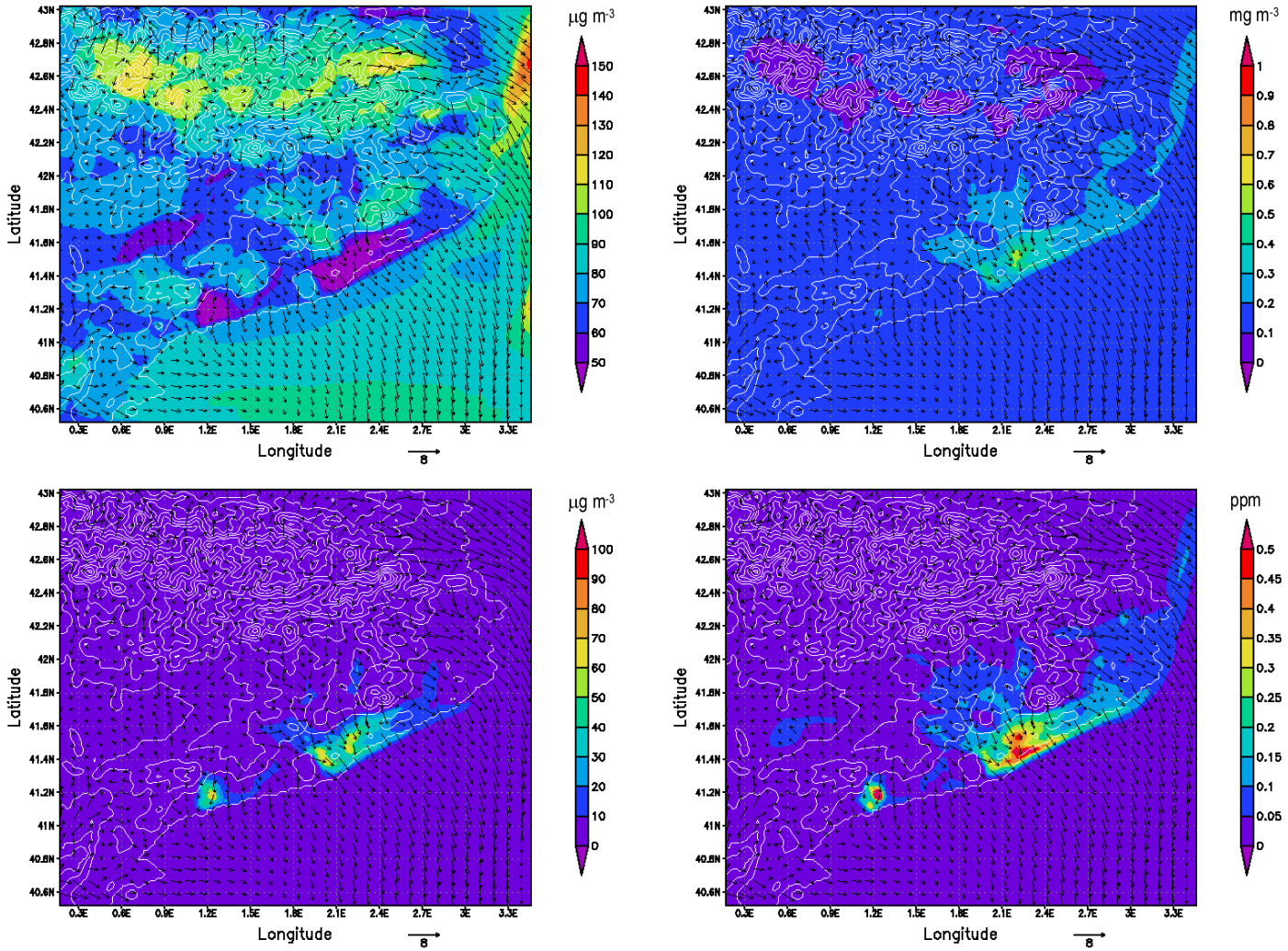

Figure 6.13. Surface concentration of O_3 (μg m^{-3}, up-left); CO (mg m^{-3}, up-right); NO_x (μg m^{-3}, down-left) and VOCs (ppm) at 0200UTC on 14 August, 2000.

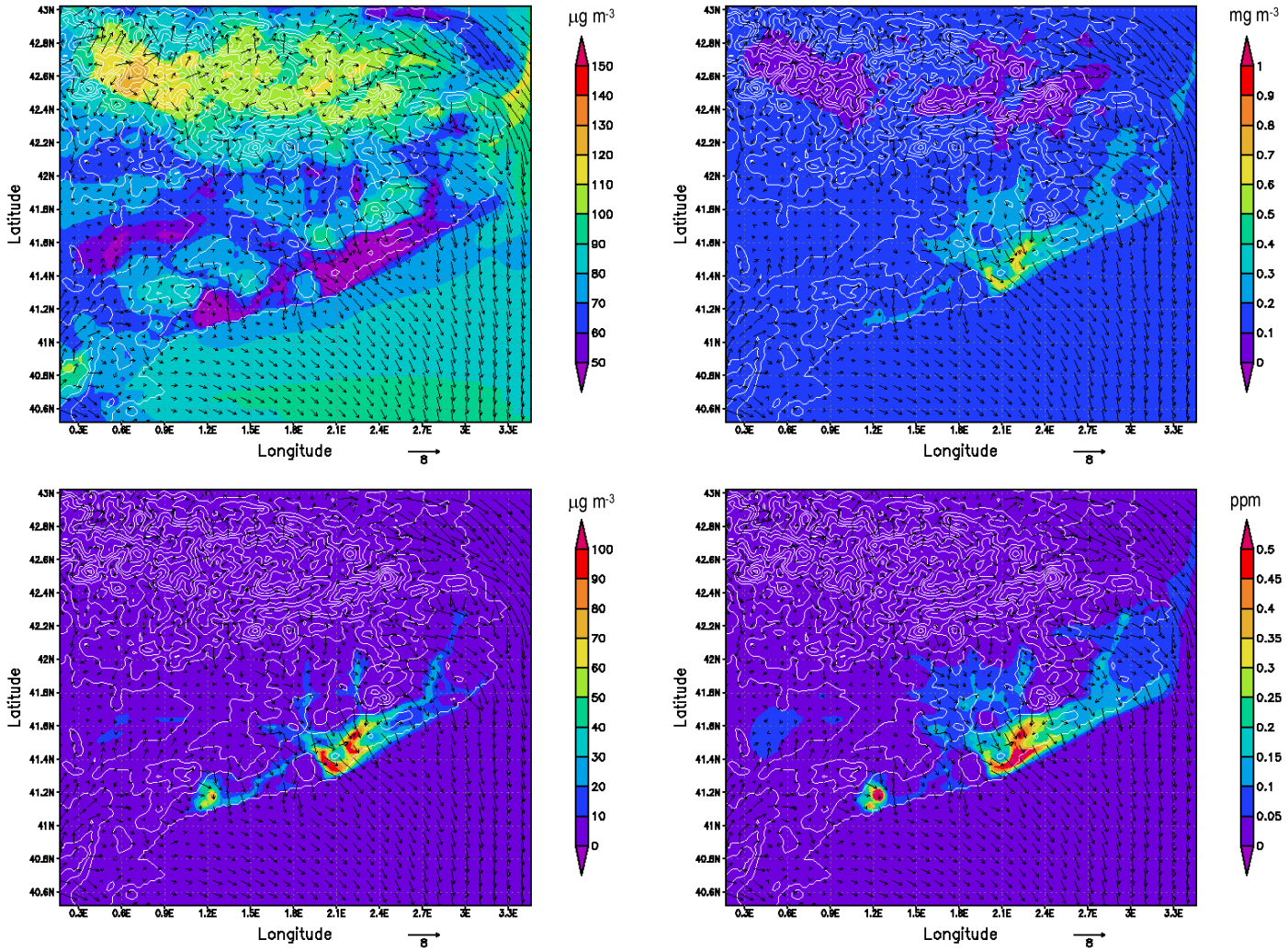

Figure 6.14. Surface concentration of O_3 ($\mu g\ m^{-3}$, up-left); CO ($mg\ m^{-3}$, up-right); NO_x ($\mu g\ m^{-3}$, down-left) and VOCs (ppm) at 0400UTC on 14 August, 2000.

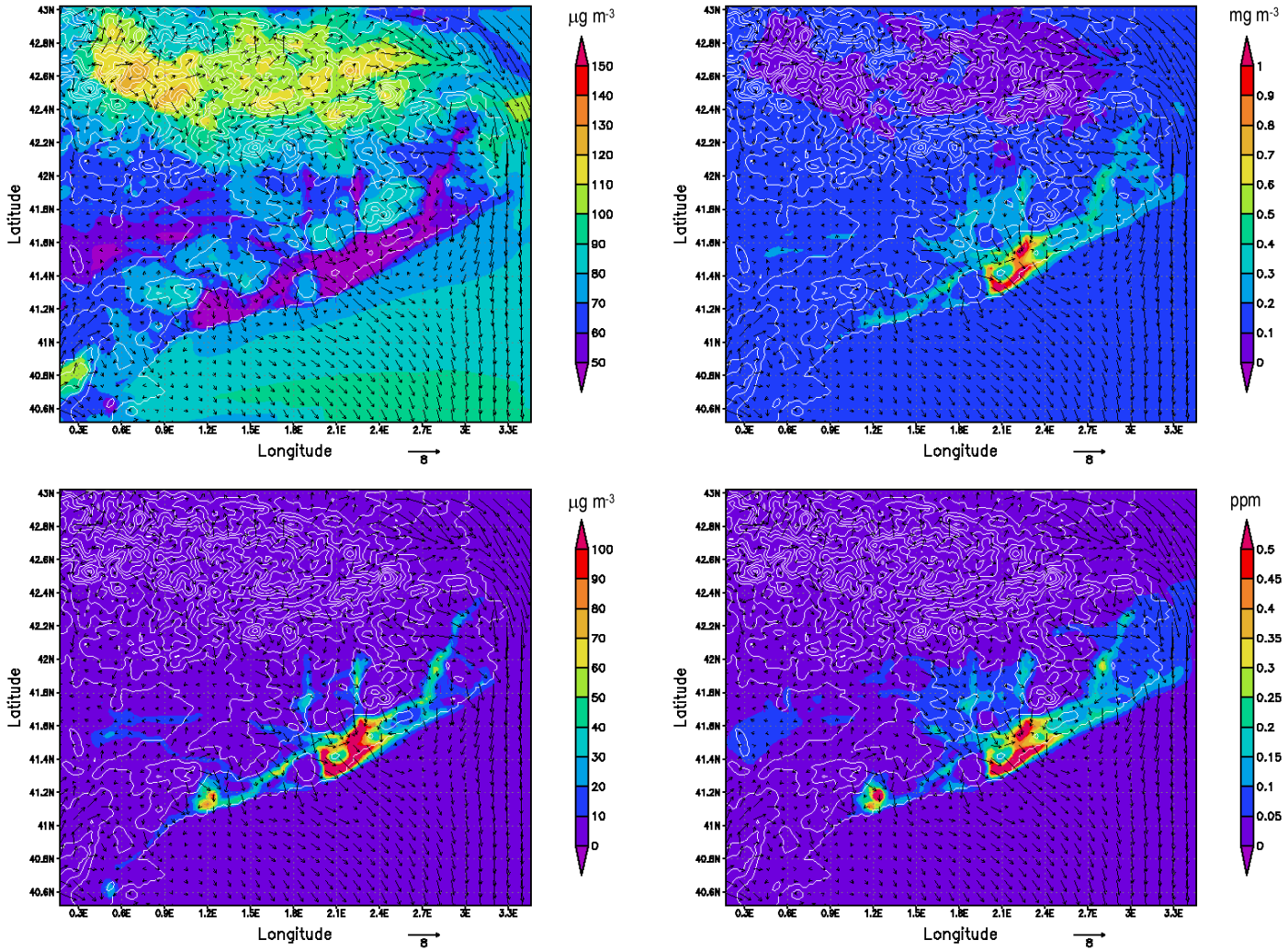

Figure 6.15. Surface concentration of O_3 ($\mu g\ m^{-3}$, up-left); CO ($mg\ m^{-3}$, up-right); NO_x ($\mu g\ m^{-3}$, down-left) and VOCs (ppm) at 0600UTC on 14 August, 2000.

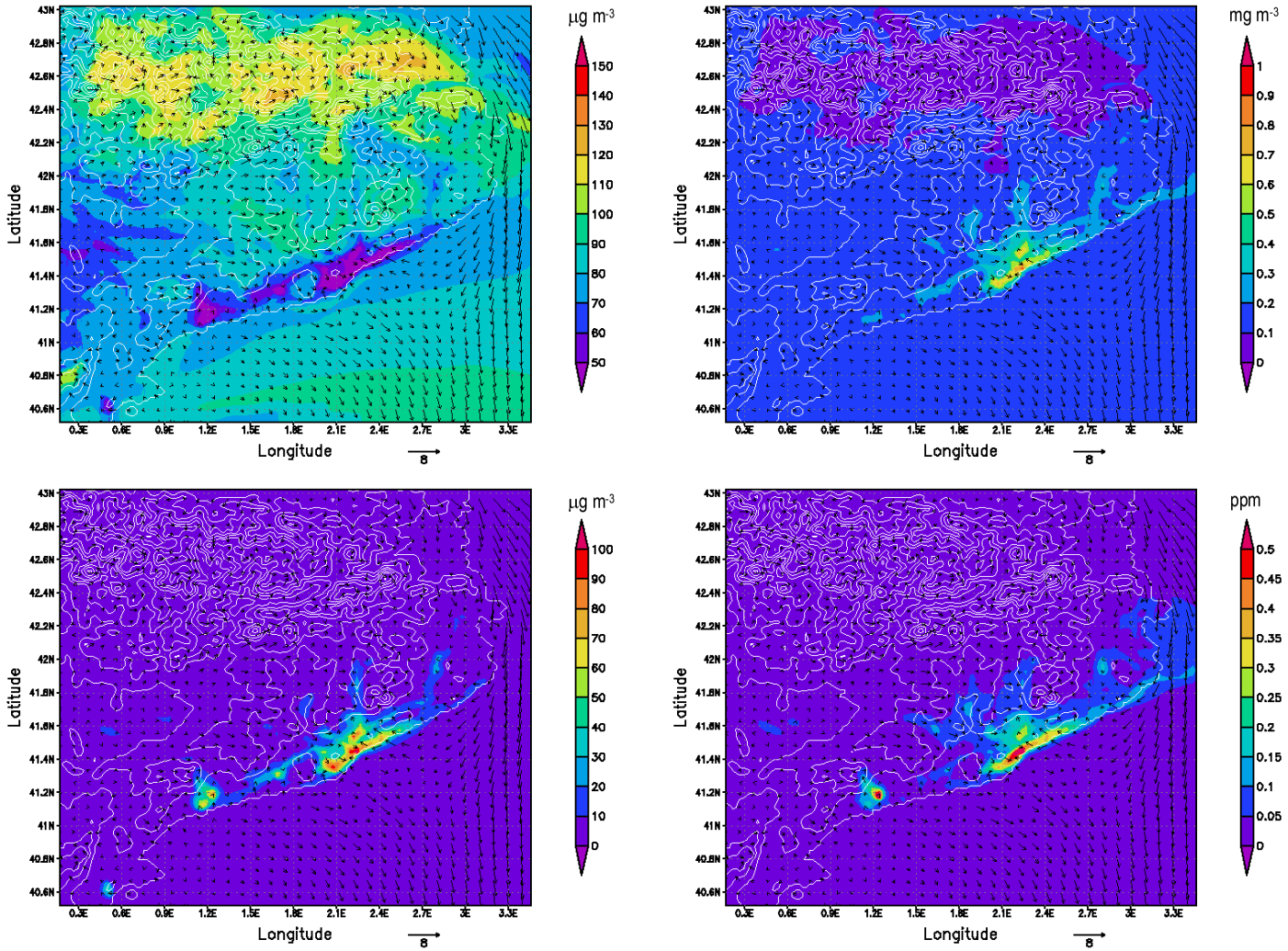

Figure 6.16. Surface concentration of O_3 ($\mu g\ m^{-3}$, up-left); CO ($mg\ m^{-3}$, up-right); NO_x ($\mu g\ m^{-3}$, down-left) and VOCs (ppm) at 0800UTC on 14 August, 2000.

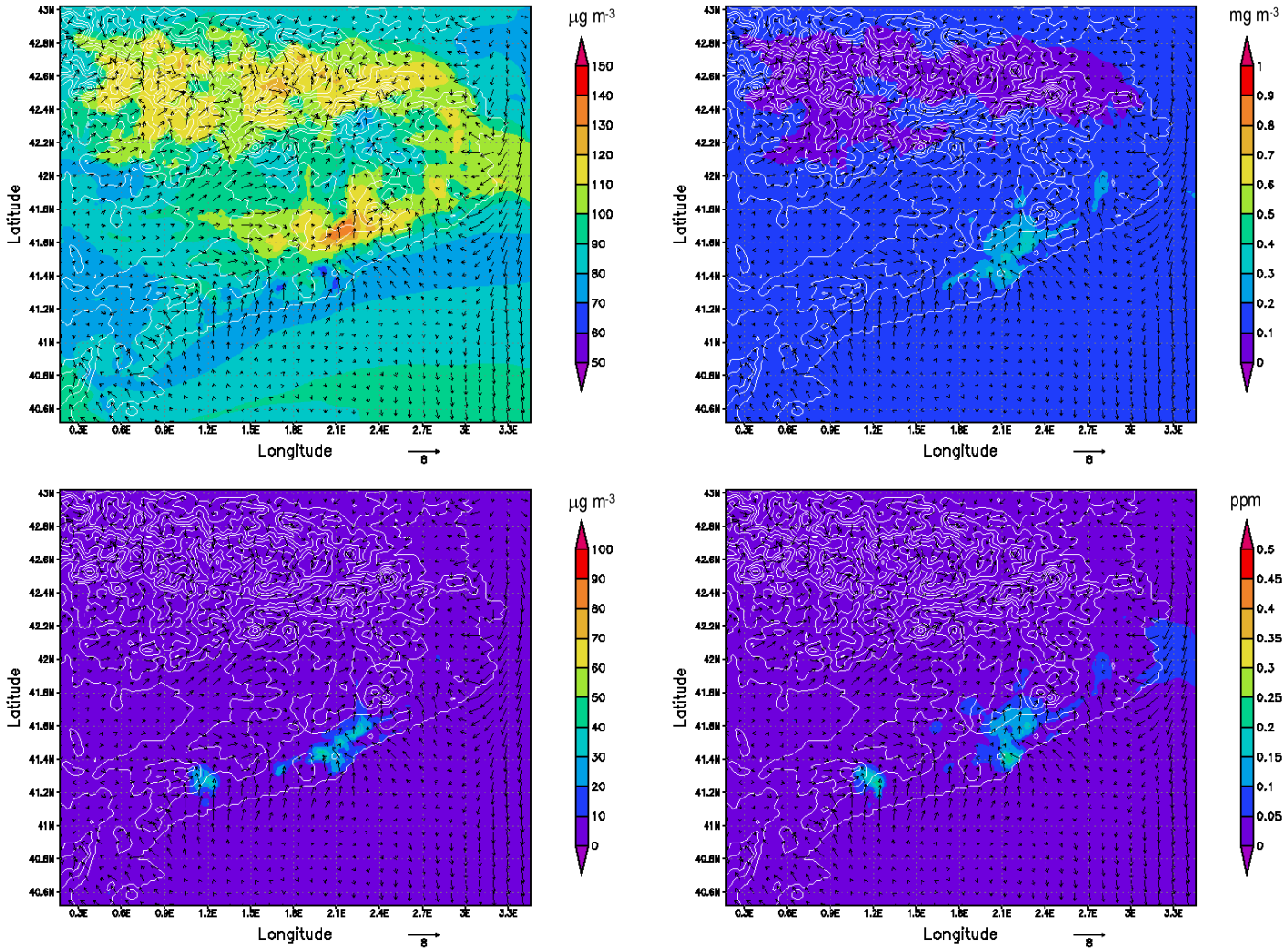

Figure 6.17. Surface concentration of O_3 (μg m^{-3}, up-left); CO (mg m^{-3}, up-right); NO_x (μg m^{-3}, down-left) and VOCs (ppm) at 1000UTC on 14 August, 2000.

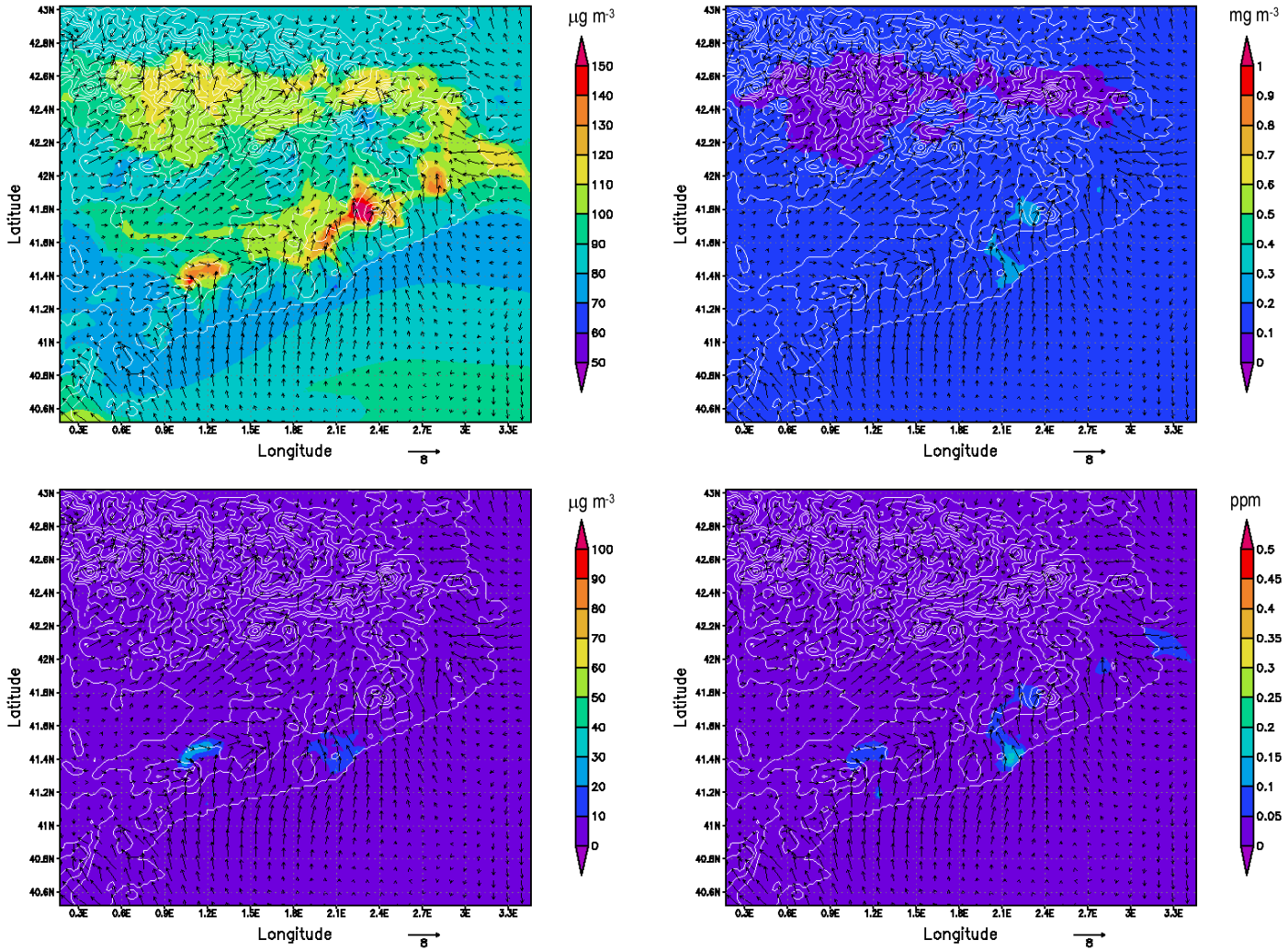

Figure 6.18. Surface concentration of O_3 (μg m^{-3}, up-left); CO (mg m^{-3}, up-right); NO_x (μg m^{-3}, down-left) and VOCs (ppm) at 1200UTC on 14 August, 2000.

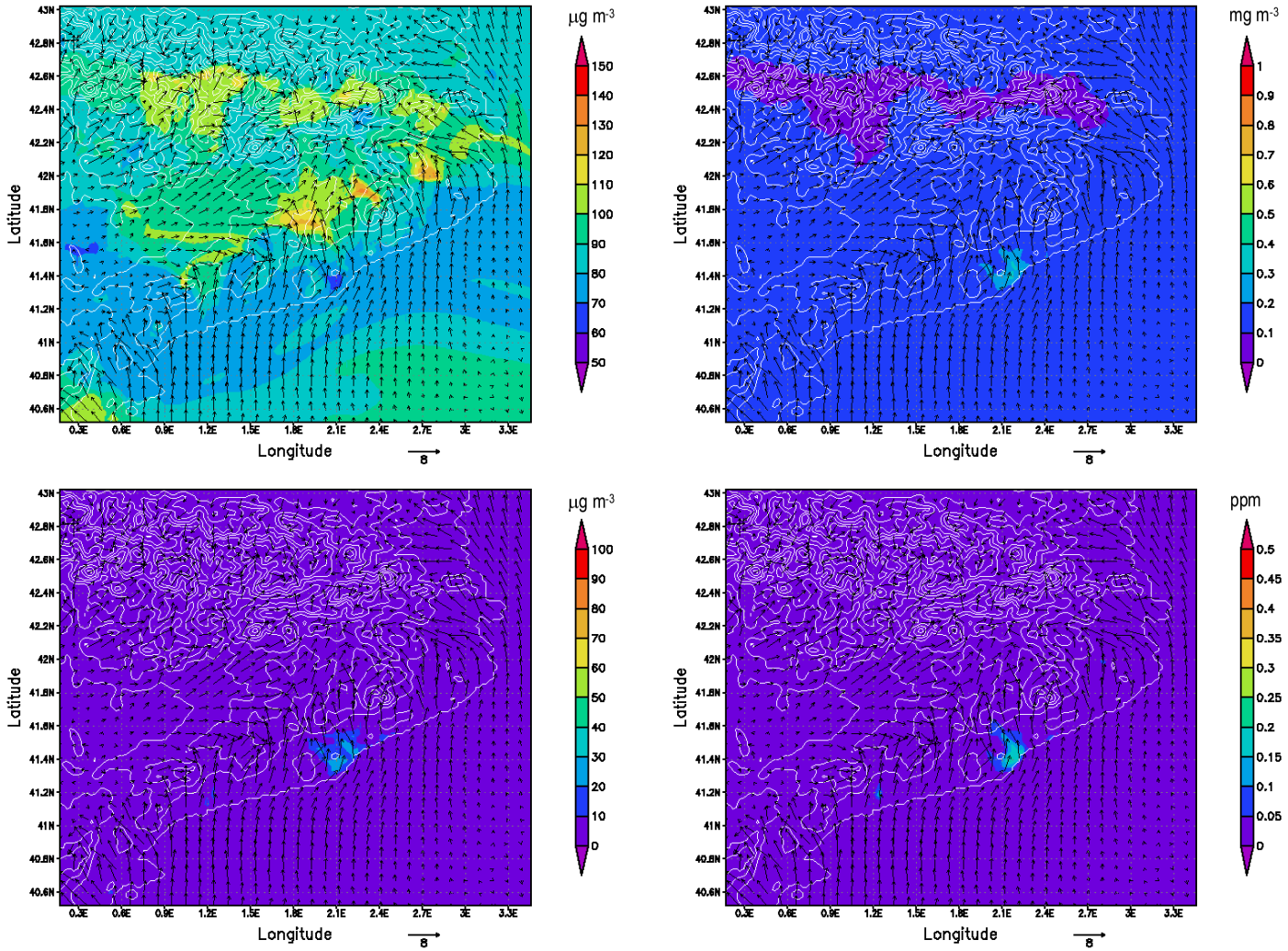

Figure 6.19. Surface concentration of O_3 (μg m^{-3}, up-left); CO (mg m^{-3}, up-right); NO_x (μg m^{-3}, down-left) and VOCs (ppm) at 1400UTC on 14 August, 2000.

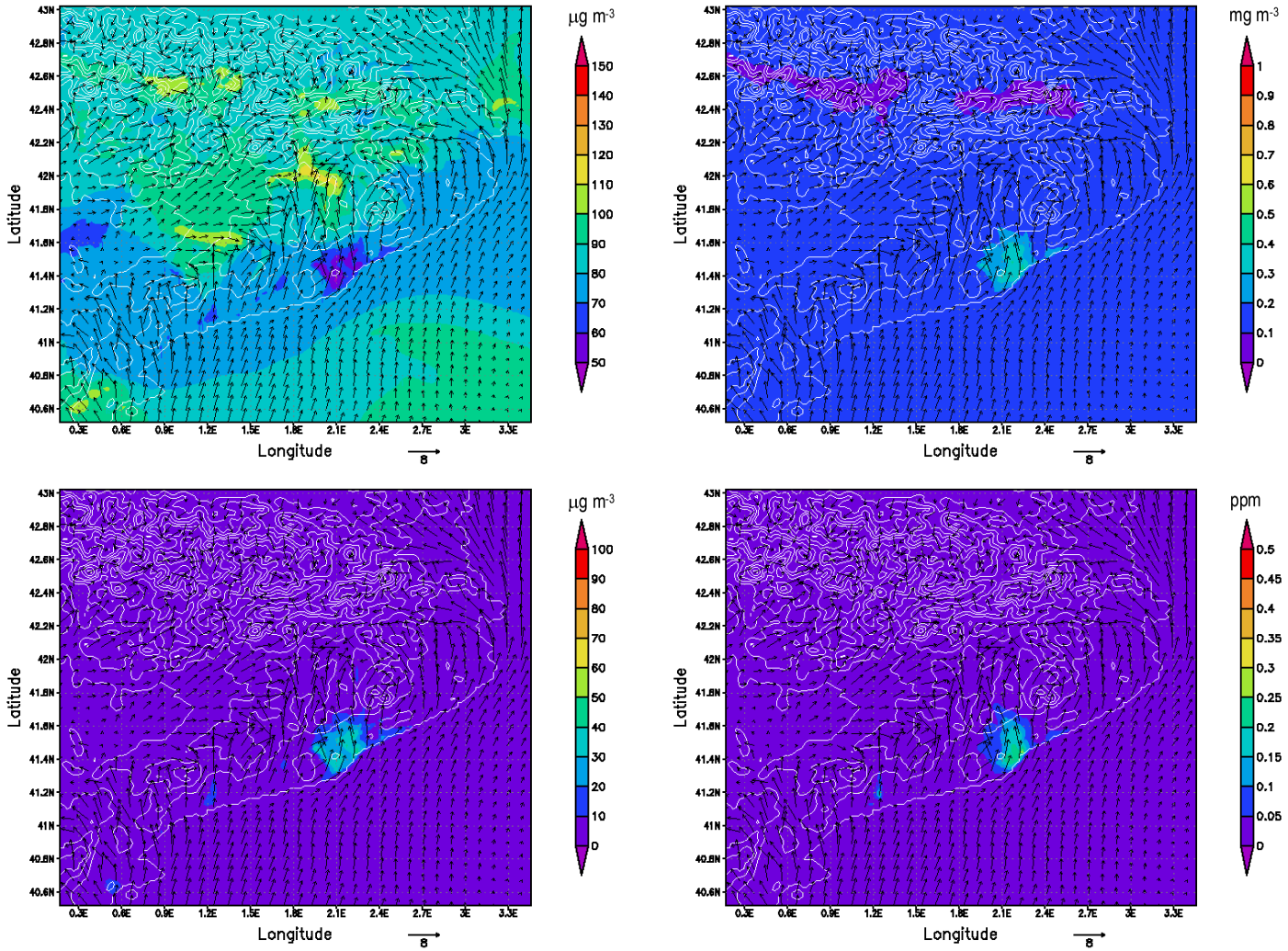

Figure 6.20. Surface concentration of O_3 ($\mu g\ m^{-3}$, up-left); CO ($mg\ m^{-3}$, up-right); NO_x ($\mu g\ m^{-3}$, down-left) and VOCs (ppm) at 1600UTC on 14 August, 2000.

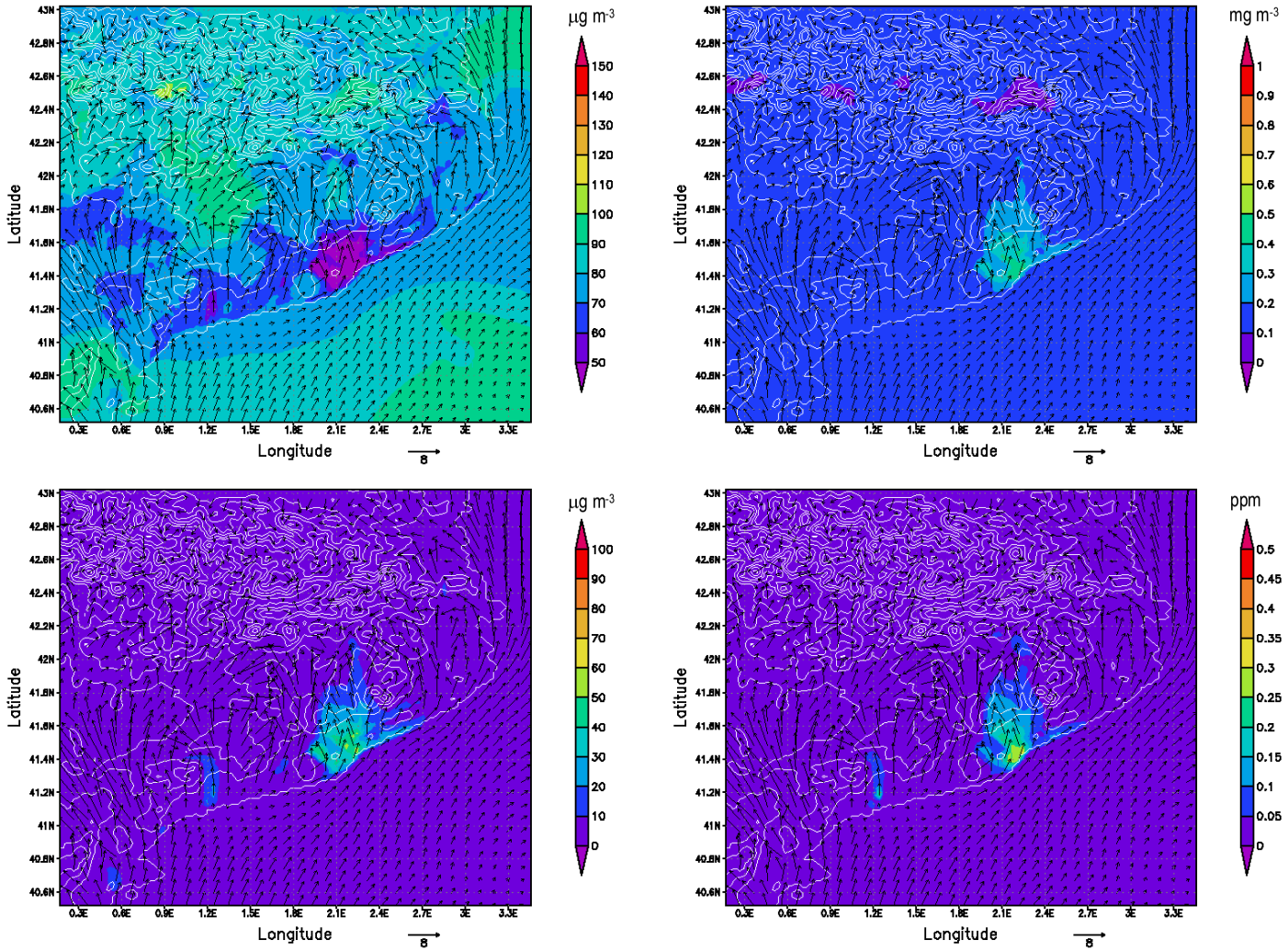

Figure 6.21. Surface concentration of O_3 (μg m^{-3}, up-left); CO (mg m^{-3}, up-right); NO_x (μg m^{-3}, down-left) and VOCs (ppm) at 1800UTC on 14 August, 2000.

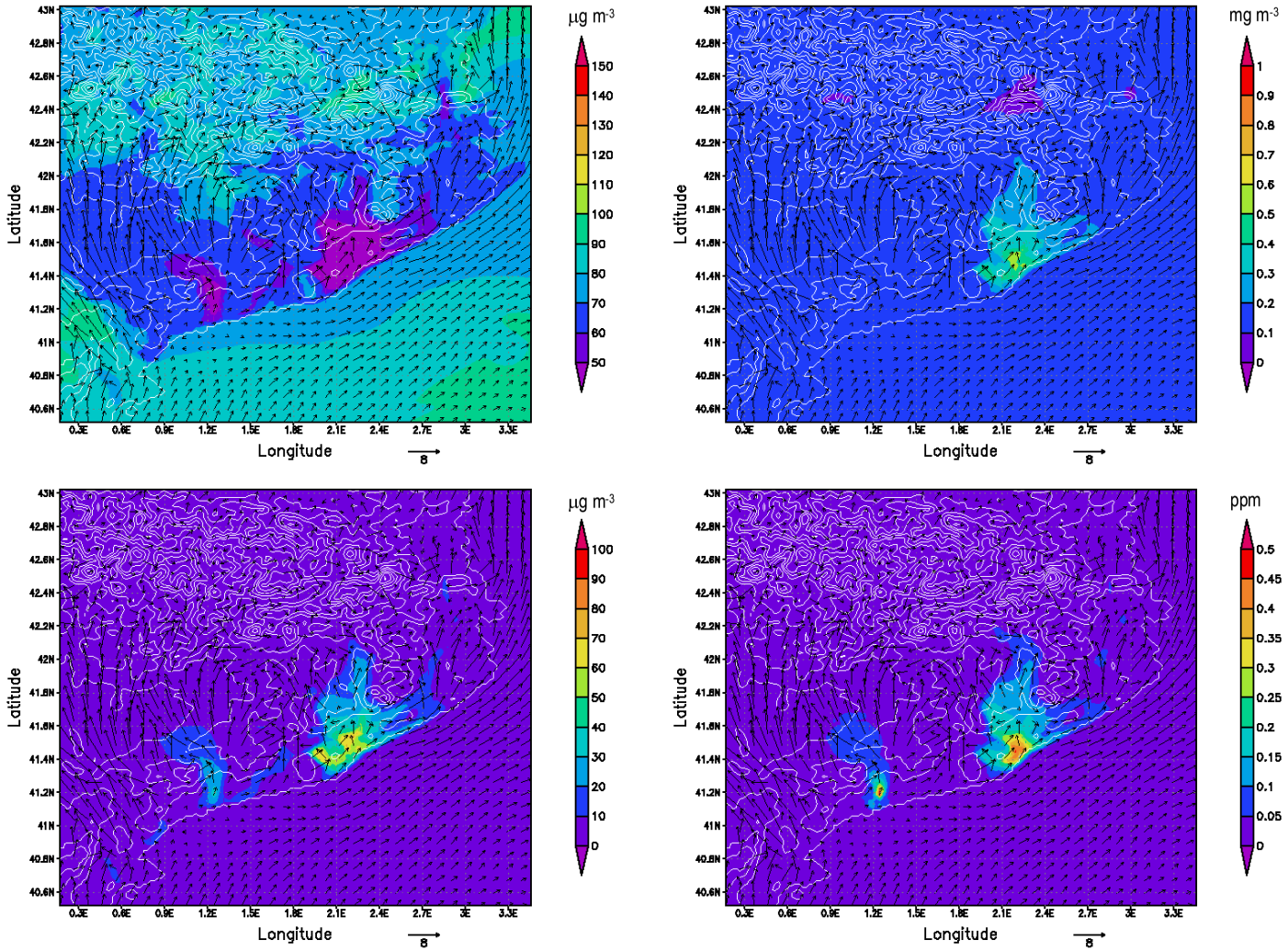

Figure 6.22. Surface concentration of O_3 ($\mu g\ m^{-3}$, up-left); CO ($mg\ m^{-3}$, up-right); NO_x ($\mu g\ m^{-3}$, down-left) and VOCs (ppm) at 2000UTC on 14 August, 2000.

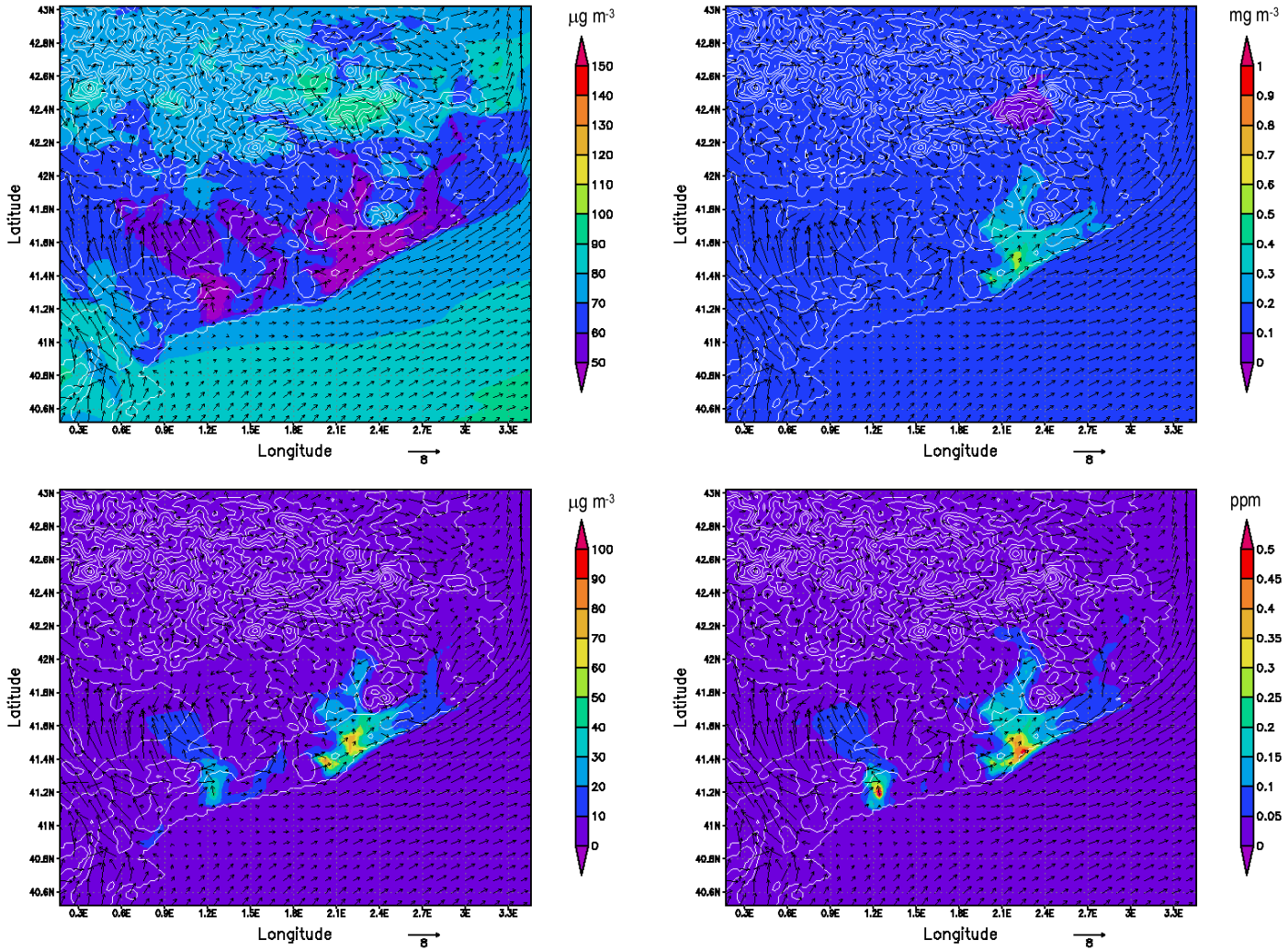

Figure 6.23. Surface concentration of O_3 (μg m^{-3}, up-left); CO (mg m^{-3}, up-right); NO_x (μg m^{-3}, down-left) and VOCs (ppm) at 2200UTC on 14 August, 2000.

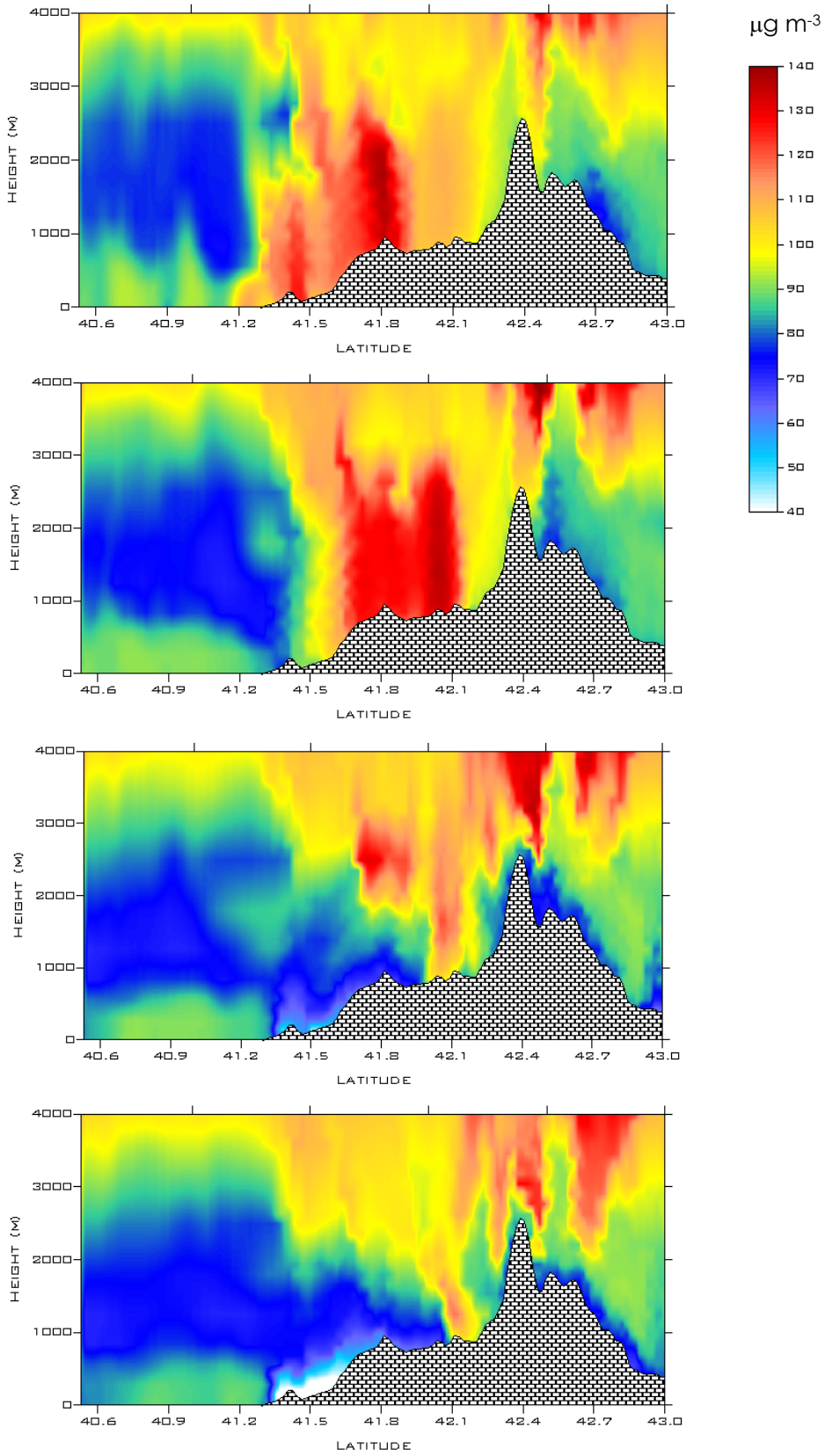

Figure 6.24. Re-circulations over the northeastern Iberian Peninsula observed from O_3 (μg m^{-3}) vertical profile Mediterranean Sea-Barcelona-Pyrenees, derived from MM5-EMICAT2000-CMAQ simulations at (up-down) 1200UTC, 1400UTC, 1800UTC and 2000UTC for 14 August, 2000.

At an altitude of 500m-1500m, backtrajectories indicate a coastal origin of air masses from the southeastern Iberian coast (Valencia). Levels of ozone and other photochemical pollutants are important in this area, especially inland, because of the presence of the industrial zone of Castellón. As observed in simulations, ECHAM5/MESSy forecasts an ozone reservoir layer at 1500m during the night over the Mediterranean Sea with concentrations above 125 $\mu g\ m^{-3}$ (Figure 6.25) that are transported inland on the following day during the development of the sea breeze cycle. The high-pressure area over the Mediterranean Sea provokes anticyclonic circulations and therefore O_3 is transported inland to Valencia.

The transport of air masses from Valencia and the eastern Iberian coast to the northeastern Iberian Peninsula is depicted through the bottom-left boundaries of the domain simulated with CMAQ during the early morning until the evening, which may reach the plateau of Lleida with concentrations of O_3 around 120 $\mu g\ m^{-3}$.

At noon, the sea breeze is not capable yet to rise above the littoral mountains and an accumulation of pollutants in the slopes of these mountain ranges, transported by the front of the sea breezes, is produced (Figure 6.26). Later, early in the afternoon, the reinforcement of the breeze combined with upslope winds produces the overcome of the topographical accidents by the sea breeze front. A fraction of pollutants undergo vertical injections (as commented before); the other fraction is transported inland, being the latter amassed in the plateau of Vic (Figure 6.27). These phenomena are observed during each day of this episode and it is characteristic of the air dynamics of the northeastern Iberian Peninsula during an episode of low pressure gradient over the Western Mediterranean Basin (Jorba *et al.*, 2003).

6.4.2 Middle Troposphere: the Iberian Thermal Low (ITL)

The intense surface heating promotes the development of the Iberian Thermal Low (ITL) inland the Iberian Peninsula. The ITL system consists of at least three main cells (Millán *et al.*, 1992; 1996): (1) the first, a coastal cell, combines the sea breeze and up-slope winds and extends to from 80 to 100 km inland from the eastern Iberian coast; (2) the second cell is located over the Central plateau; and (3) the third, a coastal cell symmetrical to that over the Western Mediterranean Basin, could be expected to develop over the Atlantic coast. The Iberian Thermal Low developed for the episode 13-16 August, 2000, persists together with the stagnant meteorological conditions.

This ITL at peninsular level forces the convergence of surface winds from the coastal areas towards the central plateau injecting polluted air masses into the middle troposphere. Once in this region, northwesterly winds transport pollutants in a stratified layer, as it is clearly shown in the backtrajectory analysis, where air masses arriving in the northeastern Iberian Peninsula show an Atlantic origin (Figure 6.28).

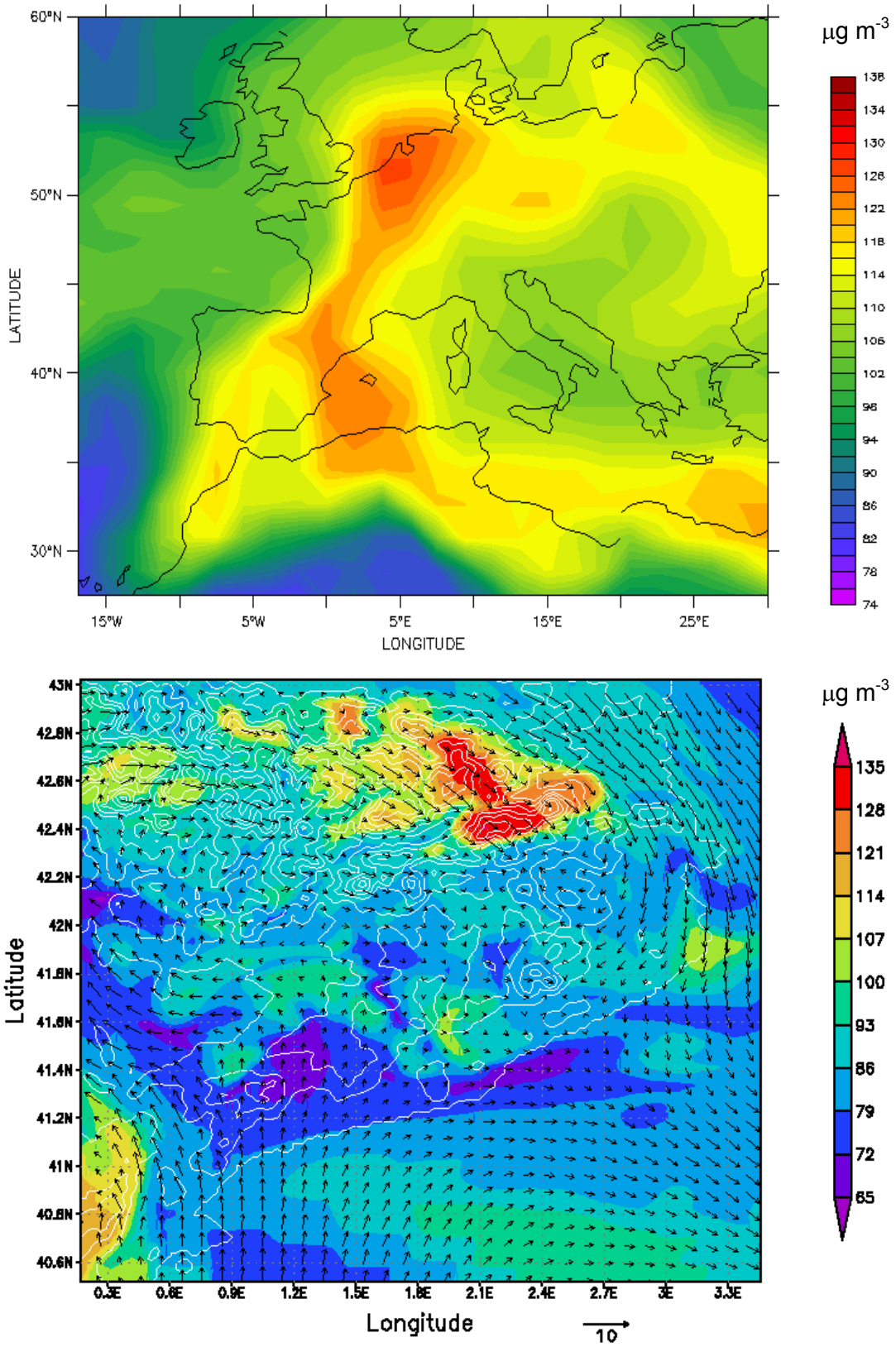

Figure 6.25. Ozone concentrations (µg m^{-3}) simulated with ECHAM5/MESSy model (up) for the WMB and O_3 concentrations (µg m^{-3}) and wind field vectors at 1000m over the northeastern Iberian Peninsula with MM5-EMICAT2000-CMAQ (down) on 14 August, 2000, at 0600UTC.

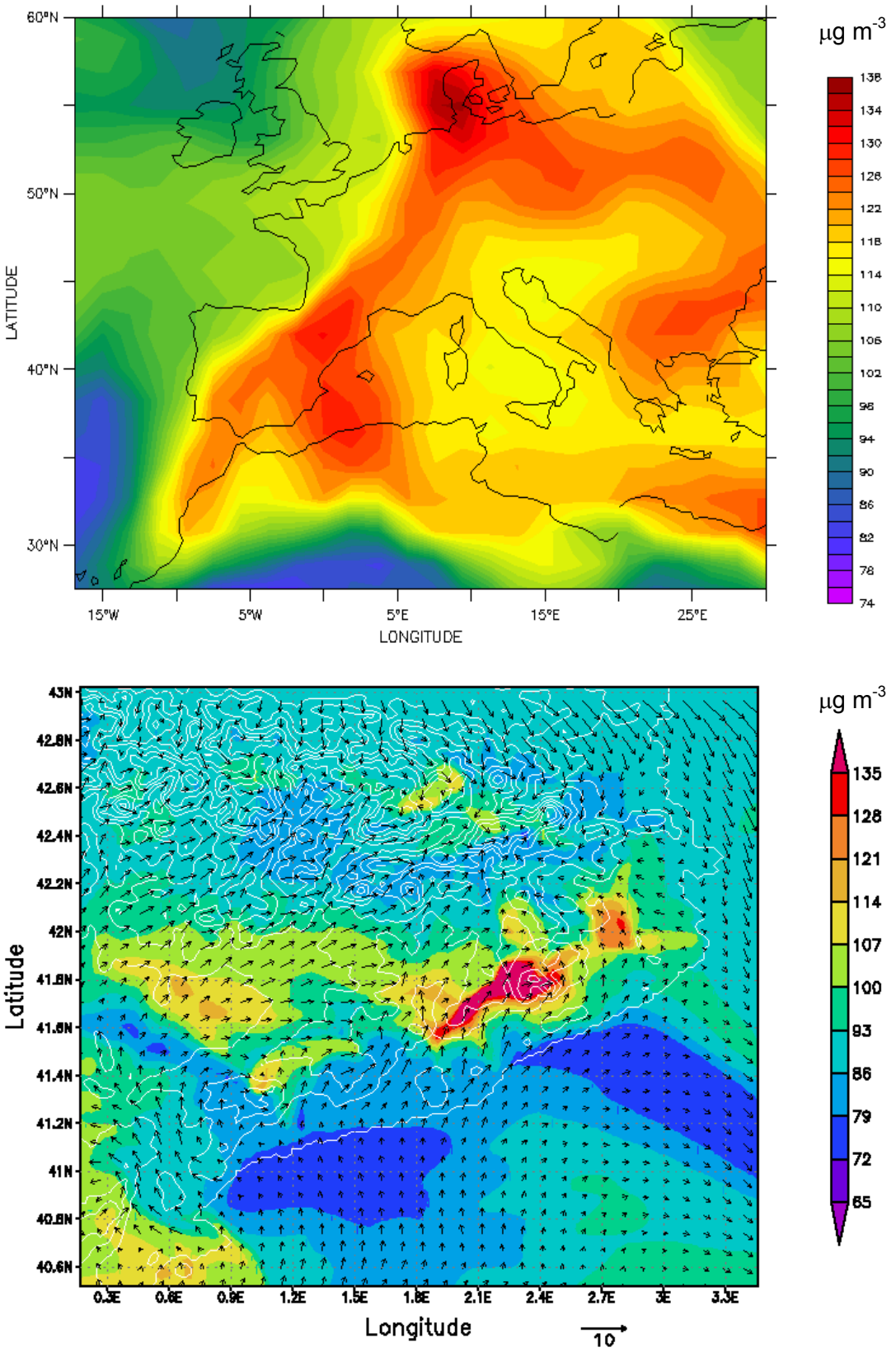

Figure 6.26. Ozone concentrations (μg m^{-3}) simulated with ECHAM5/MESSy model (up) for the WMB and O_3 concentrations (μg m^{-3}) and wind field vectors at 1000m over the northeastern Iberian Peninsula with MM5-EMICAT2000-CMAQ (down) on 14 August, 2000, at 1200UTC.

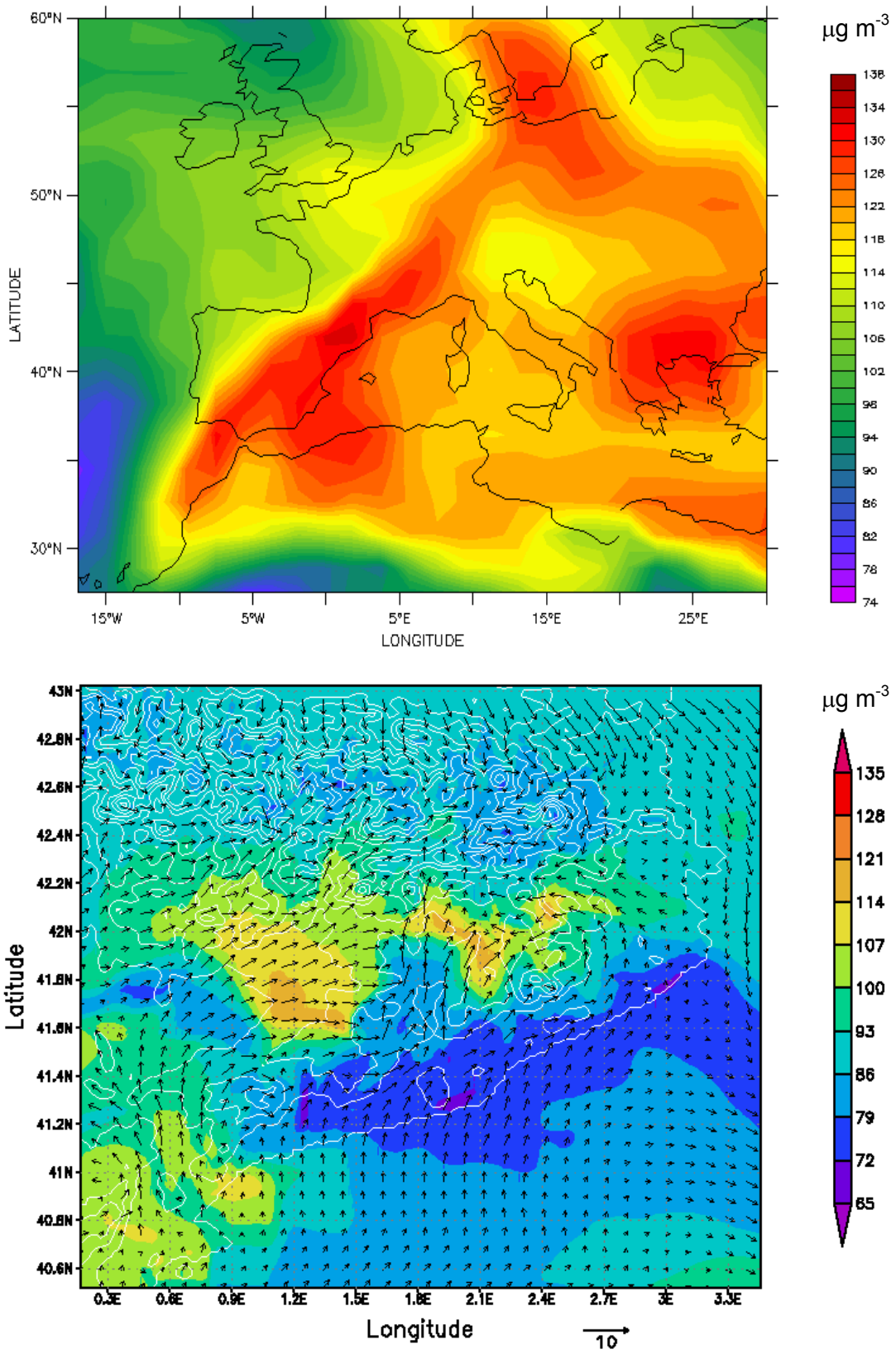

Figure 6.27. Ozone concentrations (μg m^{-3}) simulated with ECHAM5/MESSy model (up) for the WMB and O_3 concentrations (μg m^{-3}) and wind field vectors at 1000m over the northeastern Iberian Peninsula with MM5-EMICAT2000-CMAQ (down) on 14 August, 2000, at 1800UTC.

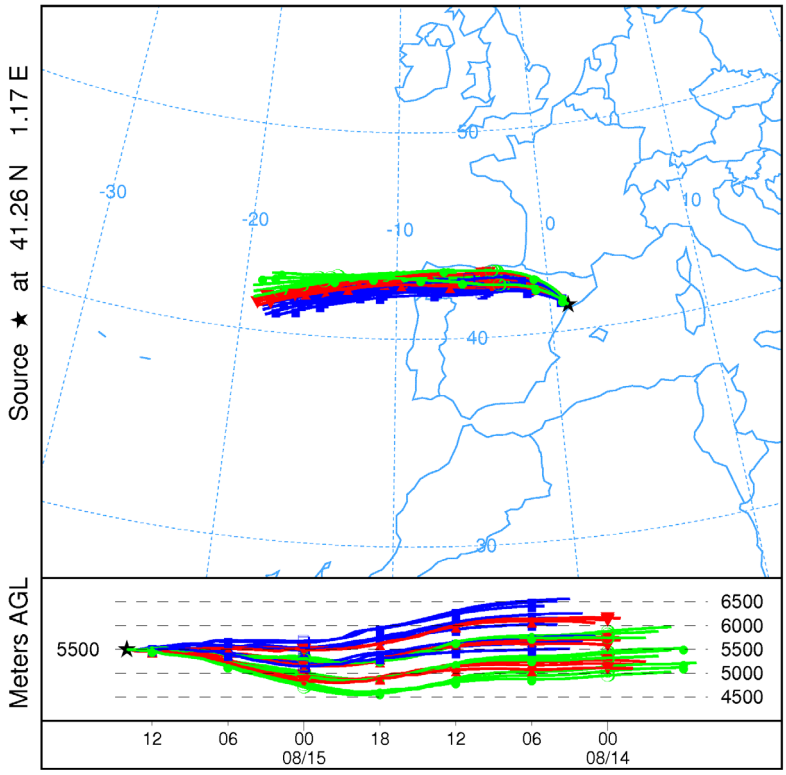

Figure 6.28. Ensemble backtrajectories arriving at the middle troposphere within the domain of the Iberian Peninsula on 15 August, 2000, at 1200UTC. Backtrajectories show a transport from Atlantic air that incorporates pollutants over the Iberian Peninsula.

Figure 6.29 indicates that this middle-tropospheric air with Atlantic origin is a clean air, with low amounts of pollutants, but it adds anthropogenic contaminants as the air masses circulate over the middle troposphere of the central Plateau of the Iberian Peninsula. Mid-tropospheric air is mainly advected from the west, and is characterized by relatively high pollutants levels, as observed from the ECHAM5/MESSy simulations at 3500m.

Simultaneous presence of both ozone and carbon monoxide indicates an anthropogenic origin of air pollution, which is not due to stratospheric ozone intrusion since CO profiles have a similar spatial pattern to those of O_3.

Pollutants are injected through convective processes in altitudes above 3500m. Once in the middle troposphere, a medium-long range transport towards the Mediterranean coast is observed in the simulations with ECHAM5/MESSy and MM5-EMICAT2000-CMAQ. Air masses with an important contribution to ozone (over 120 $\mu g\ m^{-3}$) are transported from the central plateau at 3500m due to northwesterly flows within the northeastern Iberian Peninsula through the western boundary of the domain from 0600UTC (Figure 6.30). The anticyclonic compensatory subsidence causes the sink of these pollutants and their accumulation over the littoral mountain ranges is observed at 1800UTC (Figure 6.31).

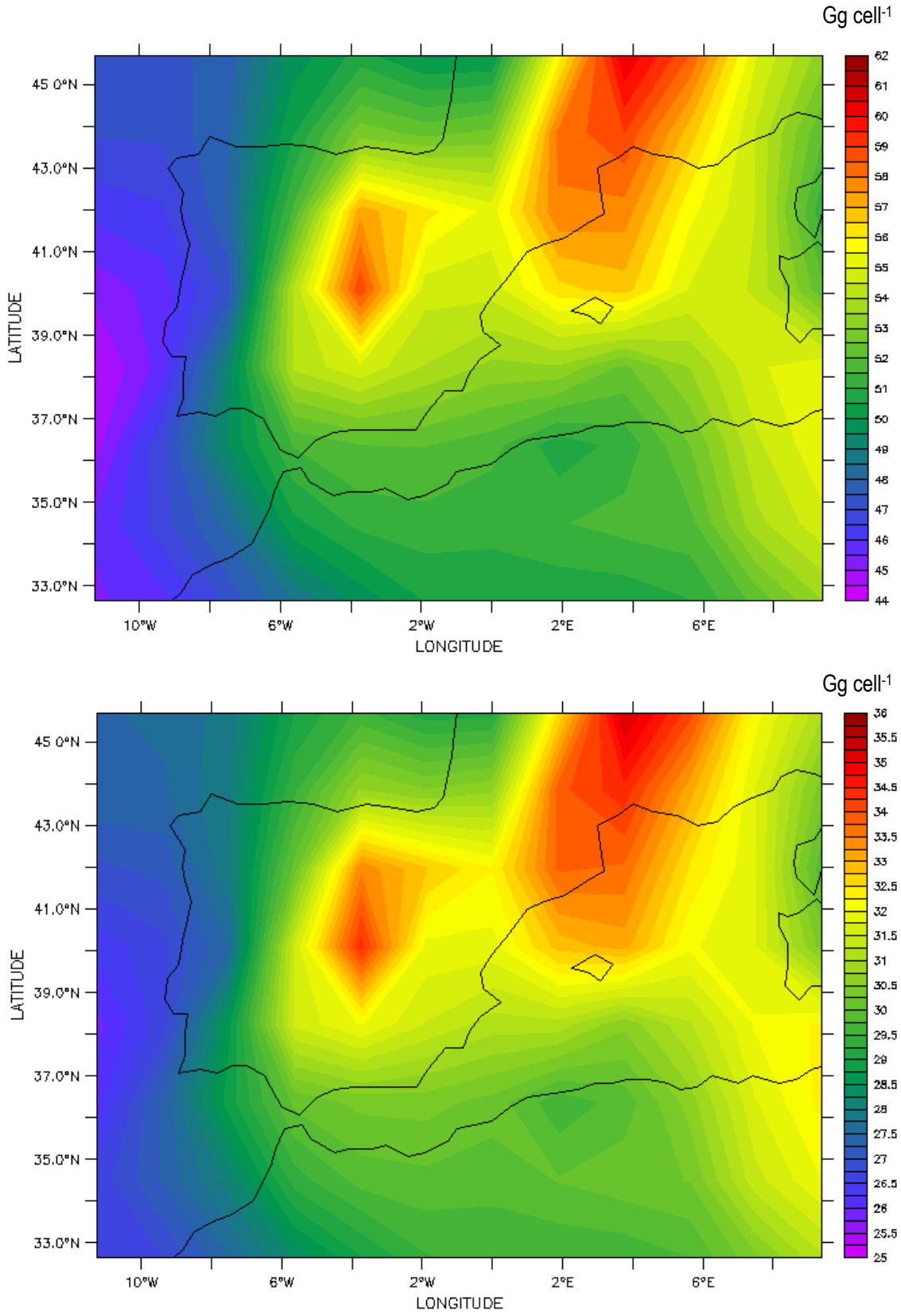

Figure 6.29. Pollutants injected in the middle troposphere as a consequence of the formation of the ITL: total O_3 (up) and CO (down) in the middle troposphere expressed in Gg cell^{-1}. Northwesterlies transport pollutants towards the coast.

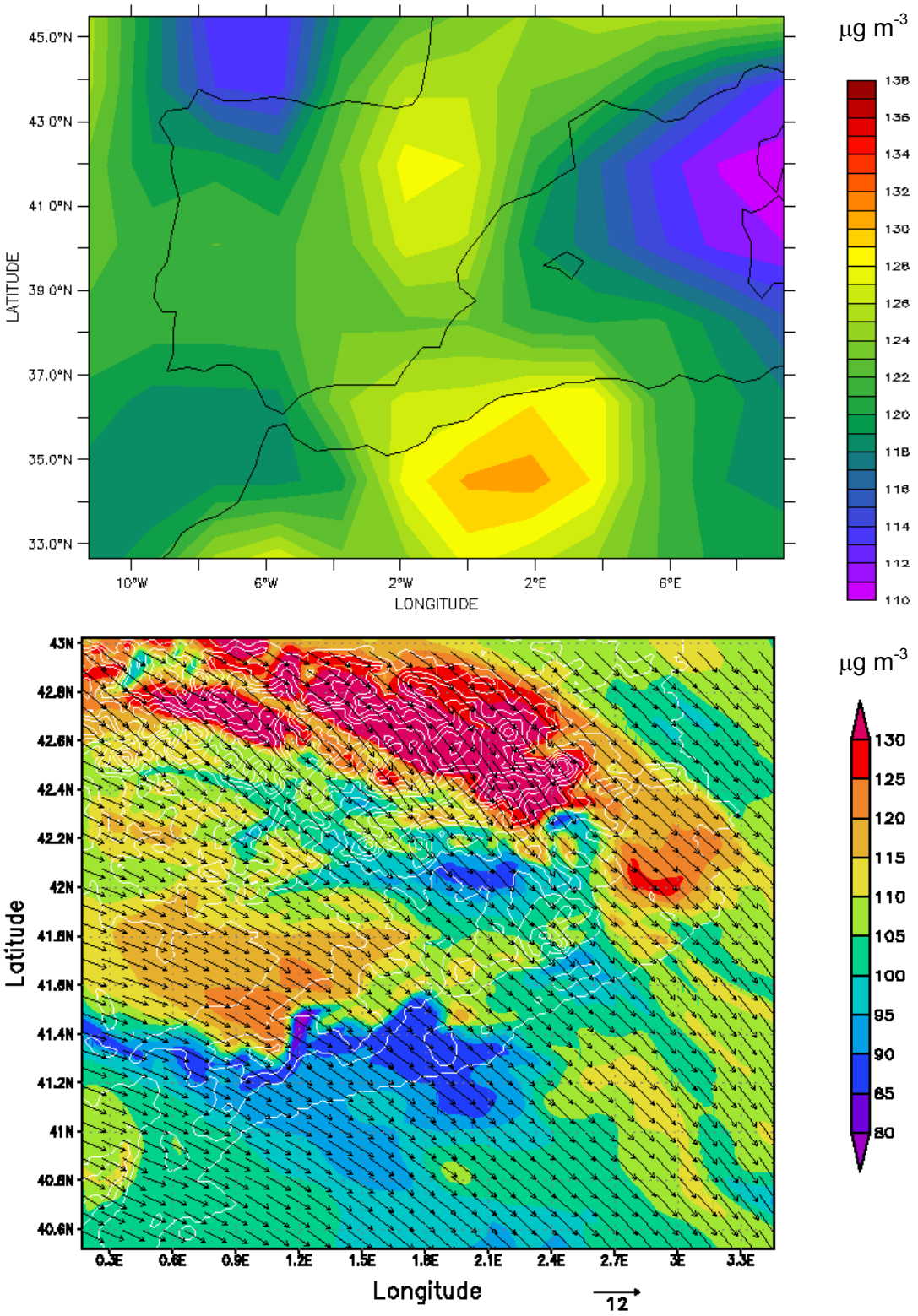

Figure 6.30. Peninsular transport of ozone (μg m^{-3}) into the domain of the northeastern Iberian Peninsula at 3500m, at 0600UTC of 14 August, 2000, simulated for the whole WMB with ECHAM5/MESSy (up) and for the NEIP with MM5-EMICAT2000-CMAQ (down).

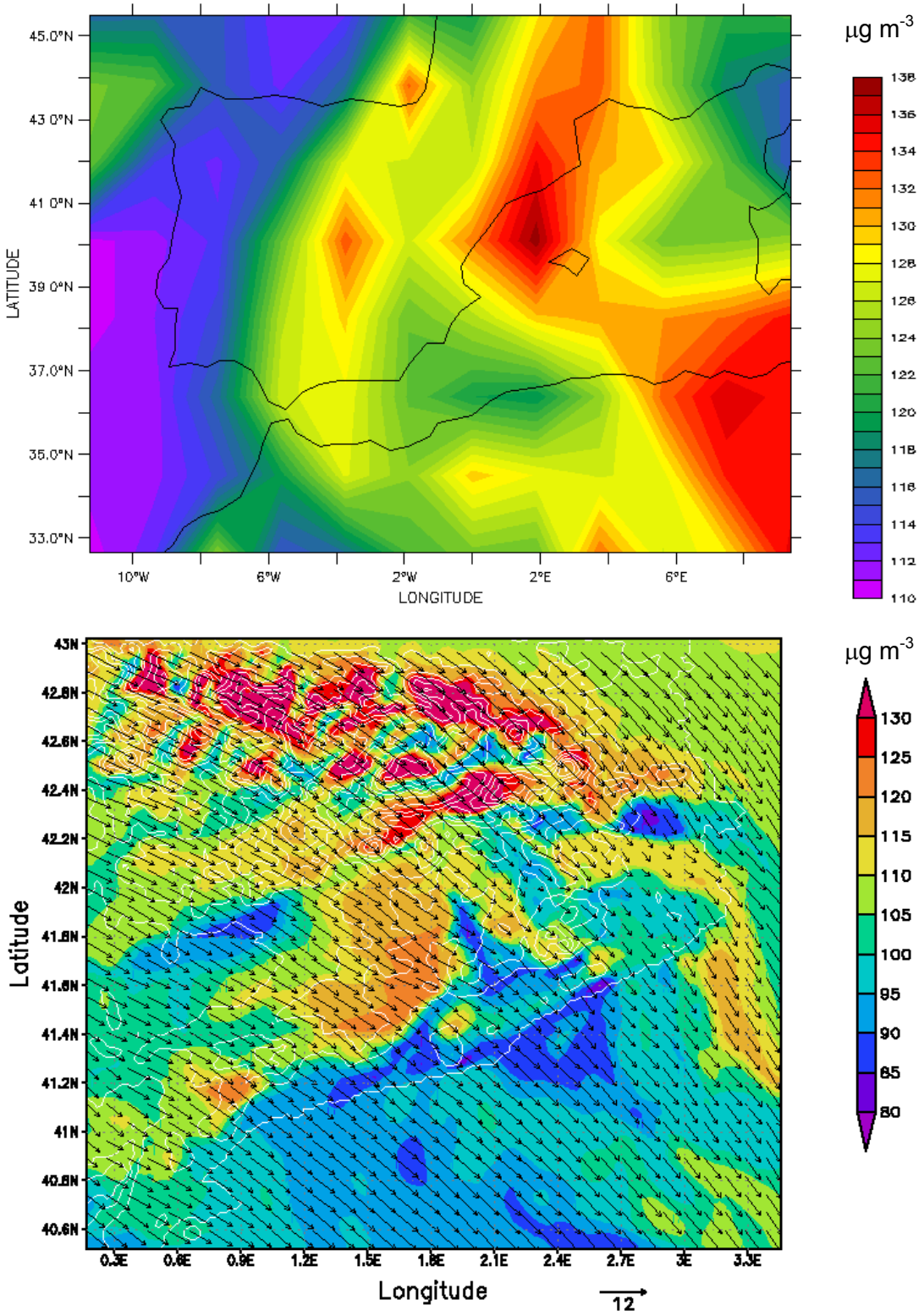

Figure 6.31. Peninsular transport of ozone (μg m^{-3}) into the domain of the northeastern Iberian Peninsula at 3500m, at 1800UTC of 14 August, 2000, simulated for the whole WMB with ECHAM5/MESSy (up) and for the NEIP with MM5-EMICAT2000-CMAQ (down).

Afterwards, the pollutants are transported towards the Mediterranean area, where they sink within the anticyclone located over the Western Mediterranean Sea; and this may cause the stabilization and layering of pollutants at the eastern coast of Iberia (Gangoiti *et al.*, 2001). A fraction of these pollutants is advected out from the domain of the northeastern Iberian Peninsula, and the other fraction is incorporated on the following morning to the sea-breeze cycle.

Another important phenomenon that affects the levels of photochemical pollution at a local scale is the convective transport on a local scale. At surface, we observe that at early afternoon, the sea-breeze front has passed over the coastal mountain range and reached the central plain (~100km from the coast), overwhelming the upslope winds in the opposite direction. Strong thermally or mechanically driven convections appear at the central plain injecting air masses up to the middle troposphere between 3500-5000m (Figure 6.32).

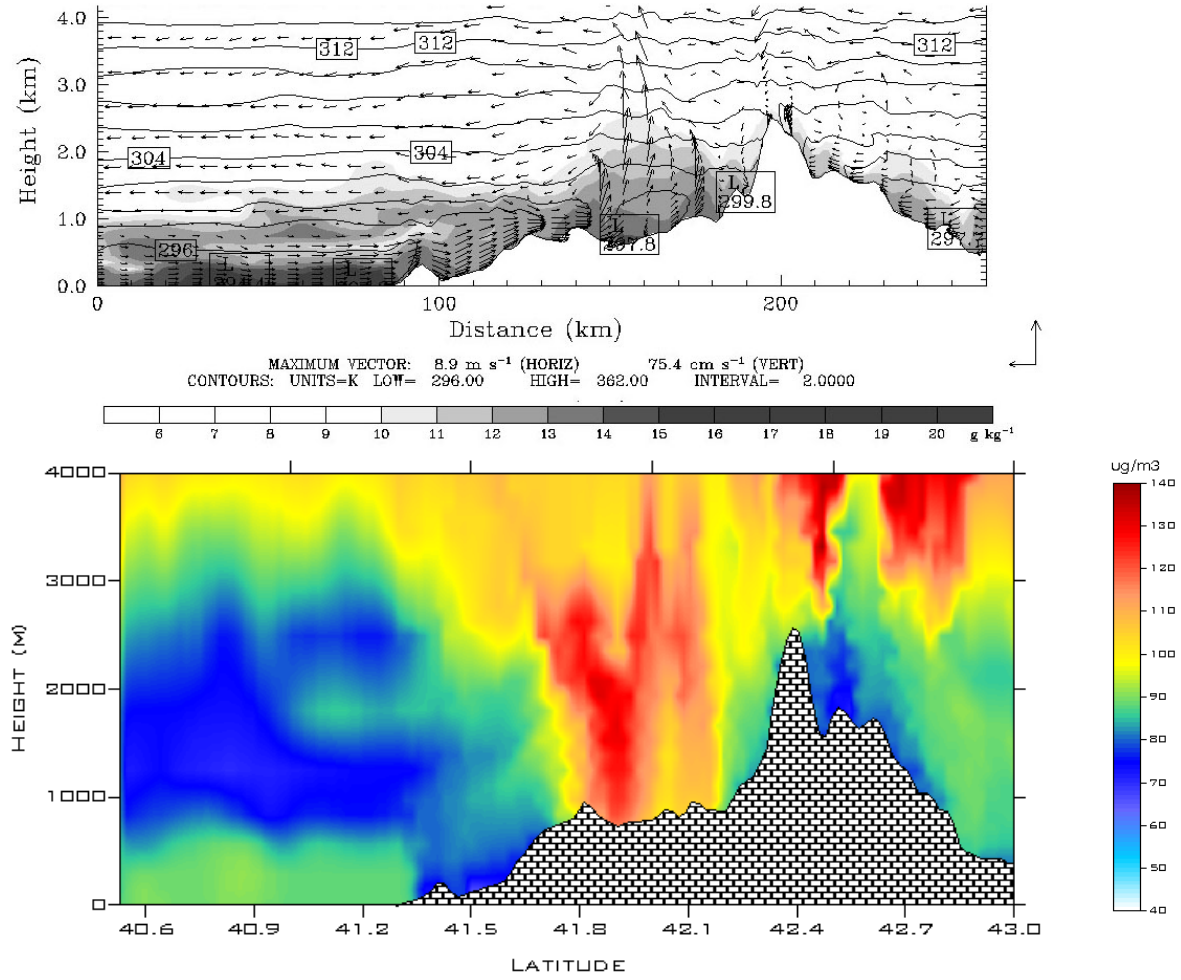

Figure 6.32. Vertical profile of the wind fields, potential temperature and mixing ratio (up) and ozone levels ($\mu g\ m^{-3}$) (down) for the vertical profile Mediterranean Sea-Barcelona-Pyrenees at 1600UTC for 14 August, 2000.

6.4.3 Upper Troposphere: the Stratosphere-Troposphere Exchange (STE)

The role of stratospheric ozone role in tropospheric ozone levels through the stratosphere-troposphere exchange (STE) has been widely studied (Stohl and Trickl, 1999; Roelofs and Lelieveld, 2000a; Lelieveld and Dentener, 2000; Traub *et al.*, 2003; among others). The downward transport from the stratosphere to the troposphere is typically associated with the formation of tropopause folds (Danielsen and Mohnen, 1977), cut-off lows (Bamber *et al.*, 1984; Wirth, 1995a; 1995b) and streamers along the polar-front jet (Appenzeller and Davies, 1992). Convective phenomena favor the downward movements of stratospheric air masses towards the middle and low troposphere (Borchi and Marenco, 2002; Tulet *et al.*, 2002).

To determine the positions of the tropopause and the possible contributions of stratospheric ozone to O_3 levels in the northeastern Iberian Peninsula, we have used the definition of potential vorticity (PV) proposed by Reed (1955). Hoerling *et al.* (1991) point out that a value of 3.5 potential vorticity units (PVU) 10^{-6} m^2 s^{-1} K kg^{-1}) represents an optimal value for the definition of the tropopause outside the tropics; this has been the criterion used also by Traub and Lelieveld (2003). Because of the difference between stratospheric and tropospheric PV, potential vorticity generation and destruction processes are essential to the exchange of air and its chemical constituents between the stratosphere and the troposphere. In addition, the turbulence index (TI) by Ellrod and Knapp (1992) has been used for diagnosis and prediction of the clean-air turbulence (non-convective turbulence typically outside the planetary boundary layer, often in the upper troposphere), whose units are 10^{-7} s^{-2}. For our further analysis, we focus on the 250-hPa level, because it is typically beneath the tropopause in the tropics and subtropics, whereas it is above the tropopause in high latitudes (Traub and Lelieveld, 2003).

The daily analysis in the upper troposphere shows high pressures that are established over Africa continent. In addition, an Atlantic depression circulates over very northern latitudes, and over the Iberian Peninsula a weak zonal circulation dominates in the middle and upper troposphere, that turns northwest over the Mediterranean coast. The mean PV distribution over the WMB at 250 hPa is depicted in Figure 6.33. A tongue-shaped area with PV values over 3.5 PVU extends along the eastern Mediterranean coast. A decreased tropopause height is also observed in the Sahara dessert and the northeaster Atlantic Ocean. Coincident with the locations of high PV, an area with enhanced TI can be seen over the eastern Mediterranean coast, the Sahara dessert and the northwestern Atlantic (Figure 6.33), with values over 8, indicating areas with an enhanced probability of turbulence. This turbulence induced by upper level convergence near the tropopause and consequential strong wind shear causes mixing of tropospheric and stratospheric air near the tropopause (Traub and Lelieveld, 2003). High concentrations of ozone associate with those tongue-shaped tropopause descends are depicted in Figure 6.34, where the influence of stratospheric ozone is observed both in the middle troposphere of regions with high PV values

and also in the upper troposphere. Horizontal transport from locations with tropopause descents can play an important role in regional O_3 levels (Bonasoni *et al.*, 2000).

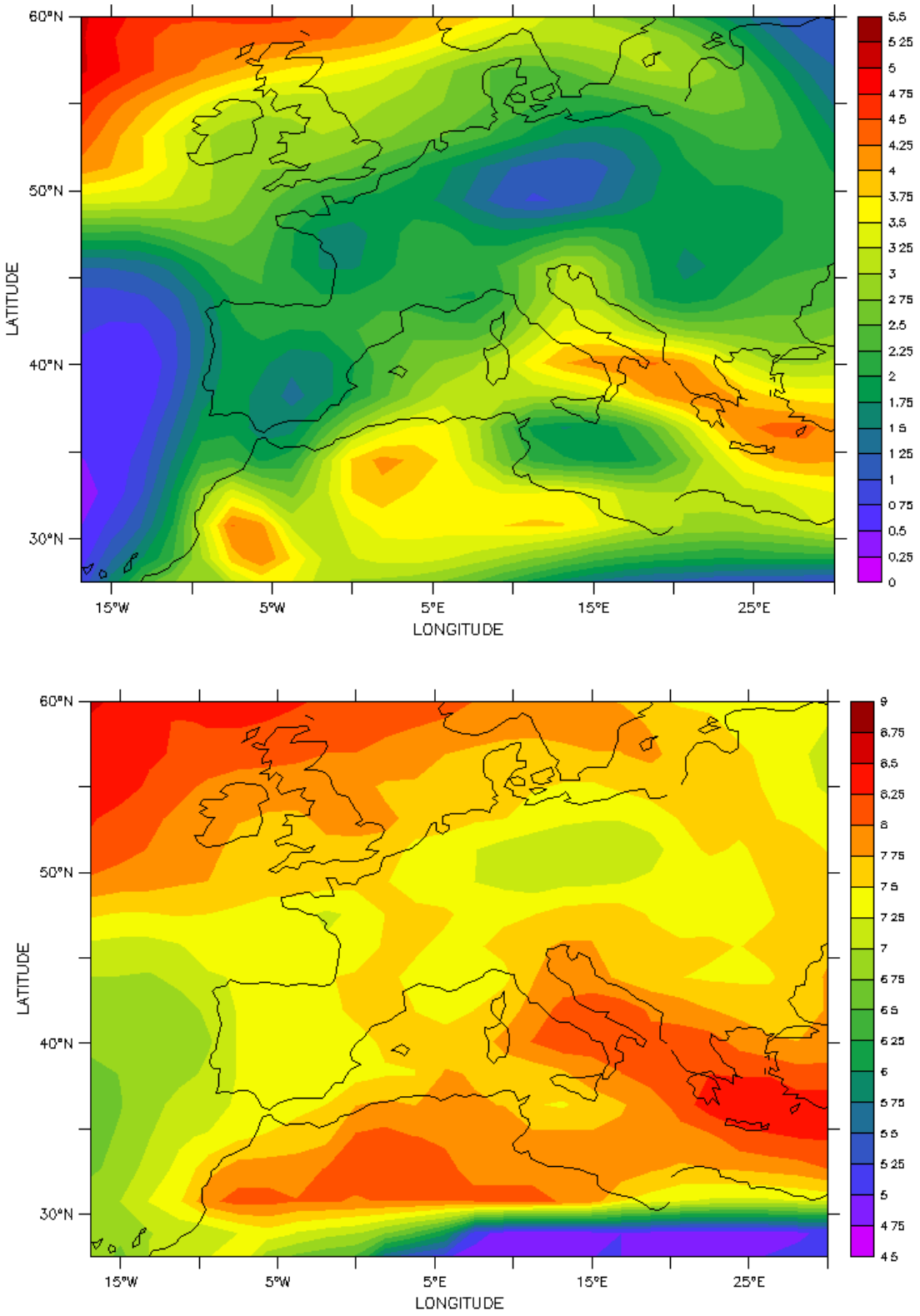

Figure 6.33. Mean PV distribution (PVU) at 250 hPa (up); and Mean TI index (10^{-7} s^{-2}) at 250 hPa (down) for the Western Mediterranean Basin during the episode of 13-16 August, 2000.

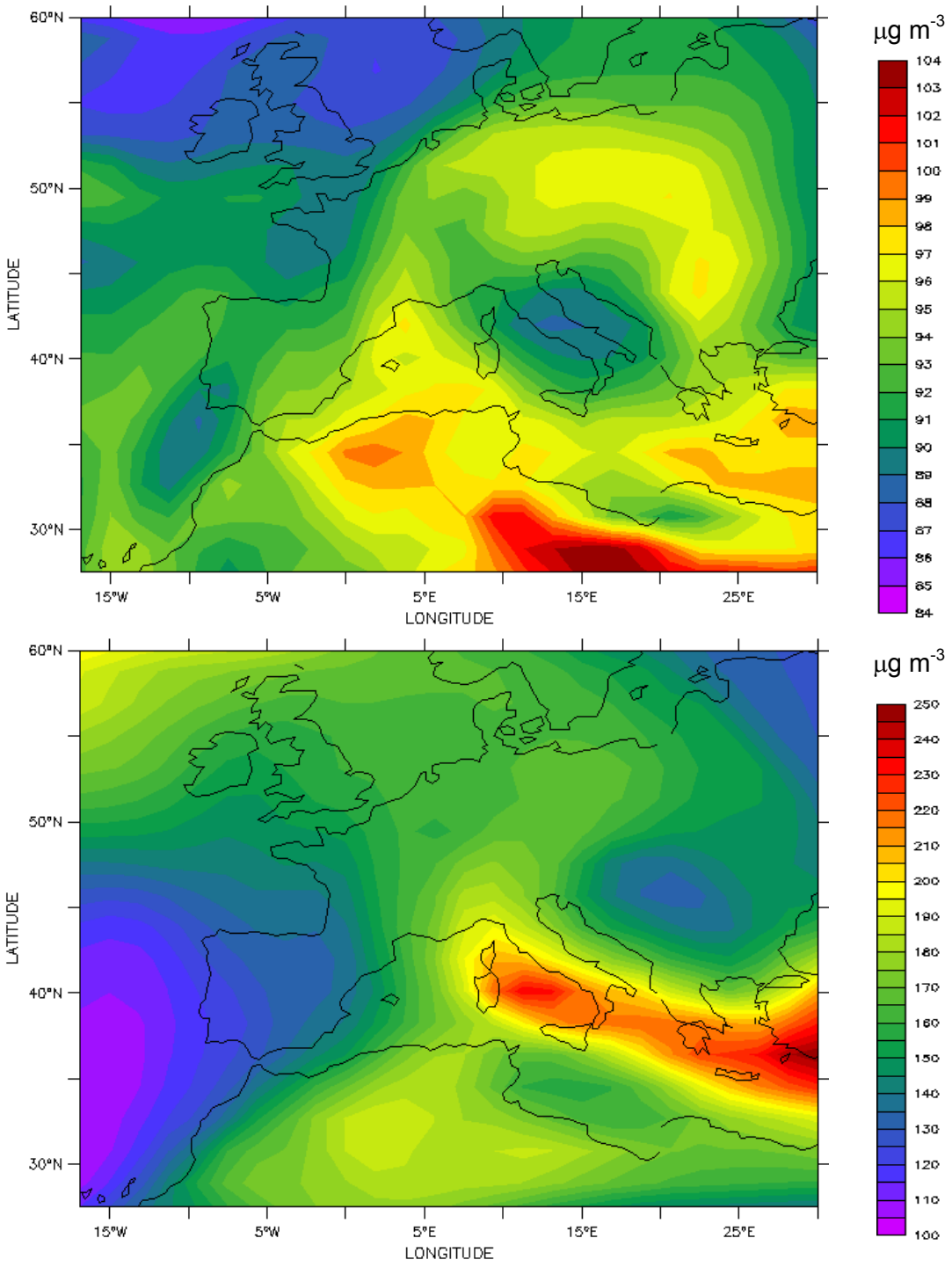

Figure 6.34. Average concentration of O_3 (μg m^{-3}) in middle troposphere (up) and upper troposphere (down) of the Western Mediterranean Basin during the episode of 13-16 August, 2000.

Backtrajectories at the upper troposphere (9000m agl) were computed in order to establish the origin of air masses arriving in the northeastern Iberian Peninsula (Figure 6.35), showing that the air with an origin in the tropopause of the Sahara dessert may be introduced into the upper troposphere of our domain of study. Nevertheless, these air masses do not show a tendency to suffer a vertical transport over the domain of study in the episode of 13-16 August, 2000.

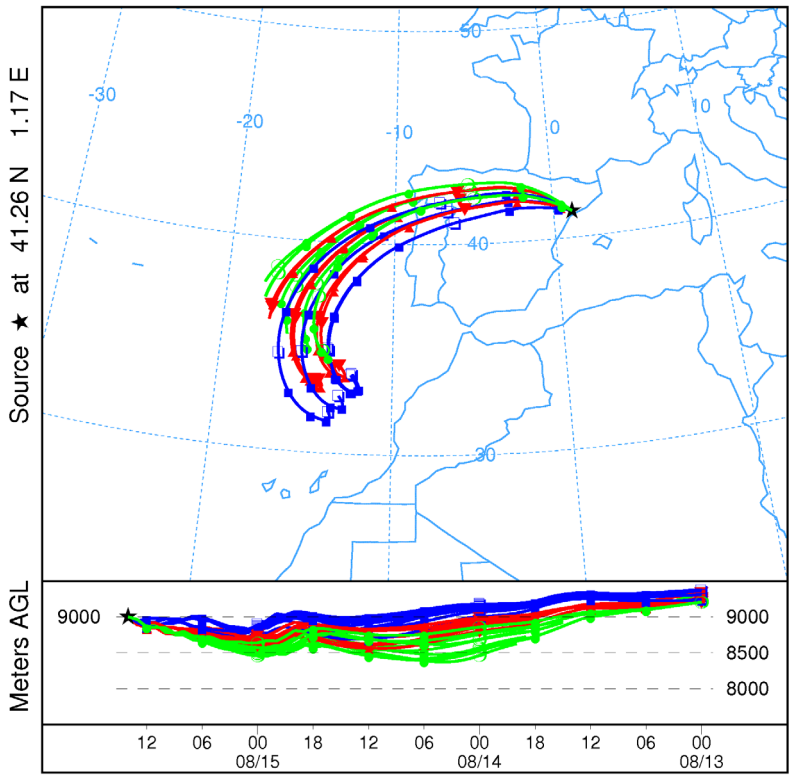

Figure 6.35. Ensemble backtrajectories arriving at 9000m at the domain of the Iberian Peninsula on 15 August, 2000, at 1200UTC. Backtrajectories indicate a Saharan origin of the air masses (area with high potential vorticity).

The high concentrations of ozone in the troposphere over 300 hPa (Figure 6.36) could be explained by the vicinity of the tropopause and the lower stratosphere. The limitation in the coupling of upper tropospheric processes with the lower troposphere provides a low horizontal gradient in ozone concentration, since the stratosphere-troposphere exchange is the process controlling the levels of O_3 in the most upper troposphere. The different chemical composition of the stratosphere and troposphere allows stratospheric air to reach the troposphere through descending in the Western Mediterranean Basin and the northeastern Iberian Peninsula. ECHAM5/MESSy provides higher ozone levels, probably because of an inaccurate representation of the stratosphere-troposphere exchange in the regional model MM5-EMICAT2000-CMAQ. Maximum ozone values are observed over the eastern Mediterranean coast and northeastern Africa, areas related with a tropopause descent.

6.5 Source Attribution to Tropospheric Ozone and Carbon Monoxide

In this section, the source attribution of main atmospheric processes to the maximum ground levels of photochemical pollutants and their budget in the troposphere is depicted in this section. Processes considered include: (1) emissions-photochemical cycle; (2) convective transport; (3) advective transport; (4) dry-wet deposition; and (5) stratosphere-troposphere exchange.

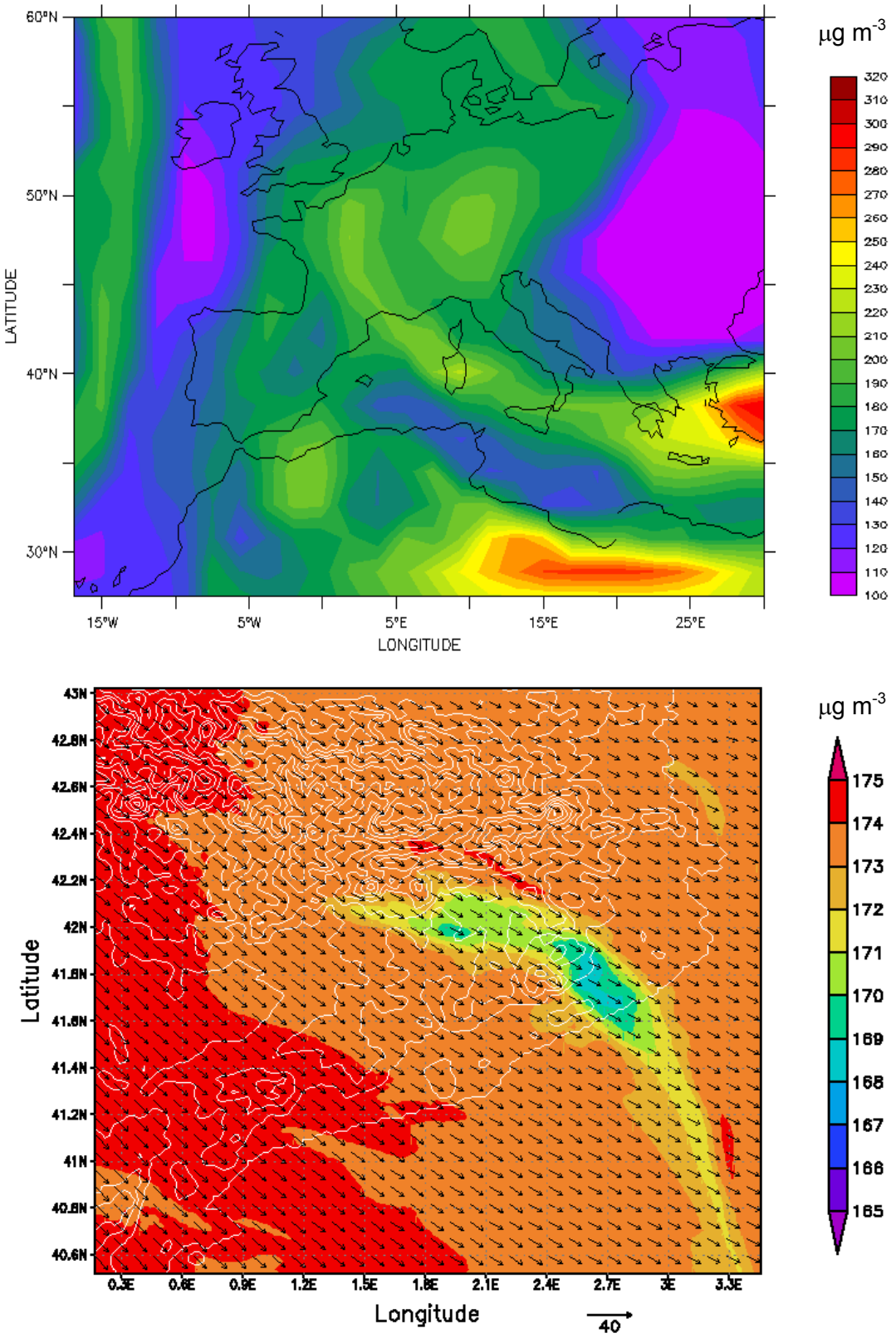

Figure 6.36. Ozone concentrations (μg m^{-3}) at 9000m, simulated for the whole WMB with ECHAM5/MESSy (up) and for the NEIP with MM5-EMICAT2000-CMAQ (down) at 1200UTC of 14 August, 2000. A low horizontal gradient is observed in the simulations, since the STE process controls the levels of this pollutant.

Table 6.4 shows the contribution of the five individual component processes to ground-level maximum concentrations of ozone and carbon monoxide estimated by ECHAM5/MESSy for the episode of 13-16 August, 2000, in the area of study of the northeastern Iberian Peninsula. The process analysis shown indicates that the occurrence of high ozone concentrations is the result of an imbalance between high local chemical production rates and dry deposition, fundamentally. The steady increase in chemical production of ozone during the day exceeds vertical convection and dry deposition removal rates and lead to peak ozone concentrations during the mid-afternoon, as was also stated by Jiang *et al.* (2003).

Table 6.4. Contribution of different physic-chemical processes to maximum ozone and carbon monoxide ground-level concentrations ($\mu g\ m^{-3}$) in northeastern Iberian Peninsula for the episode of 13-16 August, 2000, estimated with ECHAM5/MESSy.

	Ground-level O_3 concentration		**Ground-level CO concentration**	
Emissions-Photochemical Cycle	186.9 $\mu g\ m^{-3}$	114.4%	712.5 $\mu g\ m^{-3}$	97.9%
Convective Transport	-7.7 $\mu g\ m^{-3}$	-4.7%	-29.5 $\mu g\ m^{-3}$	-4.1%
Advective Transport	6.8 $\mu g\ m^{-3}$	4.2%	46.3 $\mu g\ m^{-3}$	6.4%
Dry and Wet Deposition	-26.1 $\mu g\ m^{-3}$	-16.0%	-1.4 $\mu g\ m^{-3}$	-0.2%
S-T Exchange	3.6 $\mu g\ m^{-3}$	2.2%	0.0 $\mu g\ m^{-3}$	0.0%
Total	**163.3 $\mu g\ m^{-3}$**	**100.0%**	**727.9 $\mu g\ m^{-3}$**	**100.0%**

In the northeastern Iberian Peninsula, the photochemical cycle (whose contribution is 186.9 $\mu g\ m^{-3}$ in the case of ozone and 712.5 $\mu g\ m^{-3}$ for CO) is the dominant process, while dry deposition (wet deposition is negligible in the area during this episode) and convective vertical transport are the major sinks in the case of ozone (-26.1 $\mu g\ m^{-3}$ and -7.7 $\mu g\ m^{-3}$, respectively). Meanwhile, for carbon monoxide, the contribution of deposition is just -1.4 $\mu g\ m^{-3}$, being the principal sink the convective transport that vertically exports pollutants to the middle troposphere (-29.5 $\mu g\ m^{-3}$). The stratosphere-troposphere exchange effect on superficial ozone is just around 2% (3.6 $\mu g\ m^{-3}$ for O_3), while no contribution is observed in the case of carbon monoxide.

According to ECHAM5/MESSy, the advection term contributes to maximum levels with a small quantity (6.8 $\mu g\ m^{-3}$ for O_3 and 46.3 $\mu g\ m^{-3}$ for CO) compared to the large chemical production, since the meteorological situation of the episode (low pressure gradient with a weak anticyclone over the Mediterranean) strongly limits advection processes in the area. As previously shown in Chapter 4, simulations with MM5-EMICAT2000-CMAQ indicate that the contribution of advective transport to maximum ozone levels is 4.7 $\mu g\ m^{-3}$, which signify a 2.5% of the final maximum concentrations. These results agree with those here presented by ECHAM5/MESSy (6.8 $\mu g\ m^{-3}$, 4.2% of 1-hr peak O_3 concentrations).

Table 6.5 presents an overview of the budget of tropospheric O_3 and CO for the episode of 13-16 August, 2000, over the domain of the northeastern Iberian Peninsula. The budget terms are detailed for source and sink terms, where possible. In addition, the mass balance for O_3 and CO is subdivided into different zones of the troposphere, covering from the surface to: (1) the planetary boundary layer; (2) the middle troposphere (500 hPa-5500m); and (3) the upper stratosphere (250 hPa-11000m). Percentages shown indicate the contribution of each process to the total tropospheric amount of ozone or carbon monoxide in that area of the atmosphere. Further description of the results is presented below.

Table 6.5. Budget of the contribution of different physic-chemical processes to ozone and carbon monoxide levels (Gg) within the troposphere of the entire domain of the northeastern Iberian Peninsula for the episode of 13-16 August, 2000.

	Surface-PBL			
	O_3 Balance		*CO Balance*	
Emissions-Photochemical Cycle	48.1 Gg O_3	113.3%	132.6 Gg CO	98.5%
Convective Transport	-1.5 Gg O_3	-3.5%	-5.1 Gg CO	-3.8%
Advective Transport	1.3 Gg O_3	3.2%	7.4 Gg CO	5.5%
Dry and Wet Deposition	-6.5 Gg O_3	-15.4%	-0.3 Gg CO	-0.2%
S-T Exchange	1.0 Gg O_3	2.4%	0.0 Gg CO	0.0%
Total	**42.4 Gg O_3**	**100.0%**	**134.6 Gg CO**	**100.0%**
	Surface-500 hPa (5500m)			
	O_3 Balance		*CO Balance*	
Emissions-Photochemical Cycle	141.7 Gg O_3	85.7%	281.9 Gg CO	83.2%
Convective Transport	-0.4 Gg O_3	-0.3%	-2.3 Gg CO	-0.7%
Advective Transport	20.9 Gg O_3	12.6%	59.5 Gg CO	17.6%
Dry and Wet Deposition	-6.5 Gg O_3	-3.9%	-0.3 Gg CO	-0.1%
S-T Exchange	9.6 Gg O_3	5.8%	0.0 Gg CO	0.0%
Total	**165.3 Gg O_3**	**100.0%**	**338.8 Gg CO**	**100.0%**
	Surface-250 hPa (11000m)			
	O_3 Balance		*CO Balance*	
Emissions-Photochemical Cycle	192.1 Gg O_3	75.9%	306.4 Gg CO	82.9%
Convective Transport	0.0 Gg O_3	0.0%	0.0 Gg CO	0.0%
Advective Transport	22.7 Gg O_3	9.0%	63.5 Gg CO	17.2%
Dry and Wet Deposition	-6.5 Gg O_3	-2.6%	-0.3 Gg CO	-0.1%
S-T Exchange	44.9 Gg O_3	17.7%	0.0 Gg CO	0.0%
Total	**253.1 Gg O_3**	**100.0%**	**369.6 Gg CO**	**100.0%**

6.5.1 Emissions-Photochemical Cycle

The main emission sources in the northeastern Iberian Peninsula are located on the coast, especially in the Barcelona Geographical Area and the Tarragona industrial zone (Parra, 2004). The importance of biogenic emissions is high in the entire Mediterranean coast, representing a 34% of total annual VOCs emissions, since they are a source of reactive compounds such as aldehydes and isoprene. The traffic emissions represent a 58% of the emissions of NO_x and 36%

of VOCs in the troposphere, especially olefins and aromatic compounds. During the summer months, and especially August, emissions are supposed to have an additional weight, since traffic increases because of the vacation period and the contribution of foreign vehicles. Main emitters are located in the axis of roads parallel to the littoral and the cities of Barcelona and Tarragona.

Industrial emissions are located mainly in the industrial area of Tarragona and represent a 39% of the emissions of NO_x and 17% of the emissions of VOCs; meanwhile the domestic and commercial use of solvents represents 13% of VOCs emissions in the area (Parra, 2004). The emission of precursors attributable to the industrial sector in the northeastern Iberian Peninsula adds up 41 Gg yr^{-1} of NO_x and 23 Gg yr^{-1} of VOCs. In the annual cycle, total emissions of ozone precursors in the northeastern Iberian Peninsula are 106.9 Gg yr^{-1} of NO_x (58% traffic emissions; 39% industrial emissions) and 99.3 Gg yr^{-1} of NMVOCs (34% biogenic emissions; 36% on-road traffic emissions; 17% industrial emissions).

Emissions of ozone precursors during the episode of 13-16 August, 2000, were 1.18 Gg for NO_x and 0.86 Gg for non-methane VOCs. The relation NMVOCs/NO_x, that is 1.28 for the annual cycle, increases until 1.73 for this episode of photochemical pollution due to the high temperatures and solar radiation, which promote evaporative emissions from on-road traffic and vegetation. Most of anthropogenic emissions derived from on-road traffic and domestic sector are located in the Barcelona Geographical Area and in the axis of the highways oriented parallel to the coastline.

The strong biogenic and anthropogenic forcing on emissions of O_3 precursors become an important source of tropospheric ozone and other pollutants in the northeastern Iberian Peninsula respect to other physic-chemical processes. This is not only the case at the surface, where the emissions-photochemical cycle (including background amounts) cycle accounts for 48.1 Gg O_3 and 136.2 Gg CO in the boundary layer during the episode of 13-16 August, 2000: up to approximately 5500m, more than 80% of the ozone (141.7 Gg) and carbon monoxide (281.9 Gg) derives from the emission-photochemistry cycle. For the domain studied, this cycle presently contributes more than a 70% to the tropospheric O_3 (192.1 Gg). This percentage increases over 80% in the case of CO because of the lack of contribution of the stratosphere to CO levels.

6.5.2 Convective Transport

A convective transport is a particularly efficient process for fast transport of boundary layer air into upper tropospheric zones (Hauf *et al.*, 1995; Ström *et al.*, 1999; Fischer *et al.*, 2003). As previously shown for the middle troposphere, strong thermally or mechanically driven convections appear at the central plain of the northeastern Iberian Peninsula injecting low-troposphere air masses up to 3500m. Once the air masses are injected in altitude, they incorporate to the dominant synoptic flux and are transported towards the coast (Jorba *et al.*, 2003). Here, the compensatory subsidence of the Iberian thermal low makes the polluted air masses incorporate to the breeze cell in the low troposphere. These dynamics obtained through modeling are

supported by the results described by Millán *et al.* (1992; 1997; 2000) over the eastern Iberian Mediterranean coast trough experimental campaigns. On the other side, multilayer structures associated to these phenomena have been experimentally established over the city of Barcelona with LIDAR measurements (Baldasano *et al.*, 1994; Soriano *et al.*, 2001; Pérez *et al.*, 2004).

In the case of the northeastern Iberian, convection-driven processes export 1.5 Gg of O_3 out of the planetary boundary layer to middle- and upper-troposphere levels, which accounts for a decrease of -3.5% of the total ozone within lowest troposphere. In the case of carbon monoxide, 5.1 Gg of low-troposphere CO are injected aloft (-3.8%). The pollutants extracted on a vertical convective process are mainly incorporated to the middle troposphere, between 3500-5500 m, since the extraction of O_3 and CO from the middle troposphere up to the upper troposphere is just 0.4 Gg O_3 and 2.3 Gg CO, respectively (contribution of -0.3% and -0.7% to the total amount of pollutants from surface until 500 hPa). If we consider the troposphere until the upper troposphere, the convective transport between troposphere and stratosphere (not considered in the STE) is negligible, both for O_3 and CO.

6.5.3 Advective Transport

The contribution of advective transport within the planetary boundary layer is very limited, accounting just for 1.3 Gg O_3 (3.2%) and 7.4 Gg CO (5.5%). The low-pressure gradient situation over the Mediterranean Basin limits the advective transport during this episode of 13-16 August, 2000. Local re-circulation processes (local origin of air masses) dominate the transport of pollutants in the low troposphere.

Most of the advective transport is produced in the middle troposphere, with a contribution of 19.6 Gg O_3 (to sum a total of 20.9 Gg O_3 in the domain from surface until the middle troposphere), representing a 12.6% in the northeastern Iberian Peninsula ozone from surface until the middle troposphere. In the case of CO, advective transport accounts for 17.6% in the middle troposphere (59.5 Gg CO). As previously shown in backtrajectories, this advective transport in the middle troposphere has its origin in the Iberian Peninsula and Atlantic air masses.

Stohl and Trickl (1999) and Trickl *et al.* (2003) have identified an important advection pathway for North American pollution to Europe. Air masses from the eastern coast of the United States may be transported over the Atlantic and arrive in Europe and therefore contributing to the high levels of ozone and other pollutants in the middle and upper troposphere. In addition, the aloft return flows extract part of the pollutants from the northeaster Iberian Peninsula towards the Mediterranean Sea.

In the upper troposphere, just 1.8 Gg O_3 are due to the advective transport, to totalize 22.7 Gg O_3 in total tropospheric ozone (9.0%). For CO, the contribution of advection to the total tropospheric CO is 63.5 Gg (17.2%). Here, the process of extraction of pollutants is even highlighted by the

strong northwestern winds, and therefore the introduction of pollutants into the domain of the northeastern Iberian Peninsula is balanced by the extraction of photochemical contaminants, to lead to just 1.8 Gg O_3 and 4.0 Gg CO in the range between 5500-11000m, approximately.

6.5.4 Dry and Wet Deposition

The term dry deposition represents a complex sequence of atmospheric phenomena resulting in the removal of pollutants from the atmosphere to the surface of the earth. In this work we used the approach of Ganzeveld *et al.* (1998), which derives aerodynamic and stomatal resistances from parameters calculated by ECHAM5/MESSy. Wet deposition is parameterized according to Roelofs and Lelieveld (1995). The dry deposition of ozone in the northeastern Iberian Peninsula accounts for -6.5 Gg O_3 during the episode of 13-16 August, 2000; which indicates that dry deposition extracts a -15.4% of the total amount of ozone in the area of study. The contribution of dry deposition to the ozone until the middle and upper troposphere reduces until -3.9% and 2.6%, respectively. On the other hand, the dry deposition of carbon monoxide is -0.3 Gg CO (-0.2% of the total CO) and does not greatly contribute to the budget of this pollutant. The results from simulations also indicate that a very limited wet deposition is observable over the Pyrenees, but it is negligible during this summer episode for the northeastern Iberian Peninsula.

6.5.5 Stratosphere-Troposphere Exchange

In summer, the photochemical lifetime of O_3 in the lower troposphere is of the order of days, transport is less efficient and STE has a minimum in summer (Lelieveld and Dentener, 2000). Therefore, for the episode of 13-16 August, 2000, the stratosphere-troposphere exchange has a minor contribution to total ozone inside the mixing layer (1.0 Gg O_3, 2.4%). This percentage increases to 6% in the middle troposphere, where 8.6 Gg O_3 are due to the stratospheric ozone (total of 9.6 Gg because of the STE). The model results indicate that the ozone observed in the upper troposphere is associated with the stratospheric influence (18%), while the contribution from photochemical cycle in the troposphere decreases with altitude. This result agrees with the results of Lelieveld *et al.* (2002), who state that in the free troposphere, 20 to 40% of the O_3 originates from the stratosphere. In the upper troposphere, 35.3 Gg of O_3 over the northeastern Iberian Peninsula are consequence of the STE, which totalizes 44.9 Gg of O_3 in the troposphere over the domain. This behavior in the upper troposphere is corroborated by the fact that CO is negatively related with ozone in the vertical profile shown in Figure 6.37. The relatively low levels of CO in the stratosphere make the STE contribution of this pollutant practically negligible respect to the emissions-photochemistry cycle.

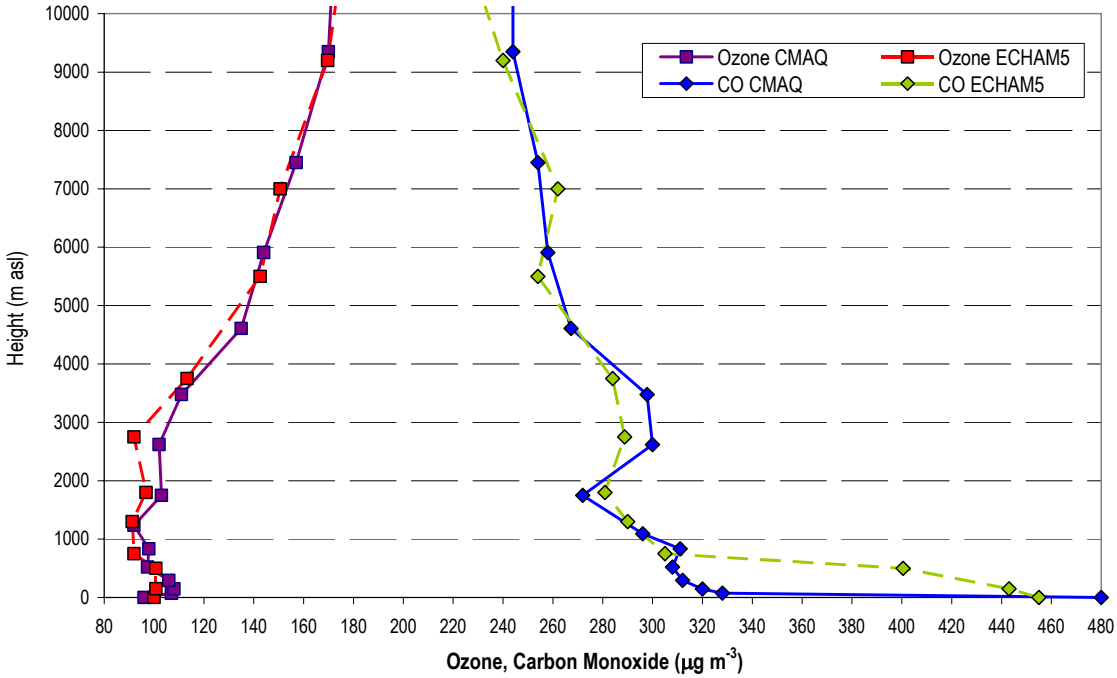

Figure 6.37. Ozone and carbon monoxide vertical concentrations (μg m^{-3}) at the city of Barcelona for 1500UTC of 14 August, 2000. Upper troposphere concentrations are anti-correlated showing the influence of stratosphere-troposphere exchange.

6.6 Conclusions

The origin of the high levels of photochemical pollutants and their dynamics over the Western Mediterranean Basin, and specifically, over the northeastern Iberian Peninsula during a typical summertime episode of photochemical pollution (13-16 August, 2000), were analyzed using the chemistry-climate model ECHAM5/MESSy and MM5-EMICAT2000-CMAQ regional model.

The models were evaluated against ambient data from 48 air quality stations in the northeastern Iberian Peninsula. They show a good behavior respect to the statistical figures analyzed. The objective set in the Directive 2002/3/EC is achieved for the whole period of study for both ECHAM5/MESSy and MM5-EMICAT2000-CMAQ. Both models, despite considering different approaches and resolutions, met the objective of ±20% set by US EPA for prediction of the peak levels of this pollutant during the episode. However, the simulation with the coarser grid (ECHAM5/MESSy) underestimates maximum ozone, carbon monoxide and nitrogen oxides levels with regards to the fine grid of MM5-EMICAT2000-CMAQ, since the grid resolution highly influences the formation and loss processes of pollutants, (especially photochemistry and vertical transport). Vertical LIDAR profiles obtained over the city of Barcelona (41.361N – 2.181E) were used for the qualitative evaluation of the vertical layering of pollutants forecasted by ECHAM5/MESSy and MM5-EMICAT2000-CMAQ. The results indicate that modeled profiles are similar to measurements, accurately capturing the layering of pollutants over the Mediterranean

produced during re-circulation processes. Both models simulate a realistic ozone gradient between the boundary layer and the free troposphere with differences between both models that focus principally in the definition of the planetary boundary layer.

The main processes that take place in the troposphere of the Western Mediterranean Basin and northeastern Iberian Peninsula are summarized in the conceptual models of Figures 6.38, 6.39 and 6.40 both for surface and vertical dynamics of pollutants. These processes may be summarized as:

1. The episode considered in this work for the analysis of processes over the Western Mediterranean Basin corresponds to 13-16 August, 2000, which is a characteristic situation of photochemical pollution by ozone in during summertime in the Western Mediterranean Basin, related to a low pressure gradient. The day was characterized by a weak synoptic forcing, so that mesoscale phenomena, induced by the particular geography of the region would be dominant (Figures 6.38 and 6.39). The air masses of the lower troposphere have a local origin mainly due to re-circulation processes (caused by the orographic forcing), which are common in the Western Mediterranean Basin during this kind of synoptic situation. The canalization between the Pyrenees and the Central Massif introduced northwestern flows of non-polluted Atlantic air masses into the northeastern Iberian Peninsula.

2. As shown in Figure 6.40, a well-developed sea-breeze regime established along the entire domain. Breeze circulation cells up to 2000m height, over the mixing height (800m), are observed in the morning. The strength of the sea breeze and the complex orography of the eastern Iberian coast produce several vertical injections and layering of pollutants. As the sea breeze front advances inland reaching the mountain ranges, orographic injections and mechanical re-circulations of air pollutants occurs during the morning in the coastal mountains (~500m). At noon, the breeze has reached the first mountainous chain, and here it is reinforced by anabatic winds producing upward motions up to 1500-2000m. At late evening (2000UTC), the photochemical activity ceases, the see-breeze regime loses intensity and winds in the coast weaken, producing drainage of pollutants towards the coast through the river valleys (Figure 6.38). Photochemical ozone is quenched by its reaction with nitrogen monoxide.

3. At an altitude of 500m-1500m, air masses arriving in the northeastern Iberian Peninsula have their origin in the southeastern Iberian coast. An ozone reservoir layer at 1500m is presented during the night over the Mediterranean Sea with ozone concentrations above 125 $\mu g\ m^{-3}$. The high-pressure area over the Mediterranean Sea provokes anticyclonic circulations and therefore pollutants are transported inland to the northwestern Mediterranean on the following day during the development of the sea breeze cycle (Figure 6.39).

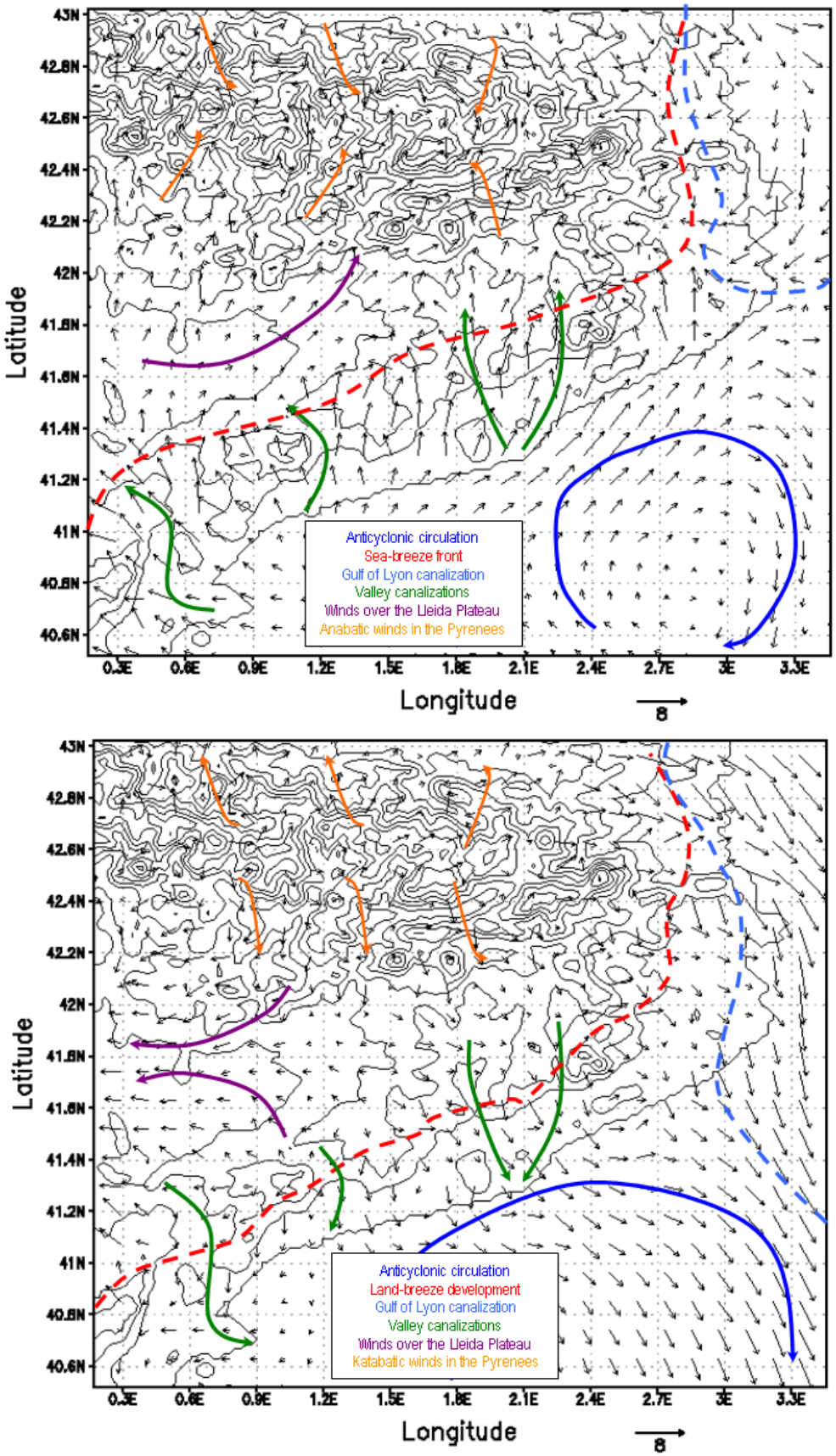

Figure 6.38. Conceptual model for surface air pollutants dynamics over the northeastern Iberian Peninsula during a typical summertime episode, at daytime (up) and nighttime (down).

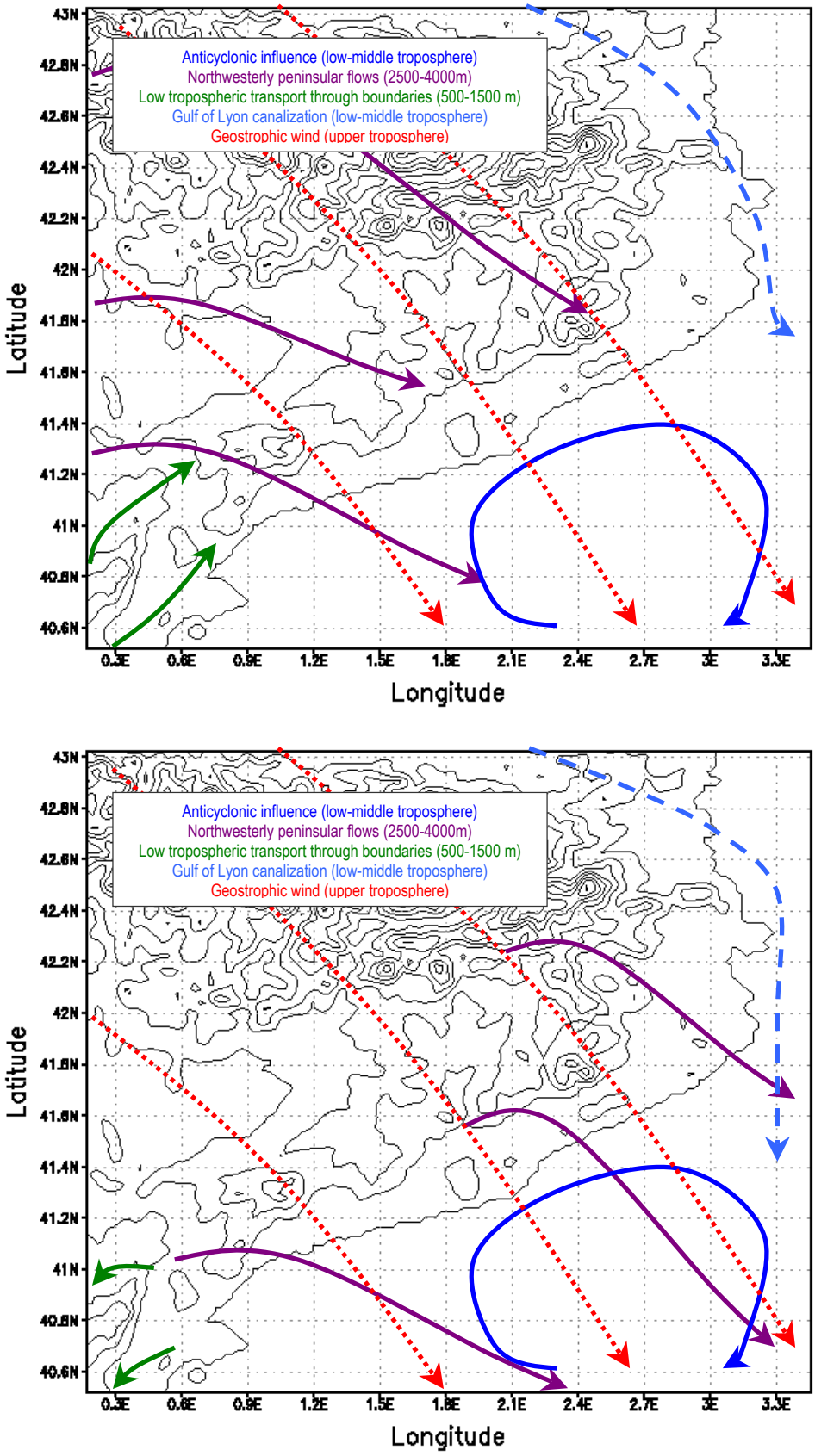

Figure 6.39. Conceptual model for aloft air pollutants dynamics over the northeastern Iberian Peninsula during a typical summertime episode, at daytime (up) and nighttime (down).

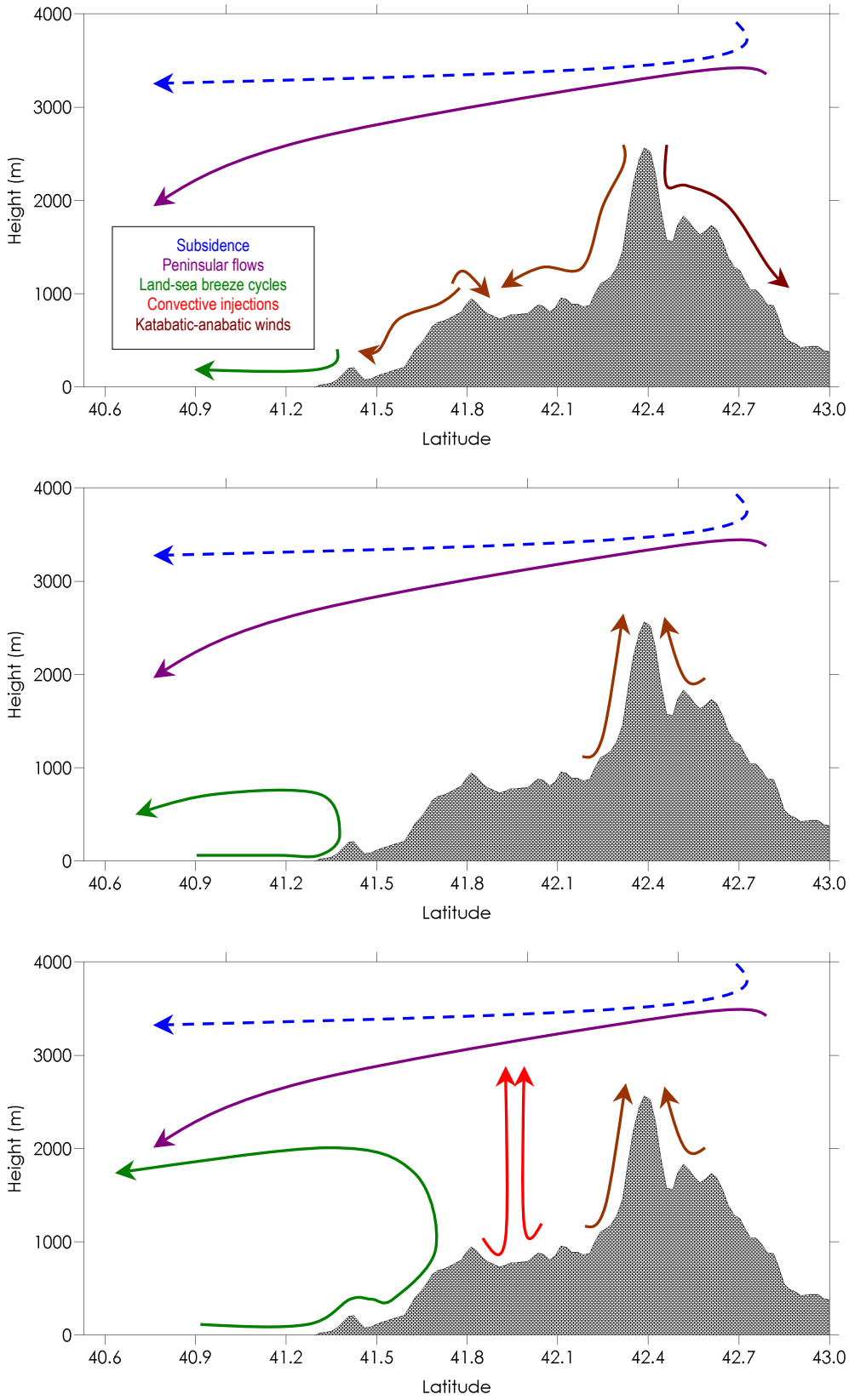

Figure 6.40. Conceptual model for a vertical profile (Mediterranean Sea-Barcelona-Pyrenees) of air pollutants dynamics over the northeastern Iberian Peninsula during a typical summertime episode, at night (up), morning (center) and afternoon (down).

4. The intense surface heating promotes the development of the Iberian Thermal Low (ITL) inland the Iberian Peninsula. The ITL developed for the episode 13-16 August, 2000, persists together with the stagnant meteorological conditions, and forces the convergence of surface winds from the coastal areas towards the central plateau injecting polluted air masses into the middle troposphere. Once in this region, northwesterly winds transport pollutants in a stratified layer in an altitude of 3500m towards the northwestern Mediterranean Basin, where they sink as a consequence of the compensatory subsidence (Figures 6.39 and 6.40).

5. Strong thermally or mechanically driven convections appear at the central plain of the northeastern Iberian Peninsula injecting low-troposphere air masses rich in photochemical pollutants up to middle troposphere (3500-5000m). Once the air masses are injected in altitude, they incorporate to the dominant synoptic flux and are transported towards the coast. Here, the compensatory subsidence of the Iberian thermal low makes the polluted air masses incorporate to the breeze cell in the low troposphere (Figure 6.40).

6. In the upper troposphere, air masses arriving in the northeastern Iberian Peninsula show an origin in the tropopause of the Sahara dessert, and are introduced in the troposphere of the northeastern Iberian Peninsula after their circulation over the Atlantic Ocean and the northern Iberian Peninsula with northewesterlies aloft (Figure 6.39). The vicinity of the tropopause explains high concentrations of ozone over 300 hPa. The limitation in the coupling of upper tropospheric processes with the lower troposphere provides a low horizontal gradient in ozone concentration, since the stratosphere-troposphere exchange is the process controlling the levels of O_3 in the most upper troposphere.

Furthermore, the contribution of different physic-chemistry processes to ground-level maximum concentrations of ozone and carbon monoxide predicted in the area of study of the northeastern Iberian Peninsula was quantified. An overview of the budget of tropospheric ozone and carbon monoxide for the episode of 13-16 August, 2000, for the area of the northeastern Iberian Peninsula is also included in this work.

The budget terms are detailed for source and sink terms, where possible. In addition, the mass balance for O_3 and CO is subdivided into different zones of the troposphere, covering from the surface to: (1) the planetary boundary layer; (2) the middle troposphere (500 hPa-5500m); and (3) the upper stratosphere (250 hPa-11000m). The process analysis indicates that the occurrence of high ozone concentrations is the result of an imbalance between high local chemical production rates and dry deposition, fundamentally.

The contribution of advective transport is limited due to the low pressure gradient, and simulations with ECHAM5/MESSy and CMAQ estimate that its contribution to maximum peak ozone levels is in the order of just 2.5-5%. The steady increase in chemical production of ozone

during the day exceeds vertical convection and dry deposition removal rates and lead to peak ozone concentrations during the mid-afternoon.

Finally, we could state that the interest of a using both a global climate-chemistry model as ECHAM5/MESSy and MM5-EMICAT2000-CMAQ regional model is the ability they provide to describe in detail the behavior of air pollutants over very complex terrains. The flows of air pollutants over very complex terrains are conditioned by the superposition of circulations of different scale (local, regional and global circulations) that may only be described by the combination of those tools.

6.7 References

Appenzeller, C., Davies, H. 1992. Structure of stratospheric intrusions into the troposphere. Nature, **358**, 570-572.

Bamber, D., Healey, P., Jones, B., Penkett, S., Tuck, A., Vaughan, G., 1984. Vertical profiles of tropospheric gases: chemical consequences of stratospheric intrusions. Atmospheric Environment, **18**, 1759-1766.

Baldasano, J.M., Cremades, L., Soriano, C., 1994. Circulation of air pollutants over the Barcelona geographical area in summer. Proceedings of Sixth European Symposium Physic-Chemical Behavior of Atmospheric Pollutants. Varese (Italy), 18-22 October, 1993. Report EUR 15609/1 EN: 474-479.

Barros, N., Toll, I., Soriano, C., Jiménez, P., Borrego, C., Baldasano, J.M., 2003. Urban Photochemical Pollution in the Iberian Peninsula: the Lisbon and Barcelona Airsheds. Journal of the Air & Waste Management Association, **53**, 347-359.

Bonasoni, P., Evangelisti, F., Bonafe, U., Ravegnani, F., Calzolari, F., Stohl, A., Tossiti, L., Tubertini, O., Colombo, T., 2000. Stratospheric Ozone intrusion episodes recorded at Mt. Cimone during the VOTALP project: case studies. Atmospheric Environment, **34**, 1355-1465.

Borchi, F., Marenco, A., 2002. Discrimination of air masses near the extratropical tropopause by multivariate analyses from MOZAIC data. Atmospheric Environment, **36**, 1123-1135.

Brühl, C., Crutzen, P., 1988. Scenarios of possible changes in atmospheric temperature and ozone concentrations due to man's activities, estimated with a one dimensional coupled photochemical climate model. Climate Dynamics, **2**, 173-203.

Danielsen, E., Mohnen, V., 1977. Ozone transport, in situ measurements and meteorological analyses of tropopause foldings. Journal of Geophysical Research, **82**, 5867-5877.

Draxler, R.R., Hess, G.D., 1998. An overview of the Hysplit_4 modelling system for trajectories, dispersion, and deposition. Australian Meteorological Magazine, **47**, 295-308.

Duclau, O., Frejafon, E., Schmidt, H., Thomasson, A., Mondelain, D., Yu, J., Guillaumond, C., Puel, C., Savoie, F., Ritter, P., Boch, J.P., Wolf, J.P., 2002. 3D-air quality model evaluation using the Lidar technique. Atmospheric Environment, **36**, 5081-5095.

Ellrod, G., and Knapp, D., 1992. An objective clean-air turbulence forecasting technique: Verification and operational use. Weather Forecast, **7**, 150-165.

Fischer, H., de Reus, M., Traub, M., Williams, J., Lelieveld, J., de Gouw, J., Warneke, C., Schlager, H., Minikin, A., Cheele, R., Siegmund, P., 2003. Deep convective injection of boundary layer air into the lowermost stratosphere at midlatitudes. Atmospheric Chemistry and Physics, **3**, 739-745.

Gangoiti, G., Millán, M.M., Salvador, R., Mantilla, E., 2001. Long-range transport and re-circulation of pollutants in the western Mediterranean during the project regional cycles of air pollution in the west–central Mediterranean area. Atmospheric Environment, **35**, 6267-6276.

Ganzeveld, L.N., Lelieveld, J., , Roelofs, G.J., 1998. A dry deposition parameterization for sulfur oxides in a chemistry-general circulation model. Journal of Geophysical Research, **103**, 5679-5694.

Hauf, T., Schulte, P., Alheit, R., Schlager, H., 1995. Rapid vertical transport by an isolated midlatitude thunderstorm. Journal of Geophysical Research, **100**, 22957-22970.

Hoerling, M., Schaak, T., Lenzen, A., 1991. Global objective tropopause analysis. Monthly Weather Review, **119**, 1816-1839.

Jang, C.J., Jeffries, H.E., Byun, D., Pleim, J.E., 1995. Sensitivity of ozone to model grid resolution – II. Detailed process analysis for ozone chemistry. Atmospheric Environment, **29**, 21, 3101-3114.

Jian, G., Lamb, B., Westberg, H., 2003. Using back trajectories and process analysis to investigate photochemical ozone production in the Puget Sound region. Atmospheric Environment, **37**, 1489-1502.

Jiménez, P., Jorba, O., Baldasano, J.M., 2004. Influence of horizontal model grid resolution on tropospheric ozone levels. In: Harmonisation 2004. 9th International Conference on Harmonisation within Atmospheric Dispersion Modelling for Regulatory Purposes. Garmish-Partenkircher, Germany, June 1-4, 2004.

Jorba, O., Gassó, S., Baldasano, J.M., 2003. Regional circulations within the Iberian Peninsula east coast. 26th International Technical Meeting of NATO-CCMS on Air Pollution Modelling and its application, Istanbul, Turkey, 26-30 May.

Jorba O., Pérez, C., Rocadenbosch, F., Baldasano, J.M., 2004. Cluster Analysis of 4-Day Back Trajectories Arriving in the Barcelona Area (Spain) from 1997 to 2002. Journal of Applied Meteorology, **43**, 6, 887-901.

Kentarchos, A.S, Roelofs, G.J., 2003. A model study of stratospheric ozone in the troposphere and its contribution to tropospheric OH formation. Journal of Geophysical Research, **108**, 10.1029/2002JD002598.

Lelieveld, J., Dentener, F.J., 2000. What controls tropospheric ozone? Journal of Geophysical Research, **105**, 3531-3551.

Lelieveld, J., Berresheim H., Borrmann, S., Crutzen, P.J., Dentener, F.J., Fischer, H., Feichter, J., Flatau, P.J., Heland, J., Holzinger, R., Korrmann, R., Lawrence, M.G., Levin, Z., Markowicz, K.M., Mihalopoulos, N., Minikin, A., Ramanathan, V., de Reus, M., Roelofs, G.J., Scheeren, H.A., Sciare, J., Schlager, H., Schultz, M., Siegmund, P., Steil, B., Stepahanou, E.G., Stier, P., Traub, M., Warneke, C., Williams, J., Zieris, H., 2002. Global air pollution crossroads over the Mediterranean. Science, **298**, 794-799.

Martín-Vide, J., 1984. Interpretación de los mapas del tiempo (Interpretation of weather charts). Ed. Ketres, 147 pp.

Millán, M.M., Artiñano, B., Alonso, L., Castro, M., Fernandez-Patier, R., Goberna, J., 1992. Mesometeorological cycles of air pollution in the Iberian Peninsula. Air Pollution Research Report 44. Commission of the European Communities. Brussels, Belgium. 219 pp.

Millán, M.M., Salvador, R., Mantilla, E., Artíñano, B., 1996. Meteorology and photochemical air pollution in southern Europe: Experimental results from EC research projects. Atmospheric Environment, **30**, 1909-1924.

Millán, M.M., Salvador, R., Mantilla, E., 1997. Photooxidant dynamics in the Mediterranean basin in summer: Results from European research projects. Journal of Geophysical Research, **102** (D7), 8811-8823.

Millán, M.M., Mantilla, E., Salvador, R., Carratala, A., Sanz, M.J., Alonso, L., Gangoiti, G., Navazo, M., 2000. Ozone cycles in the western Mediterranean basin: interpretation of monitoring data in complex coastal terrain. Journal of Applied Meteorology, **4**, 487-507.

Parra, R., 2004. Development of the EMICAT2000 model for the estimation of air pollutants emissions in Catalonia and its use in photochemical dispersion models. Ph.D. Dissertation (in Spanish), Polytechnic University of Catalonia (Spain).

Pérez, C., Sicard, M., Jorba, O., Comerón, A., Baldasano, J.M., 2004. Summertime re-circulations of air pollutants over the north-eastern Iberian coast observed from systematic EARLINET lidar measurements in Barcelona. Atmospheric Environment, **38**, 3983-4000.

Rasch, P.J., Williamson, D., 1990. Computational aspects of moisture transport in global models of the atmosphere. Quarterly Journal of the Royal Meteorological Society, **116**, 1071-1090.

Reed, R., 1955. A study of a characteristic type of upper level frontogenesis. Journal of Meteorology, **12**, 226-237.

Roeckner, E., Bäuml, G., Bonaventura, L., Brokopf, R., Ecsh, M., Giorgetta, M., Hagemann, S., Kircher, I., Kornblueh, L., Manzini, E., Rhodin, A., Schlese, U., Schulzweida, U., Tompkins, A., 2003. The atmospheric general circulation model ECHAM5: Model description. MPI Report 349, Max Planck Institute for Meteorology, Hamburg, Germany, 127 pp.

Roelofs, G.J., Lelieveld, J., 1995. Distribution and budget of O_3 in the troposphere calculated with a chemistry-general circulation model. Journal of Geophysical Research, **100**, 20983-20998.

Roelofs, G.J., Lelieveld, J., 2000a. Tropospheric ozone simulation with a global chemistry-climate model: Influence of higher hydrocarbon chemistry. Journal of Geophysical Research, **105**, 22697-22712.

Roelofs, G.J., Lelieveld, J., 2000b. Model analysis of the STE of ozone and its role in the tropospheric O_3 budget. In: Chemistry and Radiation Changes in the Ozone Layer, Zerefos, C. (Ed), NATO ASI Series, Kluwer Academic Publishers, Netherlands, pp. 25-43.

Roelofs, G.J., Scheeren, H.A., Heland, J., Ziereis, H., Lelieveld, J., 2003. A model study of ozone in the eastern Mediterranean free troposphere during MINOS (August 2001). Atmospheric Chemistry and Physics, **3**, 1199-1210.

Russell, A., Dennis, R., 2000. NARSTO critical review of photochemical models and modeling. Atmospheric Environment, **34**, 2283-2324.

Sicard M., Pérez C., Comerón A., Baldasano J.M, Rocadenbosch F., 2003. Determination of the Mixing Layer Height from Regular Lidar Measurements in the Barcelona Area. Remote Sensing of Clouds and the Atmosphere VIII (Ed. K.P. Schäfer *et al.*) Proc. Of SPIE, Vol. 5235: 505-516.

Soriano, C., Baldasano, J.M., Buttler, W.T., Moore, K., 2001. Circulatory patterns of air pollutants within the Barcelona air basin in a summertime situation: Lidar and numerical approaches. Boundary-Layer Meteorology, **98** (1), 33-55.

Steil, B., Dameris, M., Brühl, C., Crutzen, P.J., Grewe, V., Ponater, M., Sausen, R., 1998. Development of a chemistry module for GMCs: first results of a multiannual integration. Annals of Geophysics, **16**, 205-228.

Stohl, A., Trickl, T., 1999. A textbook example of long-range transport: simultaneous observation of ozone maxima of stratospheric and North American origin in the free troposphere over Europe. Journal of Geophysical Research, **104**(D32), 30445-30462.

Ström, J., Fischer, H., Lelieveld, J., Schröder, F., 1999. In-situ measurements of aerosol microphysical properties and trace gases in two cumulonimbus anvils over Western Europe. Journal of Geophysical Research, **104**, 12221-12226.

Toll, I., Baldasano, J.M., 2000. Modeling of photochemical air pollution in the Barcelona area with highly disaggregated anthropogenic and biogenic emissions. Atmospheric Environment, **34**, 19, 3060-3084.

Traub, M., Fischer, H., de Reus, M., Kormann, R., Heland, J., Yiereis, H., Schlager, H., Holzinger, R., Williams, J., Warneke, C., de Gouw, J., Lelieveld, J, 2003. Chemical characteristics assigned to trajectory clusters during the MINOS campaign. Atmospheric Chemistry and Physics, **3**, 459-468.

Traub, M., Lelieveld, J., 2003. Cross-tropopause transport over the Eastern Mediterranean. Journal of Geophysical Research, **108**(D23), 4712, doi:10.1029/2003JD003754, 2003.

Trickl, T., Cooper, O.R., Eisele, H., James, P., Mücke, R., Stohl, A., 2003. Intercontinental transport and its influence on the ozone concentrations over central Europe: Three case studies. Journal of Geophysical Research, **108**(D12), 8530, doi:10.1029/2002JD002735, 2003.

Tulet, P., Suhre, K., Mari, C., Solmon, F., Rosset, R., 2002. Mixing of boundary layer and upper tropospheric ozone during a deep convective event over Western Europe. Atmospheric Environment, **36**, 4491-4501.

US EPA, 1991. Guideline for Regulatory Application of the Urban Airshed Model. US EPA Report No. EPA-450/4-91-013. Office of Air and Radiation, Office of Air Quality Planning and Standards, Technical Support Division. Research Triangle Park, North Carolina, US.

van Aardenne, J.A., Dentener, F.J., Olivier, J.G.J., Klein-Goldewijk, C.M.G., Lelieveld, J., 2001. A 1 x 1 degree resolution dataset of historical anthropogenic trace gas emissions for the period 1890-1990. Global Biogeochemical Cycles, **15**(4), 909-928.

von Glasow, R., Sander, R., Bott, A., Crutzen, P.J., 2002. Modeling halogen chemistry in the marine boundary layer. 1. Cloud-free MBL. Journal of Geophysical Research, **107D**, 4341, doi:10.1029/2001JD000942, 2002.

von Kuhlmann, R., Lawrence, M.G., Crutzen, P.J., Rasch, P.J., 2003. A model for studies of tropospheric ozone and nonmethane hydrocarbons: Model description and ozone results. Journal of Geophysical Research, **108D**, doi: 10.1029/2002JD002893, 2003.

Wang, Y., Jacob, D.J., Logan, J.A., 1998. Global simulation of tropospheric O_3-NO_x-hydrocarbon chemistry, 2, Model evaluation and global ozone budget. Journal of Geophysical Research, **103**, 10727-10755.

Wirth, V., 1995a. Comments on "A new formulation of the exchange of mass and trace constituents between the stratosphere and troposphere". Journal of Atmospheric Science, **53**, 2491-2493.

Wirth, V. 1995b. Diabatic heating in an axisymmetric cut-off cyclone and related stratosphere-troposphere exchange. Quarterly Journal of the Royal Meteorological Society, **121**, 127-147.